## 2.12.5 Component Analyses Using Complete Model

The following section describes the full model analyses of the TB-1 containment vessel and its detailed components. As discussed in Section 1, the components within the titanium T-Ampoule consist of either cast plutonium (Pu) cylinders with a mass of 831 g or 731 g, small sample containers (SC-1), or medium sample containers (SC-2) containing Pu material or a Be composite material. Each component will be analyzed for three orientations, the end-on impact, the side-on impact, and the CGOC impact for the high-speed aircraft impact. For the hypothetical accident conditions (HAC) dynamic crush analyses, the same sets of analyses were performed. In the NCT 4-ft-drop scenario, only the side and end impact for the SC-1 and SC-2 cases were analyzed to assure the positioning of the sample containers did not require adjustment for the HAC and high-speed aircraft impact analyses.

### *2.12.5.1 Finite Element Model*

#### *2.12.5.1.1 Common Model Components*

The common components of the models are presented in Figures 2-65 and 2-66. The T-Ampoule is designed to fit snugly inside the TB-1 and to be loaded primarily in compression during impact. The finite element models of the T-Ampoule and TB-1 have a plane of symmetry along the center axis of the TB-1 (Z=0). Figure 2-65 shows the T-Ampoule and the TB-1 model for the top impact orientation. A hexagonal mesh with .015-in. elements is used to model the top of the T-Ampoule. This results in four elements through the thickness of the T-Ampoule shell. Since the primary strains are compressive, this allows for a time step which keeps the problem tractable, while providing adequate resolution of the T-Ampoule strain field. The mesh of the TB-1 is refined in the upper region with a hexagonal element size of 0.040 in. to adequately model the contact between the T-Ampoule top and the TB-1. The titanium Ring Filler, which fills the small void between the T-Ampoule and the TB-1 near the bottom of the TB-1 lid, is installed during preparations for shipment to provide uniform support to the ellipsoid T-Ampoule. As shown in Figure 2-66, the Ring Filler is not modeled explicitly, but is modeled as an integral part of the TB-1 body, with PH13-8-Mo material properties. Although the elastic moduli do differ, the yield strengths of the 13-8 (141 ksi) vs. Ti-6-4 (141.7 ksi) materials do not differ significantly, and this small gap-filling component was simplified to be continuous with the TB-1 since it provides no additional strength and only provides a smoothed inner surface for contact with the T-Ampoule and its contents. The stresses in this region are monitored to ensure that they do not threaten the integrity of the Ring Filler. For end impacts, the lower region of the TB-1 is modeled with a coarser mesh; for side impacts, the non-impact side has the coarser mesh. The TB-1 halves are tied together using the tied contact algorithm.

In the TB-1 finite element model, the lid and the body are modeled as one unit. The bolted connection is not modeled. There is a separate analytical bolt analysis in Section 2.12.6. This analysis uses the peak impulse force from the component finite element models to determine the bolt loading.

The model developed for the side-on impact analyses is presented in Figure 2-66. The model is similar to the top impact model except that the mesh for the TB-1 is refined on the sides of the component. The mesh discretization of the T-Ampoule top and T-Ampoule bottom is the same

0.015-in. hexagonal element size as that used in the end-on impact analysis. The thread region, where the top and bottom of the T-Ampoule are joined, is modeled using coincident nodes.

The SC-1 and SC-2 are fit inside a support structure within the T-Ampoule. This structure, shown in Figures 2-67 and 2-68, is constructed from Titanium 6Al-4V (see Section 2.12.4.14). The support structure consists of two dishes placed on each end of the T-Ampoule for vertical positioning (with a thickness that varies from 0.055 in. at the edge to 0.025 in. at the center), 4 upper and lower legs which centrally position the containers within the T-Ampoule (with a thickness of 0.063 in.), two rings which hold the legs in place (0.094 in. diameter), and either one or two spacers for the SC-1 and SC-2, respectively to separate the containers (with a thickness of 0.043 in. and a height of 0.749 in. and 1.008 in., respectively). The legs and rings were meshed to have 4 elements through the thickness, while the dishes have 5 elements through the thickness (see Figure 2-69 for mesh refinement). Figure 2-67 shows the support structure as used for the 0° rotated models while Figure 2-68 shows the structure used for the 45° rotated models. These two orientations were used to ensure worst cases analyses were performed in terms of loads on the support structure and loads on the T-Ampoule.

As detailed in Section 2.12.4.9, the high-strength PH13-8Mo stainless steel TB-1 is modeled using an elastic-plastic, power-law constitutive model to assure accurate capture of denting internally within the TB-1. The Ti-6Al-4V T-Ampoule and support structure are modeled using an elastic-plastic, power-law constitutive model.

The PRONTO3D code used in this analysis uses the Flanagan-Belytschko hexahedral element with one center integration point. The results are presented with contour plots showing element integration point values; they are not smoothed contours of extrapolated nodal values. Although the plots will look rough, the integration point strains are the primary variable of concern, since these values will be used in the strain locus plots. Therefore, integration point contours will be used throughout the analysis.

Included in the high speed aircraft analysis results and the HAC results are plots of kinetic energy versus time. These were included to demonstrate that the peak loads were captured in the analyses. The models were all run without built-in units, thus the kinetic energy plots presented for the high speed aircraft analyses and HAC analyses do not have labels. The x-axis of these plots, time, is in units of seconds. The y-axis of these plots, kinetic energy, is in units of pounds inches.

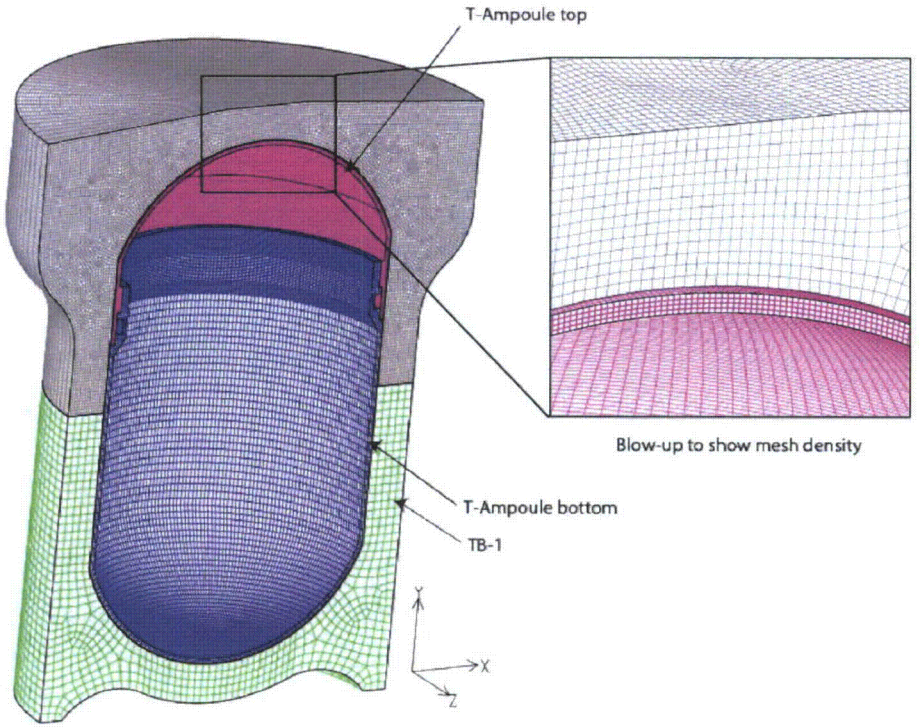


**Figure 2-65. Common Components of the Model for Top and CGOC Impact Orientation**

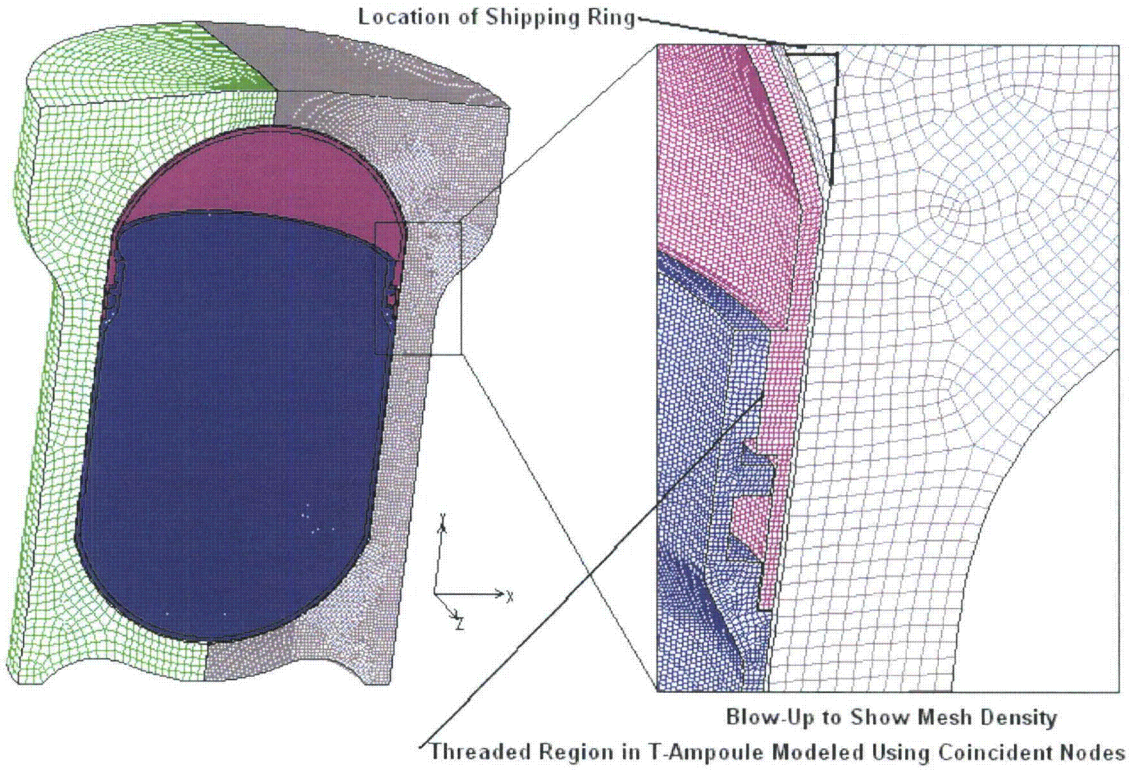


**Figure 2-66. Common Components of the Model for a Side Impact Orientation**

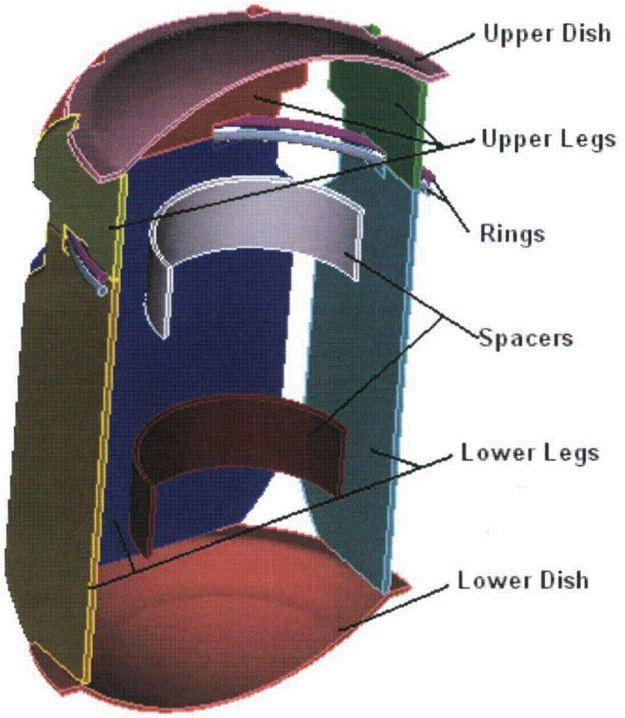


**Figure 2-67. Support Structure with 0° Rotation and Spacers for SC-1**

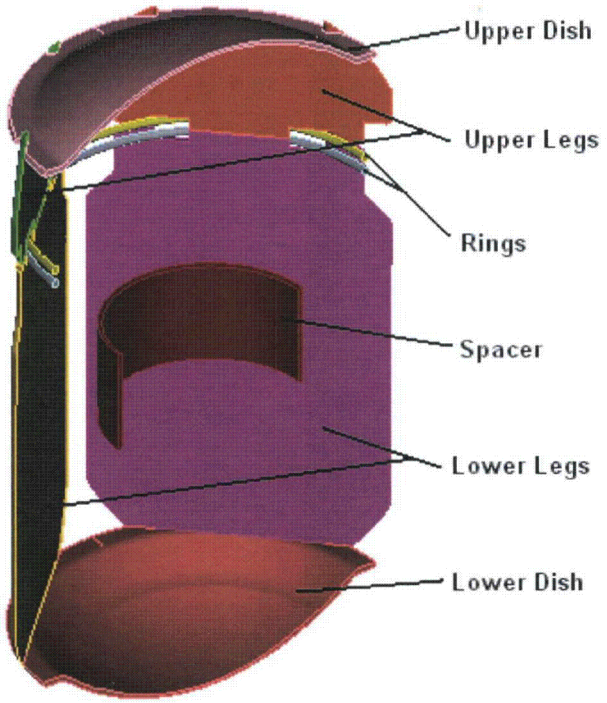


**Figure 2-68. Support Structure with 45° Rotation and Spacer for SC-2**

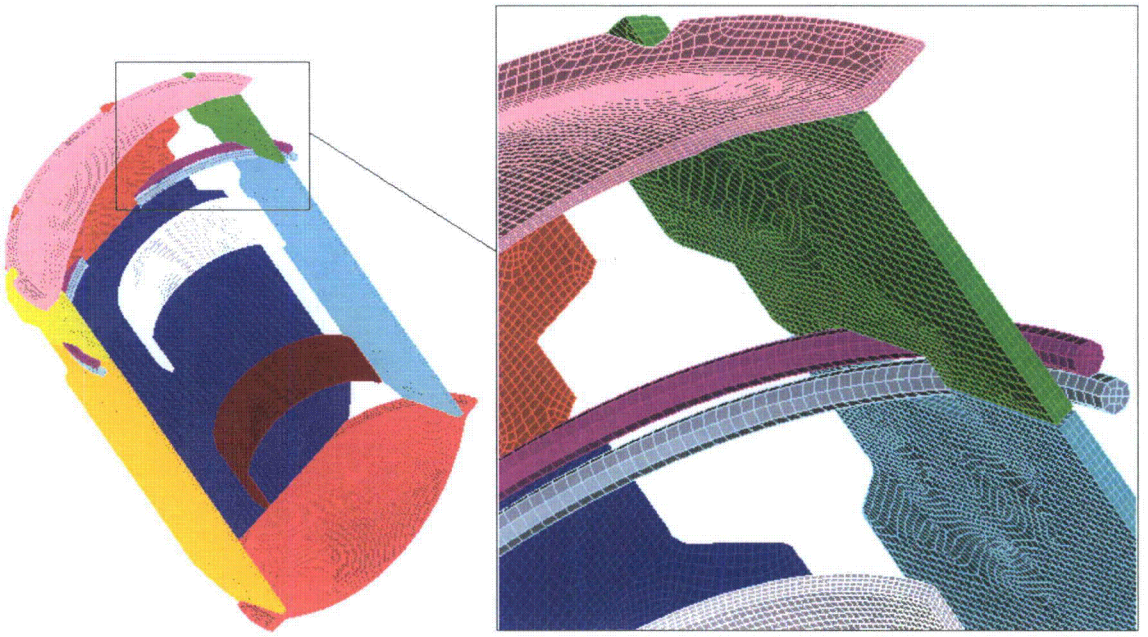

**Figure 2-69. Mesh Refinement in Support Structure with 0° Rotation and Spacer for SC-1**

### *2.12.5.2 Component Models*

Models of the content components consist of an 831-g plutonium metal hollow cylinder, a 731-g plutonium metal hollow cylinder, a small sample container (SC-1) and a medium sample container (SC-2). The sample containers will be used to transport Pu and a Pu/Be composite. These components are presented in Figures 2-70 through 2-73. The 831-g plutonium metal hollow cylinder shown in Figure 2-70 has a 2.51-in. diameter and a 2.903-in. length. The wall thickness is 0.118 in. It is modeled using 0.018 in. hexahedral elements, which results in 6 elements through the thickness. The material of the cylinder is modeled as alpha-plutonium as described in Section 2.12.4.16. The 731-g plutonium metal hollow cylinder model is very similar to the 831-g model, except that the length is reduced to account for the reduced material weight. It is also modeled as an alpha-plutonium material.

The finite element models for the sample containers are also similar to each other. The SC-1 model shown in Figure 2-72 is 3 in. in diameter and 2 in. high. The shell thickness is 0.065 in. The container is meshed with 0.020-in. hexagonal elements, which results in 3 elements through the shell thickness. The model is shown with the 0.88-in. diameter X 0.88-in. long right circular cylinder, which is modeled as delta-plutonium and has a mass of 174 g. Note that the Pu cylinder is located in the bottom of the sample container, which is farthest away from the T-Ampoule for a top-end impact (producing the highest net velocity difference between the two upon impact, and thus the highest load to the T-Ampoule). For a right side impact case, the Pu cylinder would be located on the far left side of the sample container, for the same reason. The contents of the sample containers are packed in the T-Ampoule with the support structure shown in Figures 2-67 and 2-68. The SC-2, shown in Figure 2-73, has the same basic geometry and mesh as the SC-1. The length of the sidewall has been lengthened by 1 in., and the mass of the

contents has been increased. The contents of the SC-2 are modeled using a 1.1 in. diameter X 1.1-in. long right circular cylinder, which has a mass of 338 g.

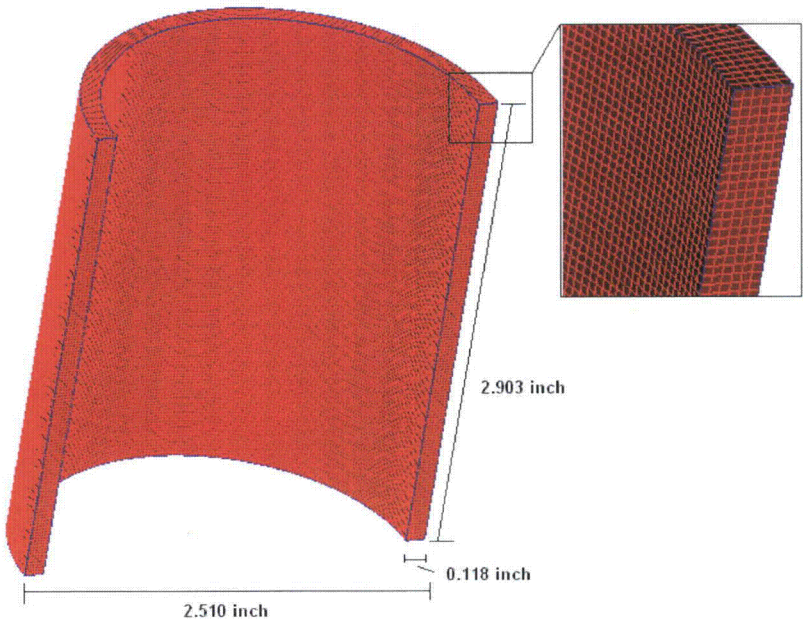


**Figure 2-70. 831-g Cylinder Finite Element Model**

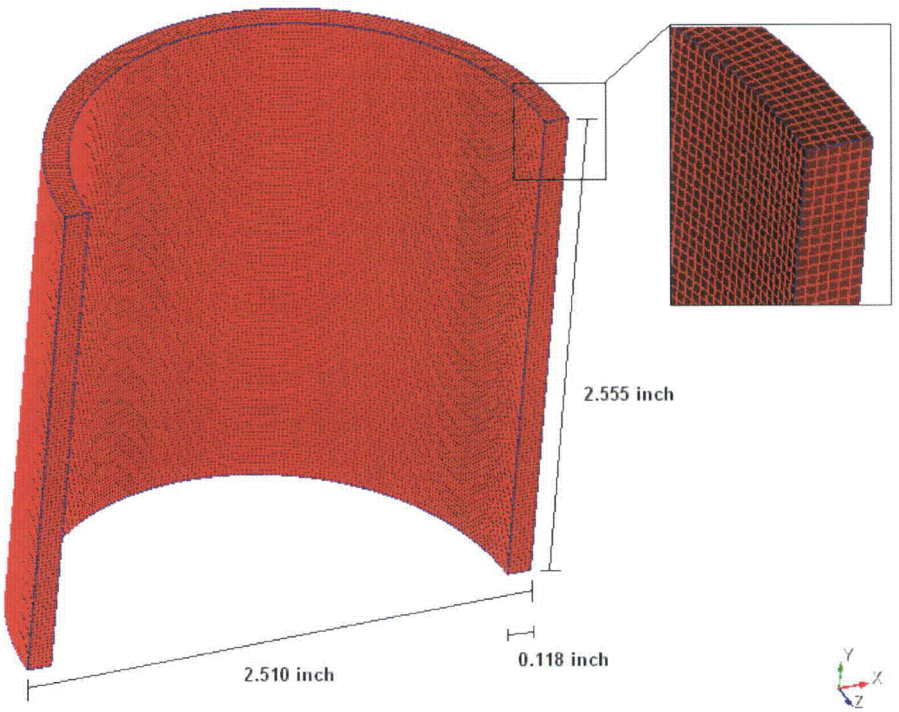


**Figure 2-71. 731-g Cylinder Finite Element Model**

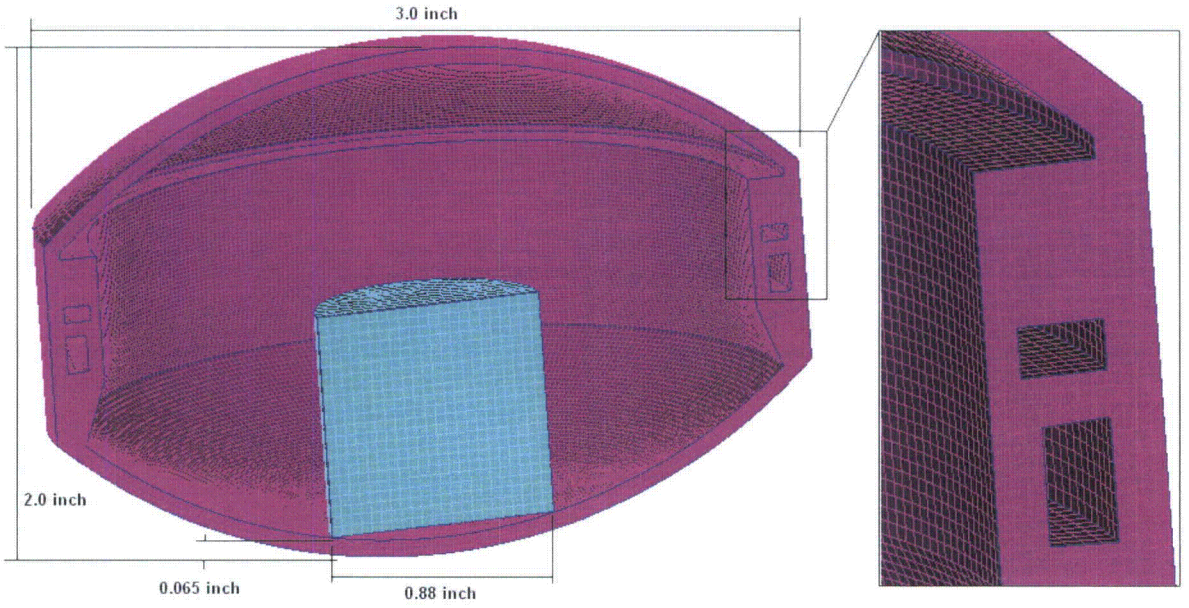


**Figure 2-72. Finite Element Model of SC-1 with Pu Cylinder Contents**

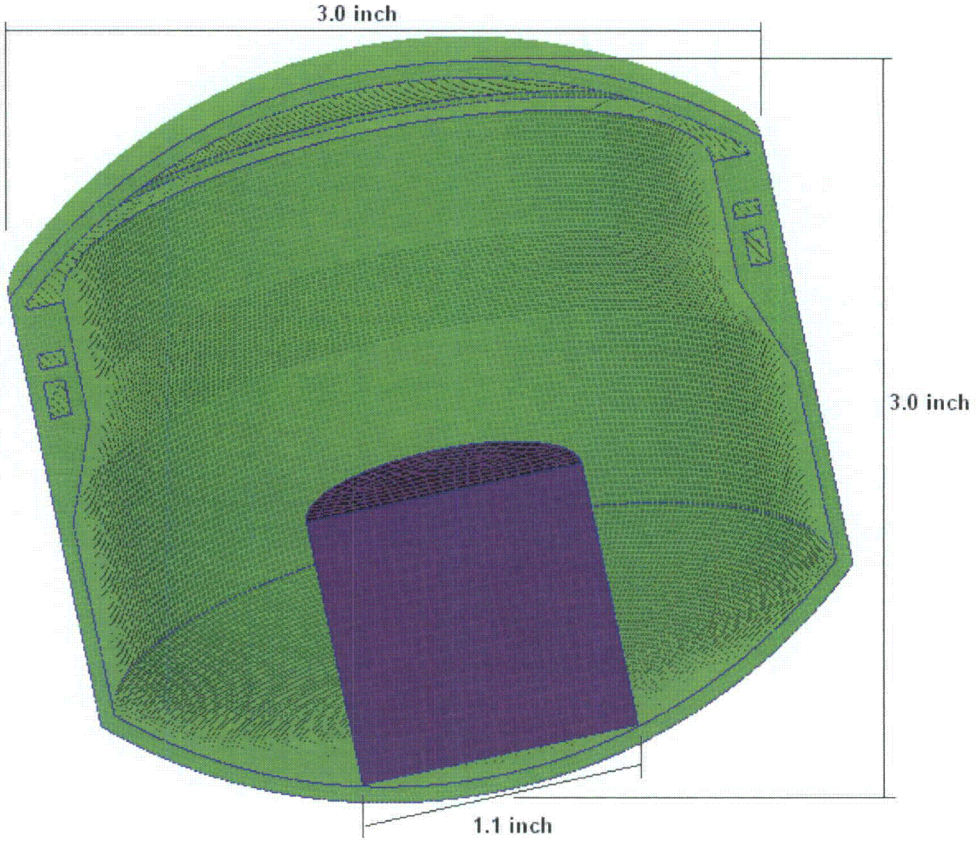


**Figure 2-73. Finite Element Model of SC-2 with Pu Cylinder Contents**

### *2.12.5.3 Normal Conditions of Transport Displacement Analyses*

The plutonium contents in the sample containers will be packaged in the T-Ampoule using the support structure shown in Figures 2-67 and 2-68. Under the NCT free drop, the support structure integrity must be assessed to assure the positioning of the sample containers for HAC and high-speed crash need not be adjusted. Therefore, the SC-1 and SC-2 were evaluated for 4-ft-drop end and side impacts. Under side impact, the model was oriented with the support structure at 0 and 45 degrees.

These analyses were completed for only the sample container components. The design of the support structure is meant to prevent the sample containers from shifting during normal operating conditions. If the Pu and Pu/Be-composite cylinders did shift to the outer edge of the T-Ampoule, and subsequently traveled across its entire width during an HAC or high speed impact, this would increase loads on the T-Ampoule and TB-1 vessel. Due to the thin walls and open shape of the hollow cylinder components which are extremely soft, the positioning of the plutonium metal hollow cylinders did not need restriction, and no support structure was designed to cradle the cylinders. The Ta foil packing material for the plutonium metal hollow cylinders and the sample container contents was conservatively neglected to allow for bounding higher net impact velocities between contents and T-Ampoule wall, and to conservatively omit any energy absorbing or load spreading from the packing material. In the high-speed impact analyses, the cylinders were positioned to allow for the maximum displacement (most conservative with the largest velocity difference between the cylinder and T-Ampoule at time of contact). The NCT analyses were performed to assure the positioning of the sample containers does not change after the 4-ft-drop. This was done by confirming the support structure does not undergo large plastic deformation throughout its thickness.

Three examples of the models created to determine the behavior of the support structure and sample containers when subjected to the NCT (10 CFR 71.71) performance tests are shown in Figures 2-74 through 2-76. Not shown are the SC-1 side impact at 45 degrees, the SC-2 side impact at 0 degrees, and the SC-2 end impact at 0 degrees, due to their similarity to the models shown. The support structure, sample containers, and plutonium are given an initial velocity of 192 in/sec, corresponding to the NCT regulatory condition. The models are half symmetry models, with the plane of symmetry passing through the center of the TB-1.

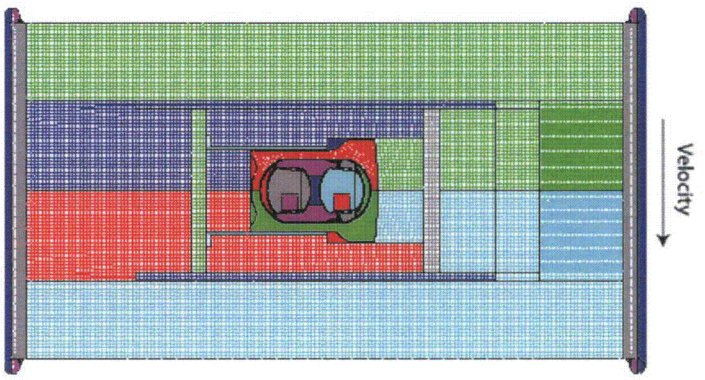


**Figure 2-74. NCT SC-2 Side Impact with Support Structure Rotated 45°**

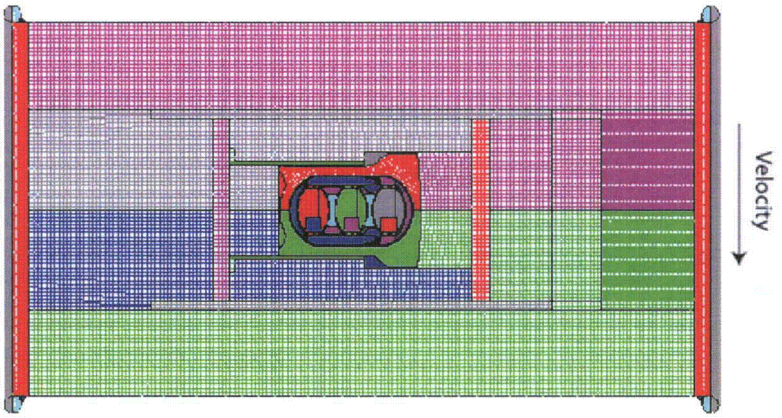


**Figure 2-75. NCT SC-1 Side Impact with Support Structure Rotated 0°**

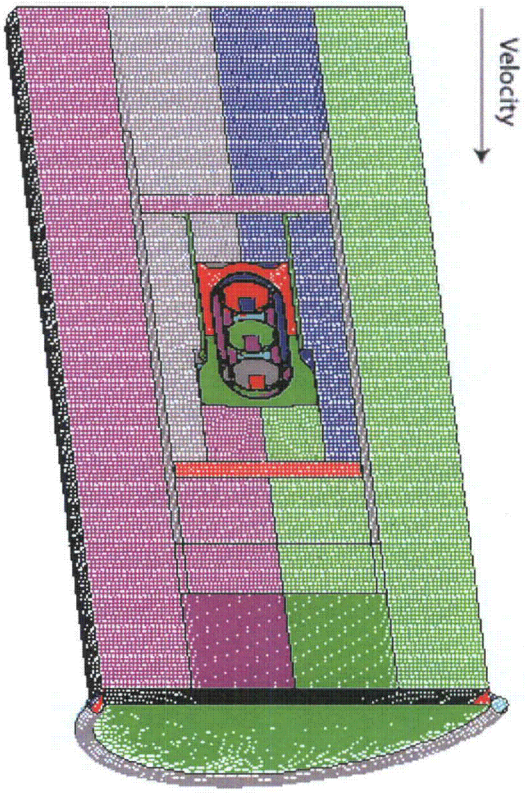


**Figure 2-76. NCT SC-1 End Impact with Support Structure Rotated 0°**

*2.12.5.3.1 NCT End Drop Analysis*

The models created for the 4-ft-drop end impact for the SC-1 and SC-2 at time 0 are shown in Figures 2-76 and 2-77, respectively. The post-4-ft-drop models are shown in Figures 2-78 and 2-79, although almost no discernable difference can be seen since the package overpack lid ring is only slightly dented. The kinetic energy histories for these two impacts are shown in Figures 2-80 and 2-81, indicating that sufficient analysis time transpired to capture the entire impact event, and the PAT-1 package actually bounced after impact. As shown in Figures 2-82 through 2-86 and Table 2-16, the minimal plasticity (less than 4%, and only in small localized areas of internal or external corners) observed in the titanium support structure, or cradle, verifies that the overall structure remained essentially elastic and the original position of the sample containers would remain unchanged.

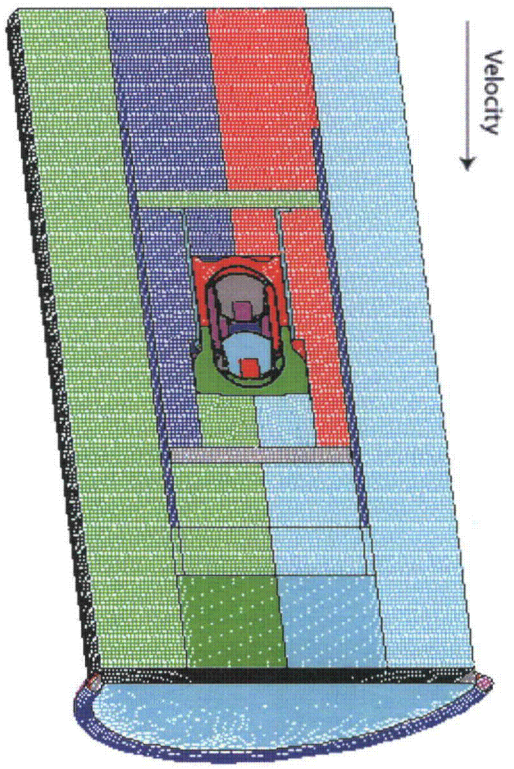


**Figure 2-77. NCT SC-2 End Impact with Support Structure Rotated 0°**

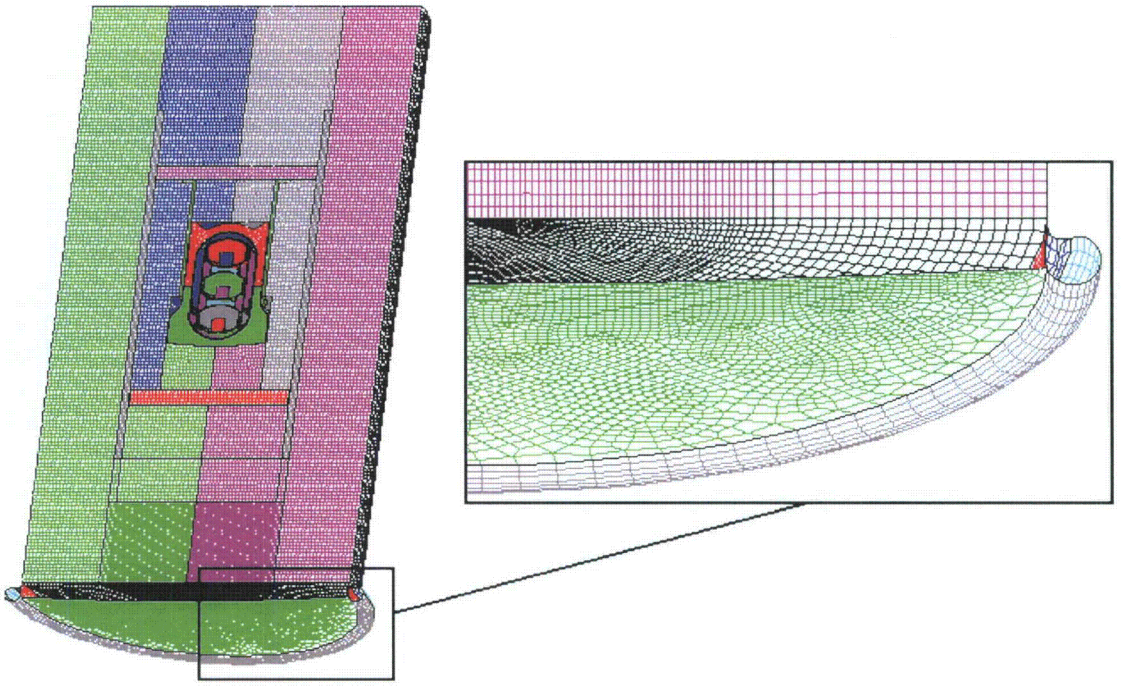

**Figure 2-78. NCT SC-1 End Impact with Support Structure Rotated 0° – Final Displacement**

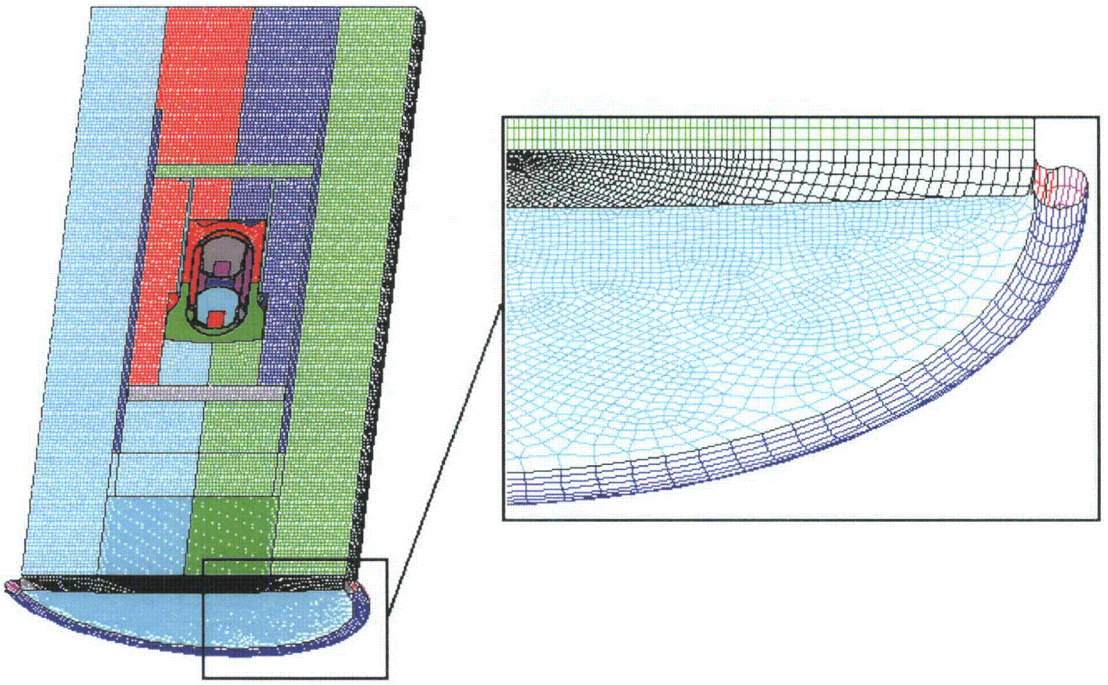

**Figure 2-79. NCT SC-2 End Impact with Support Structure Rotated 0° – Final Displacement**

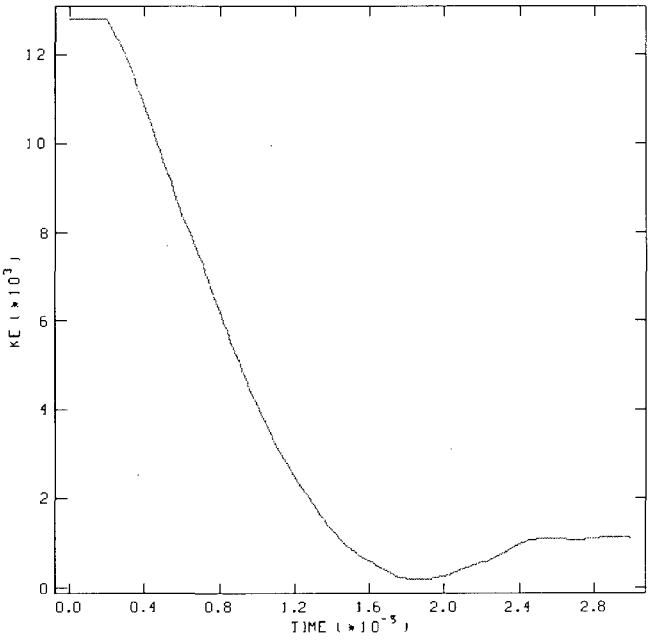


**Figure 2-80. NCT SC-1 End Impact with Support Structure Rotated 0° - Kinetic Energy Time History**

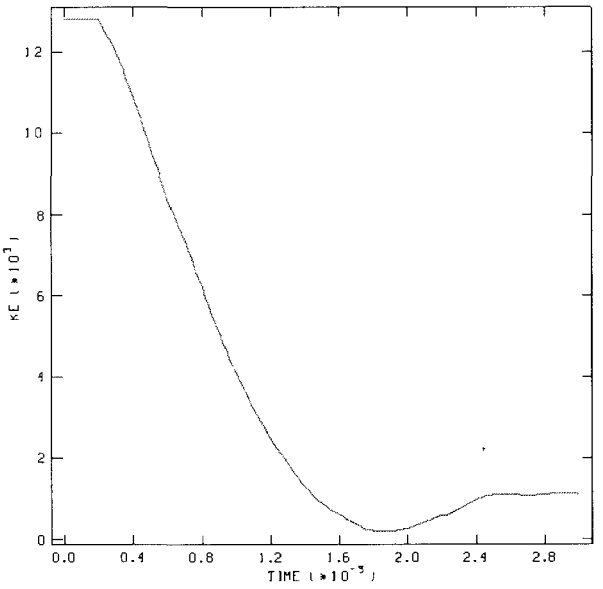


**Figure 2-81. NCT SC-2 End Impact with Support Structure Rotated 0° - Kinetic Energy Time History**

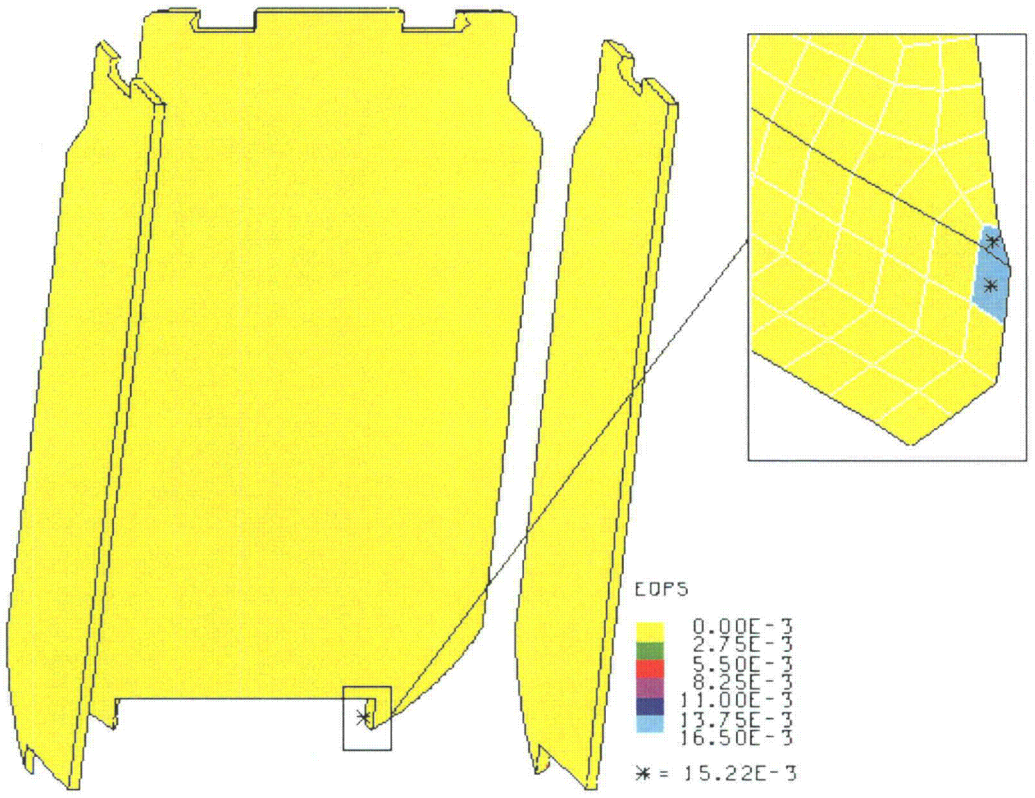


**Figure 2-82. NCT SC-1 End Impact with Support Structure Rotated 0° - EQPS in Bottom Legs**

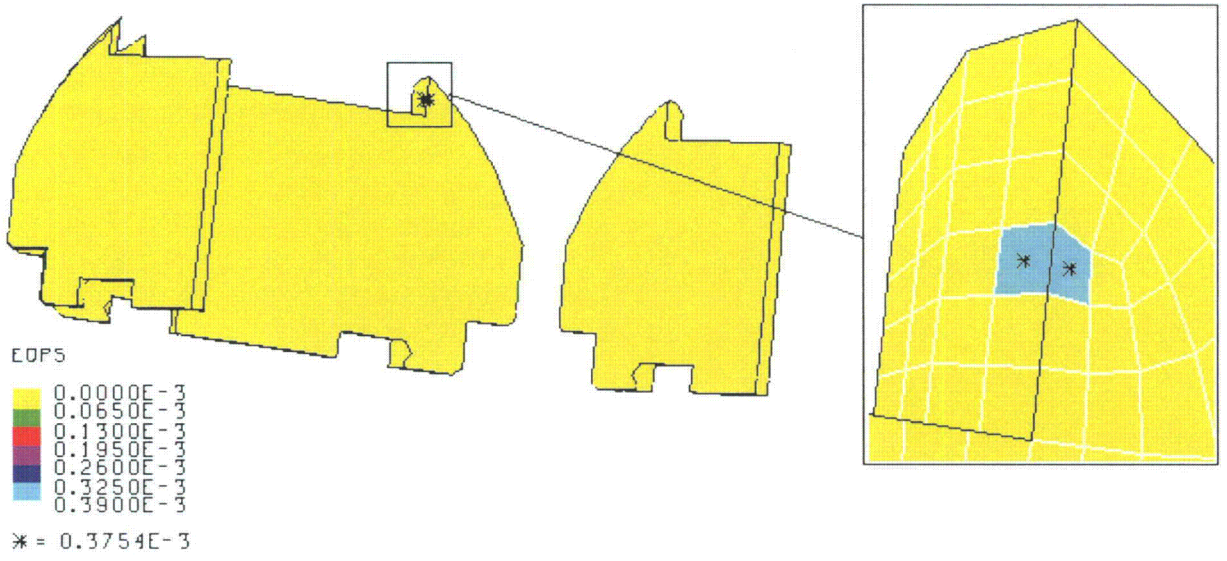


**Figure 2-83. NCT SC-1 End Impact with Support Structure Rotated 0° - EQPS in Top Legs**

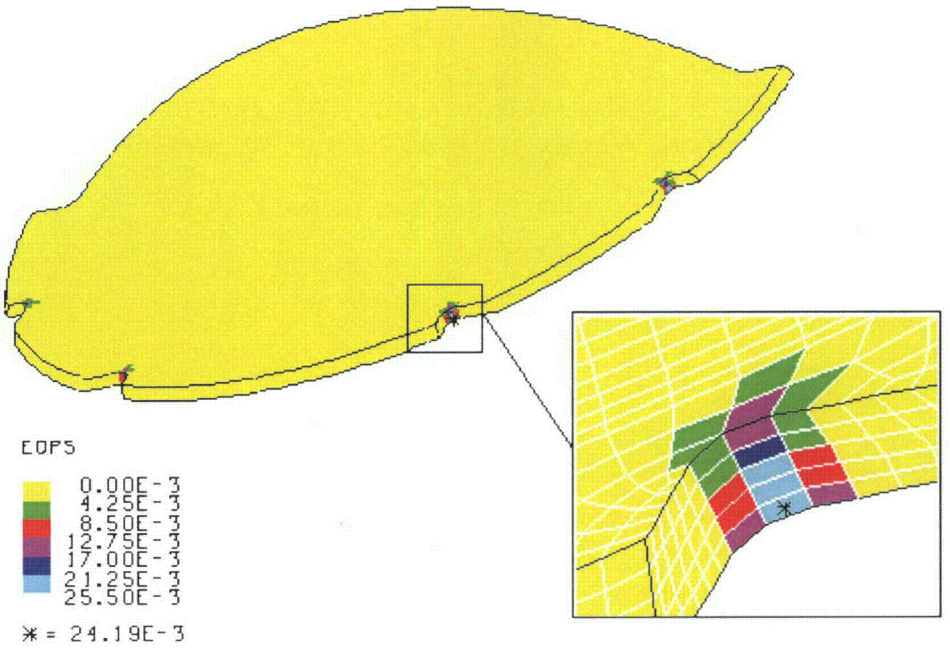


**Figure 2-84. NCT SC-1 End Impact with Support Structure Rotated 0° – EQPS in Top Dish**

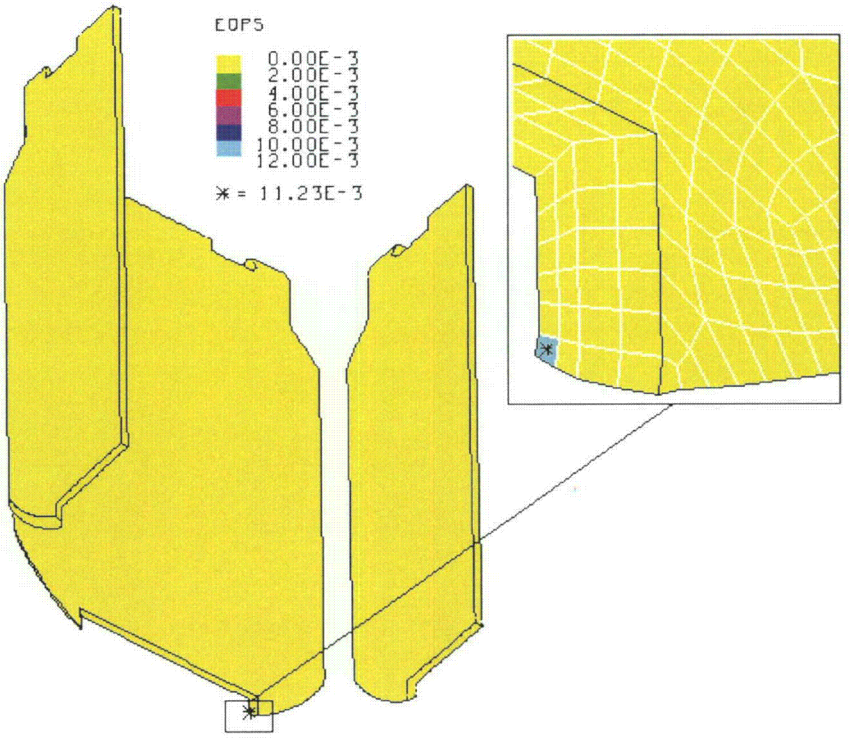


**Figure 2-85. NCT SC-2 End Impact with Support Structure Rotated 0° – EQPS in Bottom Legs**

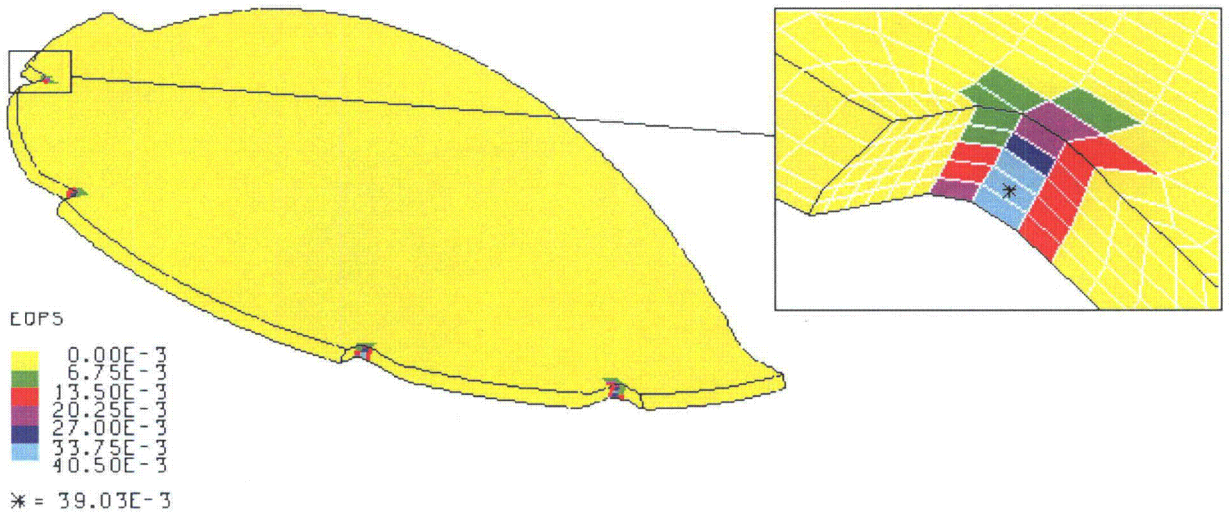


**Figure 2-86. NCT SC-2 End Impact with Support Structure Rotated 0° – EQPS in Top Dish**

**Table 2-16. Maximum Strains in 4 ft End Drop Models**

| Model/Part | EQPS |
|---|---|
| **SC-1 End Impact** | |
| Bottom Legs | 1.52e-2 |
| Upper Legs | 3.75e-4 |
| Upper Dish | 2.42e-2 |
| **SC-2 End Impact** | |
| Bottom Legs | 1.12e-2 |
| Upper Dish | 3.90e-2 |

*2.12.5.3.2 NCT Side Drop Analysis*

The models created for the 4-ft-drop side impact for the SC-1 AND SC-2 (0 and 45 degree rotated) at time 0 are shown in Figure 2-87 and Figure 2-88. The post-4-ft-drop models are shown in Figure 2-89 through Figure 2-92, and for these side impact cases more localized denting of the overpack lid rings is visible than for the end impact cases. The kinetic energy histories for these four impacts are shown in Figure 2-93 through Figure 2-96, indicating that sufficient analysis time transpired to capture the entire impact event, and the PAT-1 package actually bounced after impact. As shown in Figure 2-97 through Figure 2-105 and Table 2-17, the minimal plasticity (less than 7% and only in small localized areas of internal or external corners) observed in the titanium support structure, or inner cradle, verifies that the overall structure remained essentially elastic and the original position of the sample containers would remain unchanged. The zero plasticity post-drop condition of the T-Ampoule is shown in Figure 2-106, as well as zero plasticity in the TB-1 in Figure 2-107 and extremely low through-thickness stress intensities in Figure 2-108, below ASME limits shown in Table 2-4.

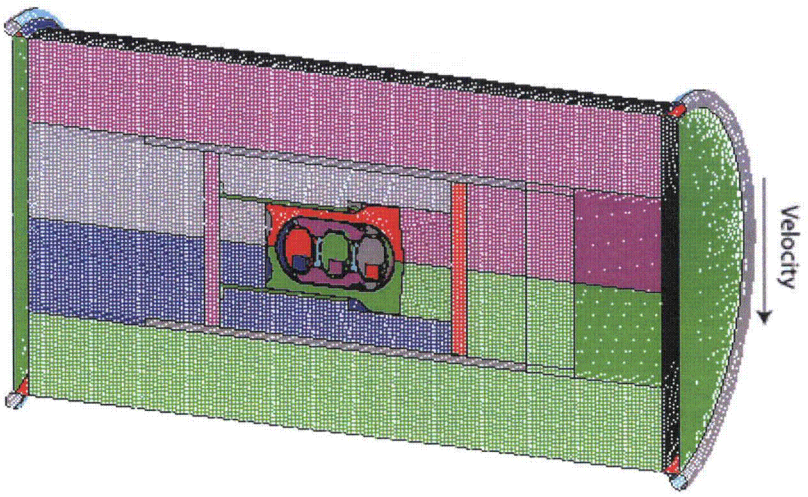


**Figure 2-87. NCT SC-1 Side Impact with Support Structure Rotated 45°**

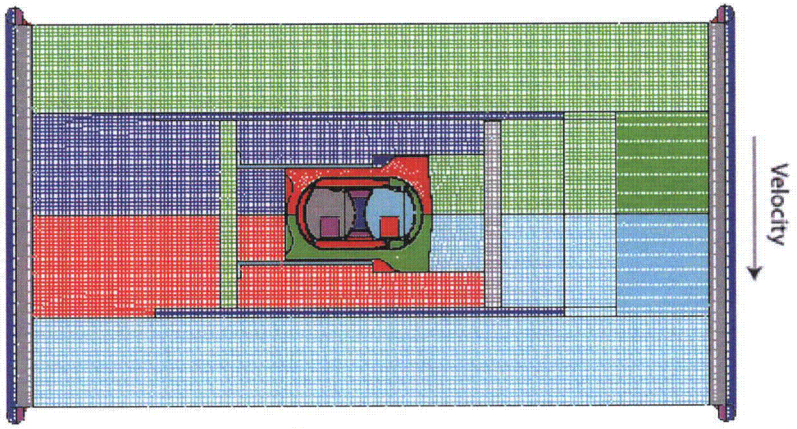


**Figure 2-88. NCT SC-2 Side Impact with Support Structure Rotated 0°**

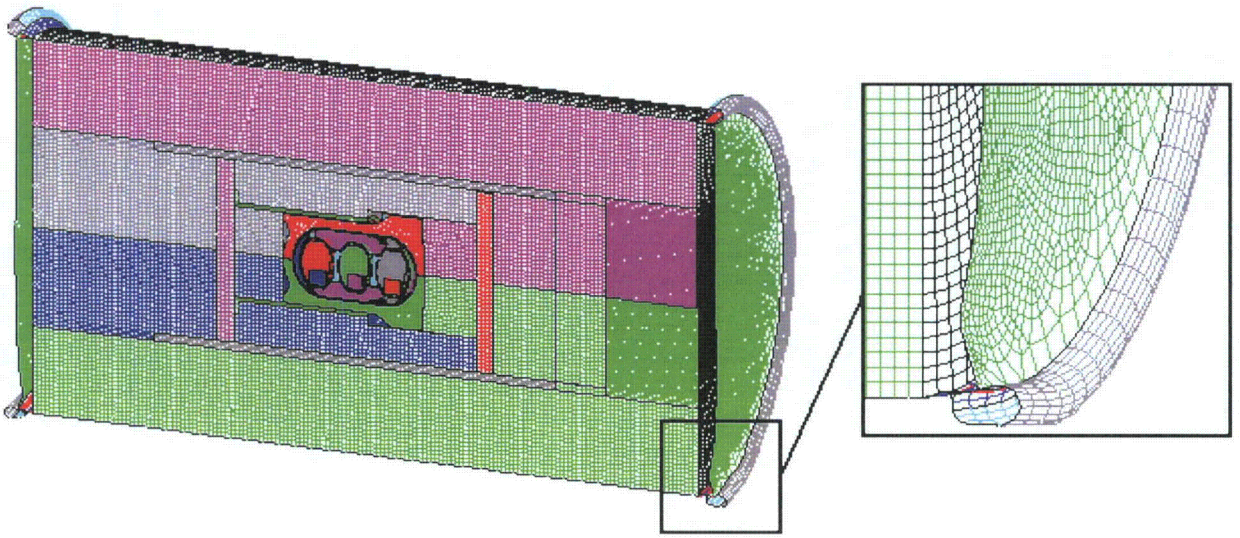

**Figure 2-89. NCT SC-1 Side Impact with Support Structure Rotated 45° – Final Displacement**

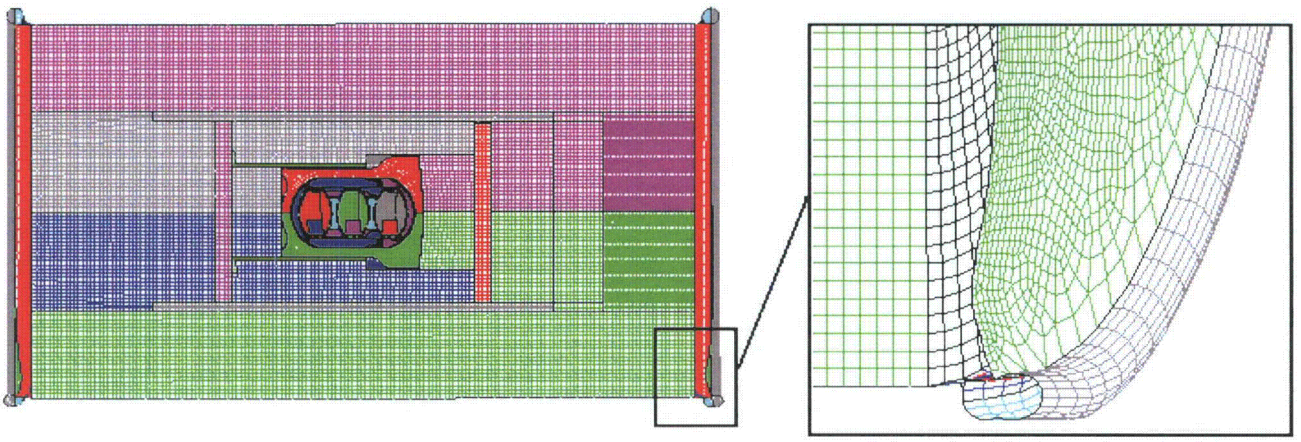

**Figure 2-90. NCT SC-1 Side Impact with Support Structure Rotated 0° – Final Displacement**

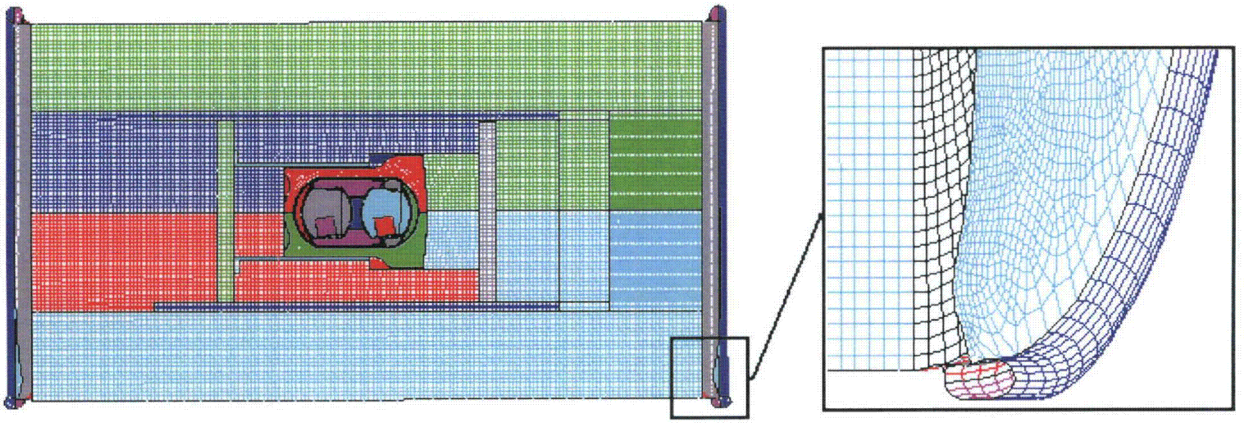

**Figure 2-91. NCT SC-2 Side Impact with Support Structure Rotated 45° – Final Displacement**

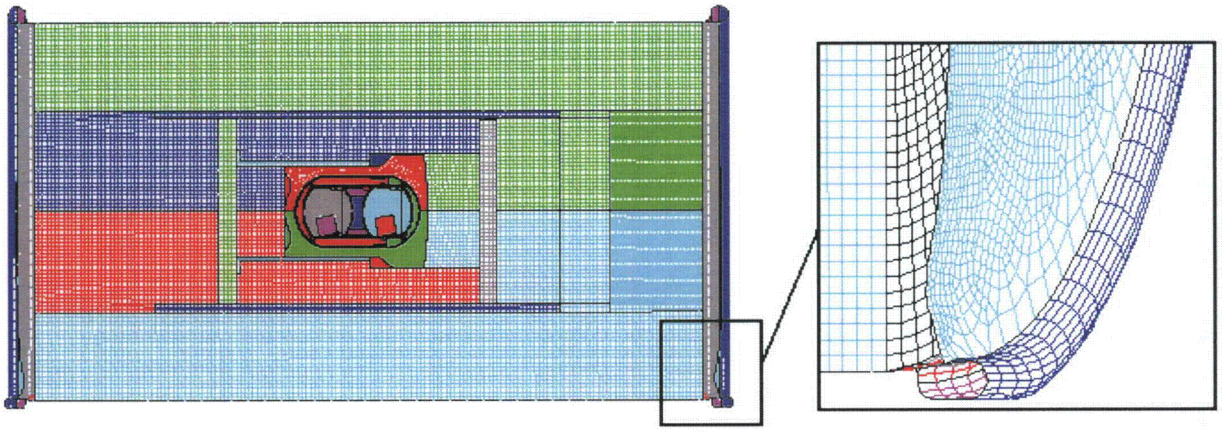

**Figure 2-92. NCT SC-2 Side Impact with Support Structure Rotated 0° - Final Displacement**

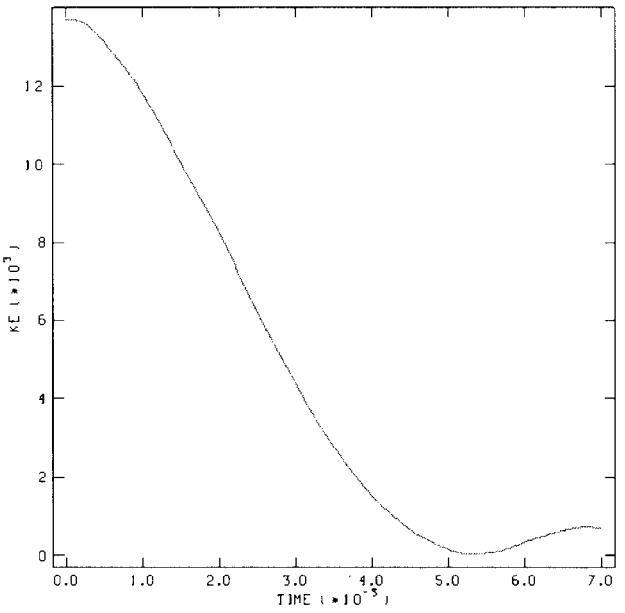


**Figure 2-93. NCT SC-1 Side Impact with Support Structure Rotated 45° - Kinetic Energy Time History**

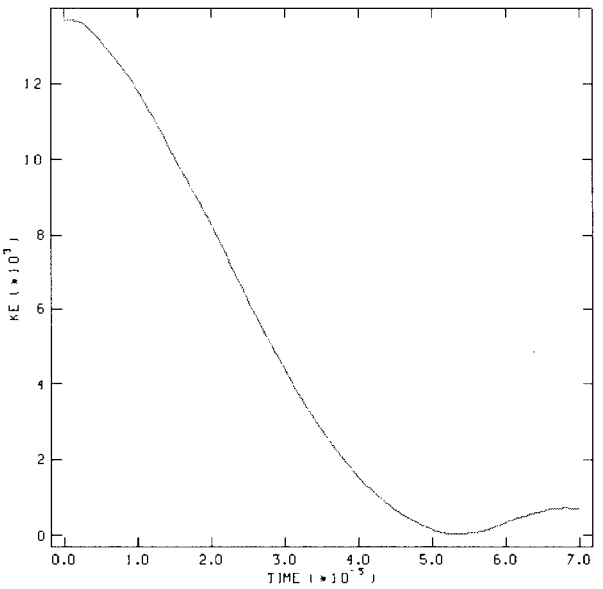


**Figure 2-94. NCT SC-2 Side Impact with Support Structure Rotated 45° - Kinetic Energy Time History**

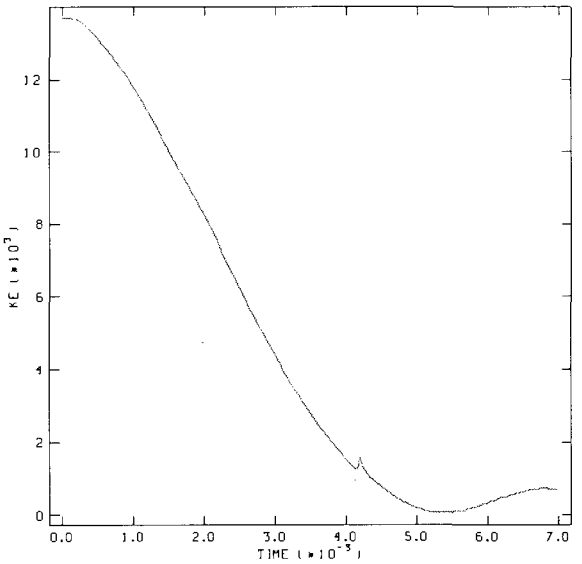


**Figure 2-95. NCT SC-1 Side Impact with Support Structure Rotated 0° – Kinetic Energy Time History**

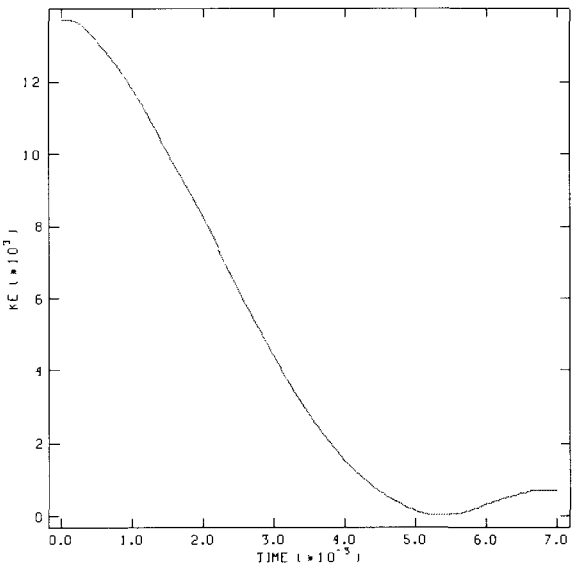


**Figure 2-96. NCT SC-2 Side Impact with Support Structure Rotated 0° – Kinetic Energy Time History**

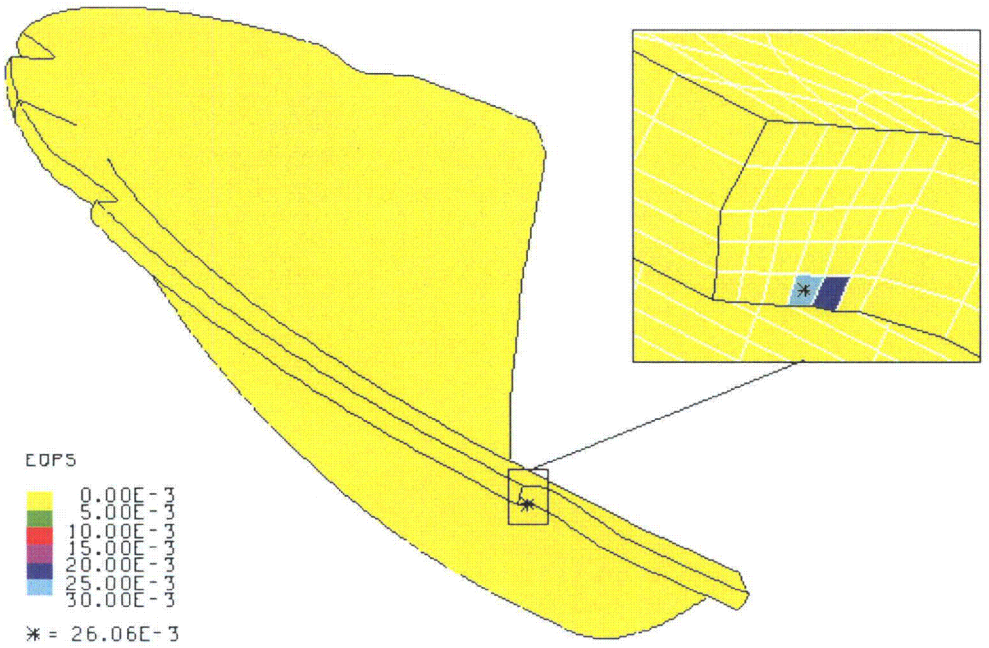


**Figure 2-97. NCT SC-1 Side Impact with Support Structure Rotated 45° – EQPS in Bottom Dish**

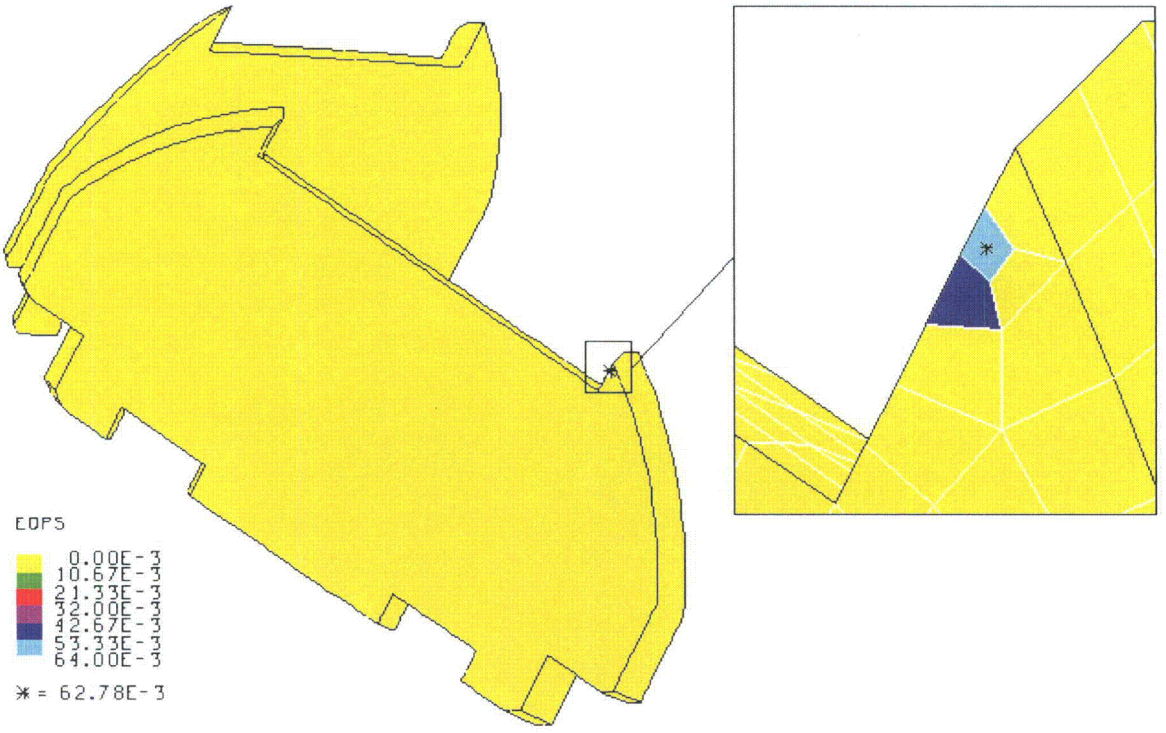


**Figure 2-98. NCT SC-1 Side Impact with Support Structure Rotated 45° – EQPS in Top Legs**

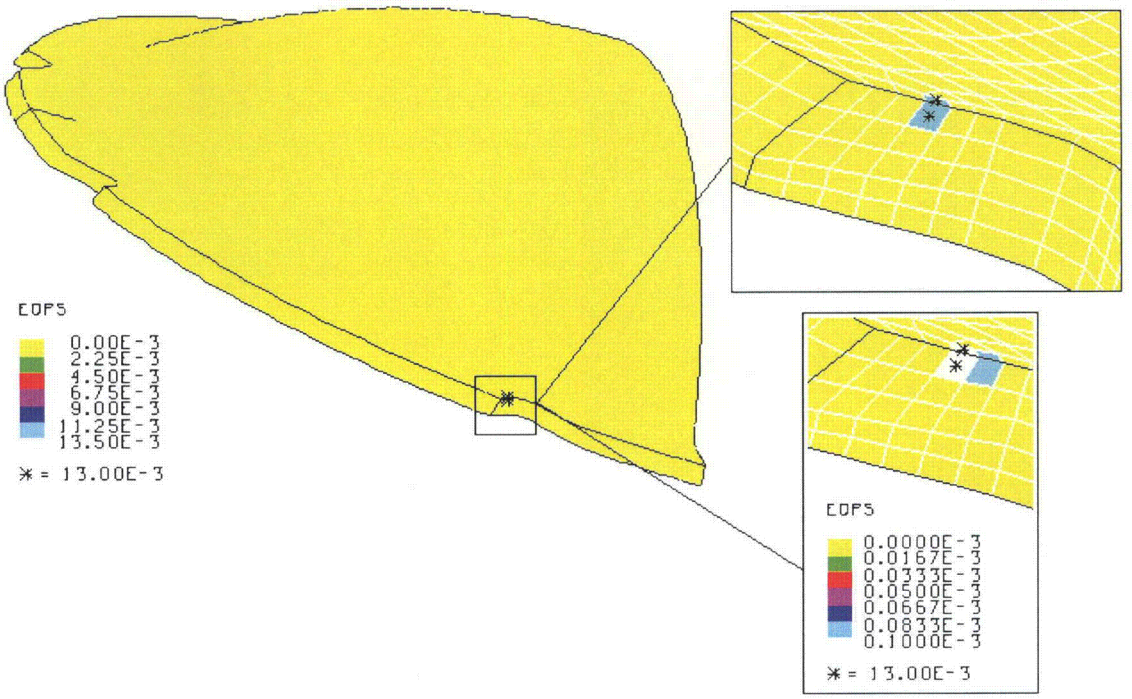


**Figure 2-99. NCT SC-1 Side Impact with Support Structure Rotated 45° – EQPS in Top Dish**

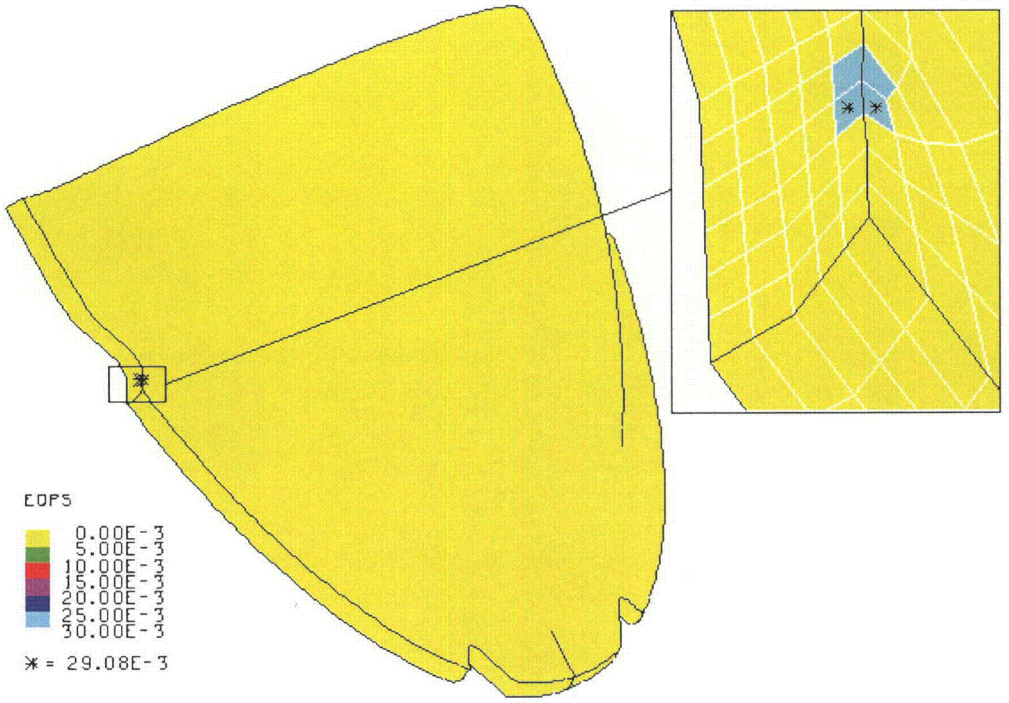


**Figure 2-100. NCT SC-2 Side Impact with Support Structure Rotated 45° – EQPS in Bottom Dish**

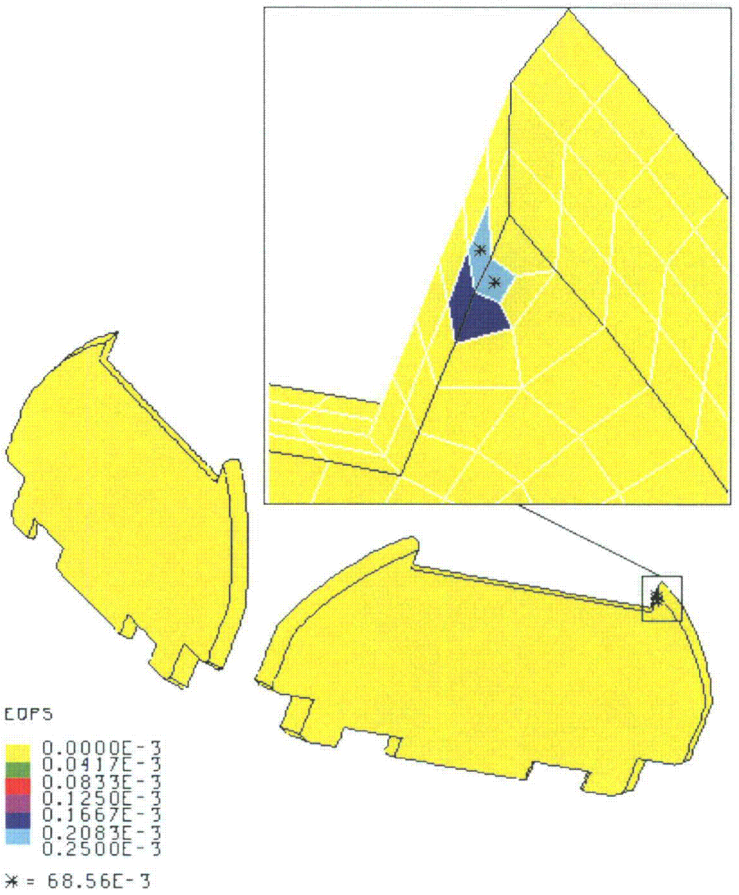


**Figure 2-101. NCT SC-2 Side Impact with Support Structure Rotated 45° – EQPS in Top Legs**

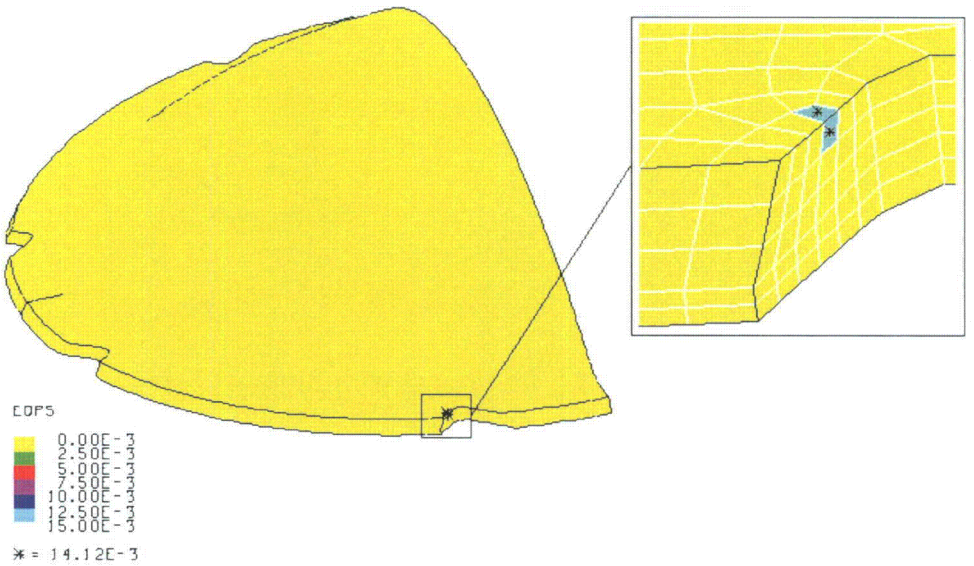


**Figure 2-102. NCT SC-2 Side Impact with Support Structure Rotated 45° – EQPS in Top Dish**

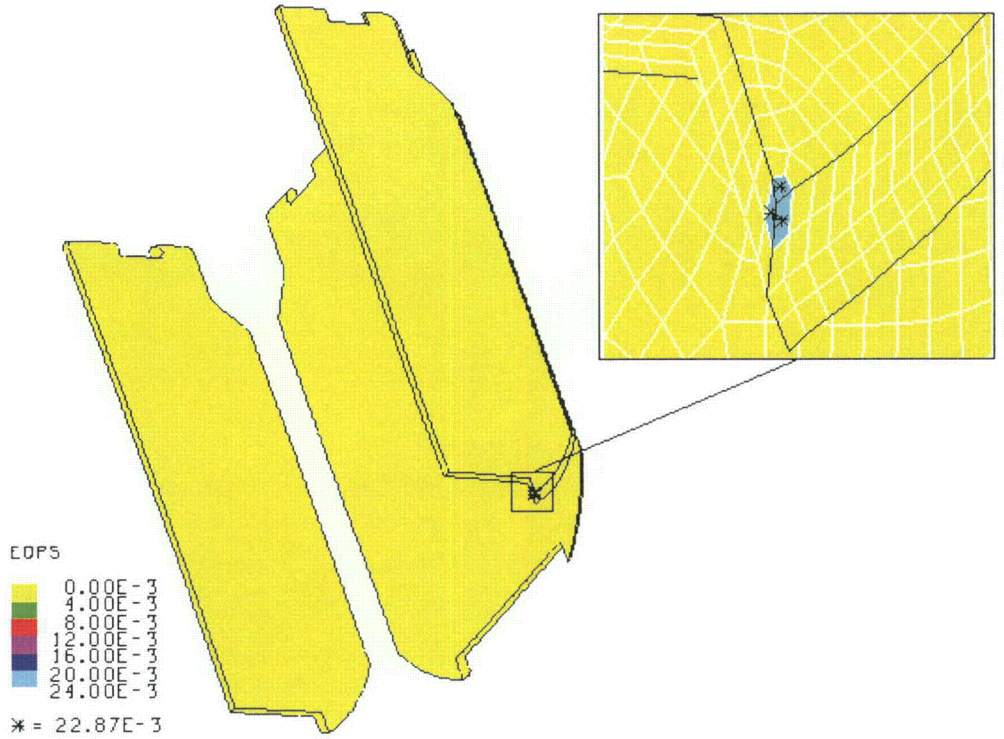


**Figure 2-103. NCT SC-1 Side Impact with Support Structure Rotated 0° – EQPS in Bottom Legs**

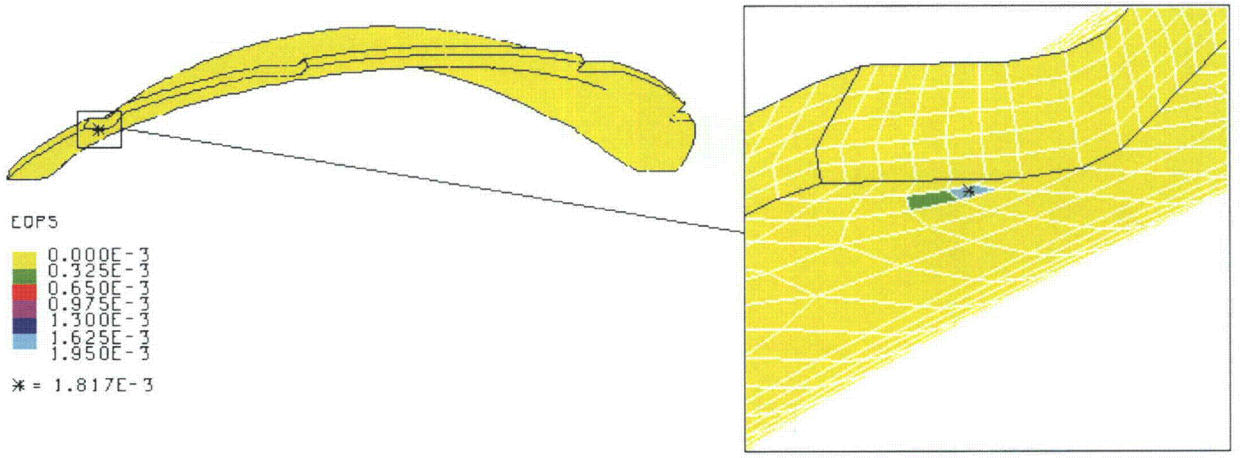


**Figure 2-104. NCT SC-1 Side Impact with Support Structure Rotated 0° – EQPS in Top Dish**

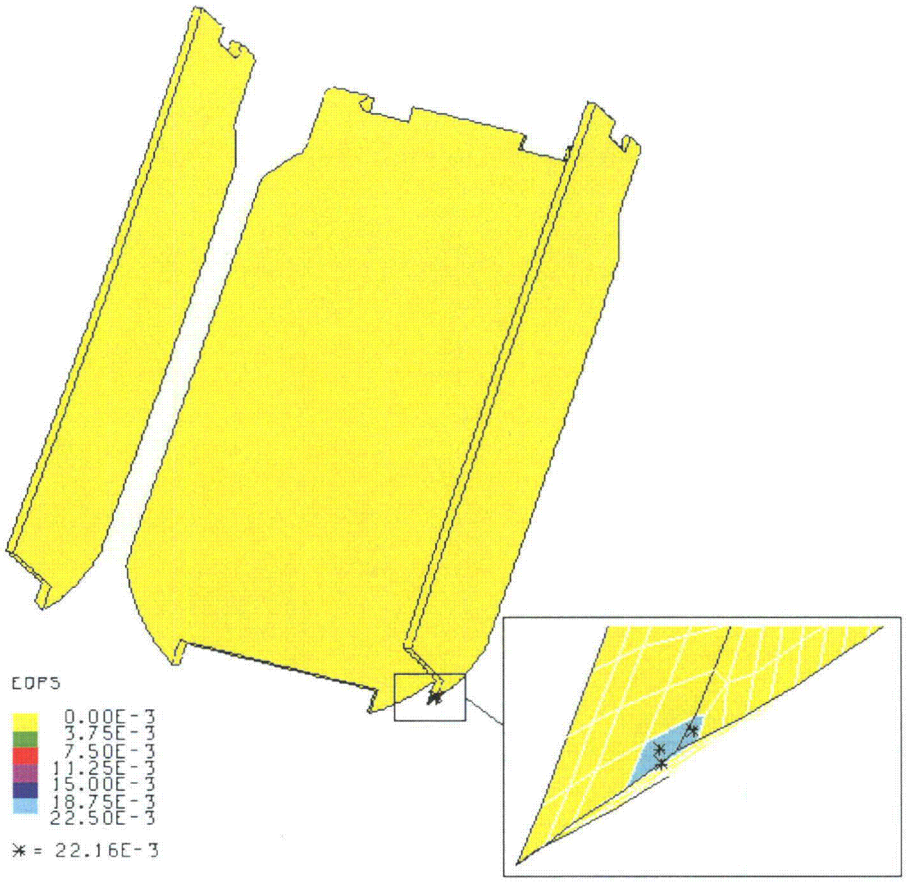


**Figure 2-105. NCT SC-2 Side Impact with Support Structure Rotated 0° – EQPS in Bottom Legs**

**Table 2-17. Maximum Strains in 4 ft Side Drop Models**

| Model/Part | EQPS |
|---|---|
| **SC-1 45° Side Impact** | |
| Bottom Dish | 2.61e-2 |
| Upper Legs | 6.28e-2 |
| Upper Dish | 1.30e-2 |
| **SC-2 45° Side Impact** | |
| Bottom Dish | 2.91e-2 |
| Upper Legs | 6.86e-2 |
| Upper Dish | 1.41e-2 |
| **SC-1 0° Side Impact** | |
| Bottom Legs | 2.29e-2 |
| Upper Dish | 1.82e-3 |
| **SC-2 0° Side Impact** | |
| Bottom Legs | 2.22e-2 |

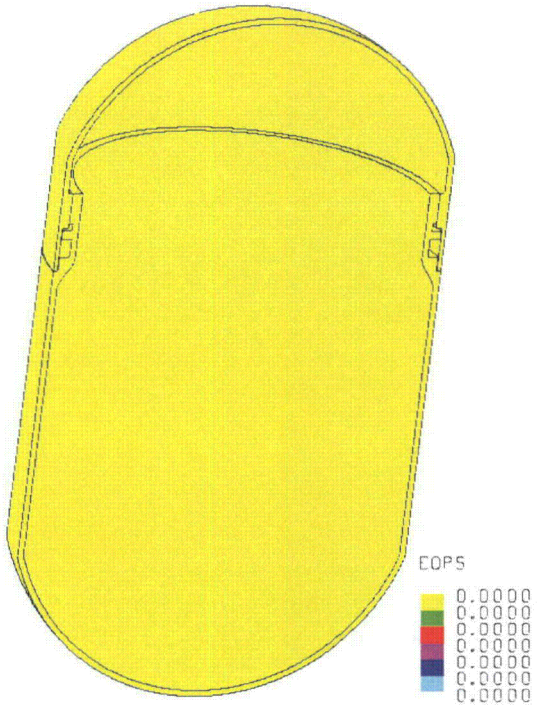


**Figure 2-106. NCT SC-2 Side Impact with Support Structure Rotated 45° - EQPS in T-Ampoule**

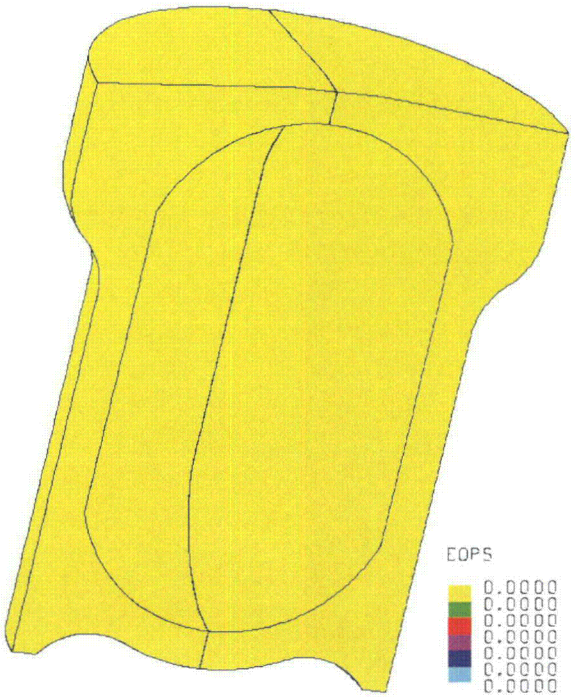


**Figure 2-107. NCT SC-2 Side Impact with Support Structure Rotated 45° - EQPS in TB-1**

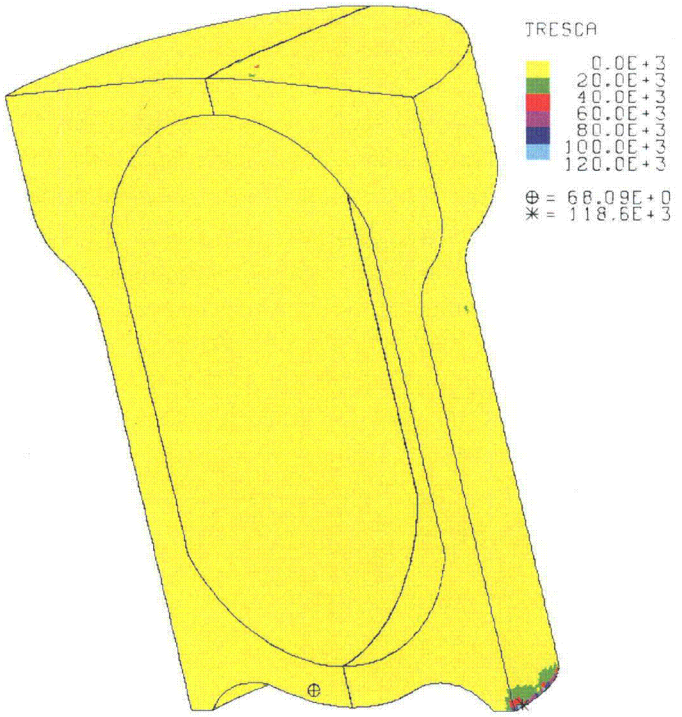


**Figure 2-108. NCT SC-2 Side Impact with Support Structure Rotated 45° - Tresca Stress in TB-1**

*2.12.5.3.1 NCT End and Side Drop Analysis Summary*

The two previous sections highlight the fact that the position of the contents within their sample containers and support cradle is essentially unchanged after 4-ft NCT drops. The titanium Inner Cradle remains essentially undeformed and the contents' positions no farther from the T-Ampoule than pre-drop, as well as no plasticity in the TB-1 and the T-Ampoule, all means that HAC and aircraft impact analyses are justified in assuming an undamaged PAT-1 package and contents before those events.

### *2.12.5.4 Aircraft Accident Impact Analyses*

Detailed PAT-1 package models identical to those shown in the previous NCT section, except for neglecting the rolled ring lid ends, were analyzed to determine the response of the T-Ampoule and TB-1 when subjected to the loading of 10 CFR 71.74 (accident conditions for air transport of plutonium). Each combination of package orientation (lid end, side, and CG-over-corner) and contents was analyzed at an initial velocity of 422 ft/sec and each package impacts onto an analytically unyielding target.

The TB-1 was shown in the SAR[1] aircraft impact tests to remain elastic and maintain containment. With similar mass contents, similar TB-1 response would be expected, excepting the possibility of minor localized denting due to more dense contents (solid Pu vs. oxide powder). Effective or von Mises stresses (which capture three-dimensional stress states well and is more conservative than Tresca stress to show avoidance of yielding) were calculated and an acceptance criterion of "below through-thickness yielding" used to demonstrate similar TB-1

behavior as in the original regulatory testing. This also means zero plasticity in the seal area of the TB-1, ensuring similar containment requirements performance of the containment vessel.

A total of twenty-seven high speed impact analyses were conducted for the five potential contents in various orientations; the analyses are listed below in Table 2-18. In the hollow-cylinder (ER cylinder) component models, as well as the sample container models, no credit is taken for the positioning of the cylinders with the tantalum packing foil. Each form contents are assumed to be unconstrained and are placed in the worst orientation and most severe location for each impact. The delta-plutonium in the sample containers is relatively soft and has a greater degree of plasticity, so although its location will affect T-Ampoule loading, its local orientation would not. However, the beryllium composite cylinders are much harder and stronger, so their orientation is always rotated such that they present a sharp corner (CGOC, actually) towards the normal surface of the T-Ampoule, parallel with the impact direction.

**Table 2-18. Aircraft Accident Impact Analyses, Components, and Orientations**

| Run No. | Component | Submodel Orientation |
|---|---|---|
| 1 | 831 g Plutonium Metal Hollow Cylinder, alpha Pu | Bottom position, top impact |
| 2 | 831 g Plutonium Metal Hollow Cylinder, alpha Pu | Bottom position (angled), top impact |
| 3 | 831 g Plutonium Metal Hollow Cylinder, alpha Pu | Bottom position (angled), CGOC impact |
| 4 | 831 g Plutonium Metal Hollow Cylinder, alpha Pu | Far side position, side impact |
| 5 | 831 g Plutonium Metal Hollow Cylinder, alpha Pu | Far side position (angled), side impact |
| 6 | 731 g Plutonium Metal Hollow Cylinder, alpha Pu | Bottom position, top impact |
| 7 | 731 g Plutonium Metal Hollow Cylinder, alpha Pu | Bottom position (angled), top impact |
| 8 | 731 g Plutonium Metal Hollow Cylinder, alpha Pu | Bottom position (angled), CGOC impact |
| 9 | 731 g Plutonium Metal Hollow Cylinder, alpha Pu | Far side position, side impact |
| 10 | 731 g Plutonium Metal Hollow Cylinder, alpha Pu | Far side position (angled), side impact |
| 11 | SC-1 – Pu | Bottom position, support structure 0°, top impact |
| 12 | SC-1 – Pu | Far side position, support structure 0°,side impact |
| 13 | SC-1 – Pu | Far side position, support structure 45°, side impact |
| 14 | SC-1 – Pu | Bottom position, support structure 0°, CGOC impact |
| 15 | SC-1 – Pu | Bottom position, support structure 45°, CGOC impact |

**Table 2-18. Aircraft Accident Impact Analyses, Components, and Orientations (Continued)**

| Run No. | Component | Submodel Orientation |
|---|---|---|
| 16 | SC-2 – Pu | Bottom position, support structure 0°, top impact |
| 17 | SC-2 – Pu | Far side position, support structure 0°,side impact |
| 18 | SC-2 – Pu | Far side position, support structure 45°, side impact |
| 19 | SC-2 – Pu | Bottom position, support structure 0°, CGOC impact |
| 20 | SC-2 – Pu | Bottom position, support structure 45°, CGOC impact |
| 21 | SC-1 – Be | Bottom position, angled Be, support structure 0°, top impact |
| 22 | SC-1 – Be | Far side position, angled Be, support structure 0°, side impact |
| 23 | SC-1 – Be | Far side position, angled Be, support structure 45°, side impact |
| 24 | SC-1 – Be | Bottom position, angled Be, support structure 0°, CGOC impact |
| 25 | SC-1 – Be | Bottom position, angled Be, support structure 45°, CGOC impact |
| 26 | SC-2 – Pu | Far side position, support structure 45°, side impact, friction 0.4 |
| 27 | SC-2 – Pu | Far side position, support structure 45°, side impact, friction 0.2 |

*2.12.5.4.1 ER Cylinder Analyses*

Ten separate plutonium metal hollow cylinder, high-speed impact analyses were conducted. There are several inherent conservatisms in this model:

1. The tantalum foil used to package the plutonium metal hollow cylinders inside the T-Ampoule is not modeled. The small quantity of energy it would absorb, and load spreading it would provide, is conservatively ignored. In addition, any initial positioning that would be provided by the foil is also ignored. Each analysis is run with the plutonium metal hollow cylinder in a location farthest from the impact surface.

2. The Pu material is modeled using a power-law hardening constitutive model without fracture. Hecker and Stevens[3] present two curves for alpha-plutonium; one curve depicts a very brittle material, and the other represents a finer-grain material with more ductility. To maximize the energy and impulse load applied to the T-Ampoule wall, the plutonium metal was modeled as a continuously hardening material that does not fracture, which is extremely conservative in terms of the reaction loading of the T-Ampoule. This conservatism (stronger alpha material, continuously hardening) allows for the possibility that the cylinder could also consist of delta Pu, if transport of that material were desired instead.

3. The dimensions of the plutonium metal hollow cylinders are conservatively assumed to be the "strongest" possible. Within the bounds of LANL-defined tolerances of machining these cylinders, they are the most resistant to buckling (shortest, thickest wall,

maximum OD and minimum ID, see Figures 2-70and 2-71), which allows for the greatest loading of the T-Ampoule.

*2.12.5.4.2 Run 1 - 831-g Plutonium Metal Hollow Cylinder with Bottom Initial Location and a Top Impact*

The top end impact model for the plutonium metal hollow cylinder, oriented axially (with the impact direction, as opposed to angled) is shown in Figure 2-109. Note that the cylinder is located at the bottom of the T-Ampoule so that its net impact velocity with the top of the T-Ampoule is maximized. The post-impact deformation is shown in Figure 2-110 and its kinetic energy history in Figure 2-111. Note the similar degree of overpack crush up as compared to the certification test end impact analysis in Figure 2-12, despite the slightly reduced impact velocity of 422 ft/sec versus the tested 445 ft/sec. The plutonium metal hollow cylinder exhibits significant buckling, despite its conservatively "strongest shape" definition.

Equivalent Plastic Strain (EQPS) in the TB-1 vessel is shown in Figures 2-112 and 2-113 to be less than 2.3%, and only in some localized outer contact regions with the redwood overpack. This localized ring of plasticity in the top outer surface of the TB-1 lid is due to a minor contact over closure between the TB-1 and the redwood; it is only a minor modeling artifact. This minor modeling artifact is not a concern because even though it produces elevated localized stresses and even miniscule plasticity, it does not increase through-thickness stresses or in any way negatively affect the integrity of the containment vessel. The von Mises stresses (see Figures 2-114 and 2-115) peak at 147.5 ksi, just above the elevated-temperature minimum yield strength for the TB-1 of 141 ksi, but more importantly, through-thickness TB-1 stress values are in the less-than-50 ksi range, below yield. The time at which the peak value of the von Mises stress occurs coincides with the peak value of the contact force (summed over the lid area). A plot of this force as a function of time is shown in Figure 2-116. A maximum contact load of 66,000 lbs is applied to the inner surface of the TB-1 lid during the impact, which is below the 108,000 lb preload in the bolts. No T-Ampoule elements exceeded the tested B-W strain locus, and the peak Tearing Parameter value (see Table 2-11, High Velocity (Aircraft) Impact Analyses Peak Tearing Parameter Values, run #1) of 0.0528 was below the critical Tearing Parameter value of 1.012 for Ti-6Al-4V.

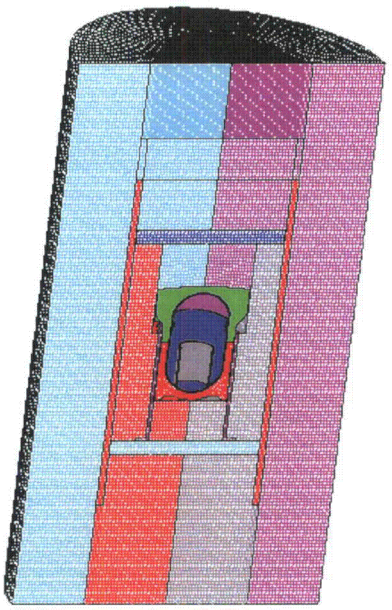

**Figure 2-109. Finite Element Mesh for the 831-g, Plutonium Metal Hollow Cylinder, Bottom Position, End Impact**

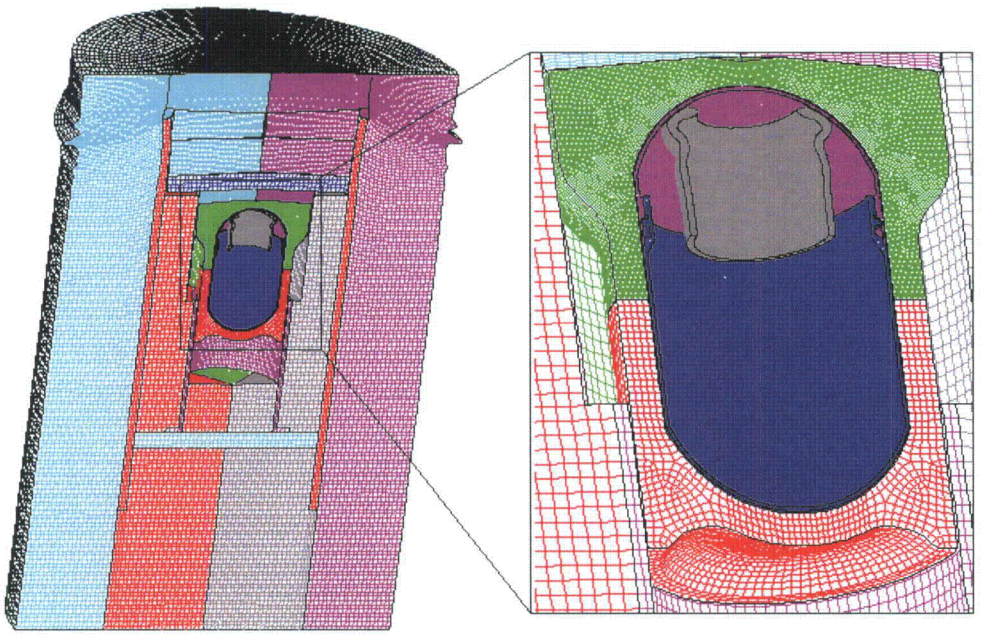

**Figure 2-110. Finite Element Mesh for the 831-g, Plutonium Metal Hollow Cylinder, Bottom Position, End Impact – Final Displacement**

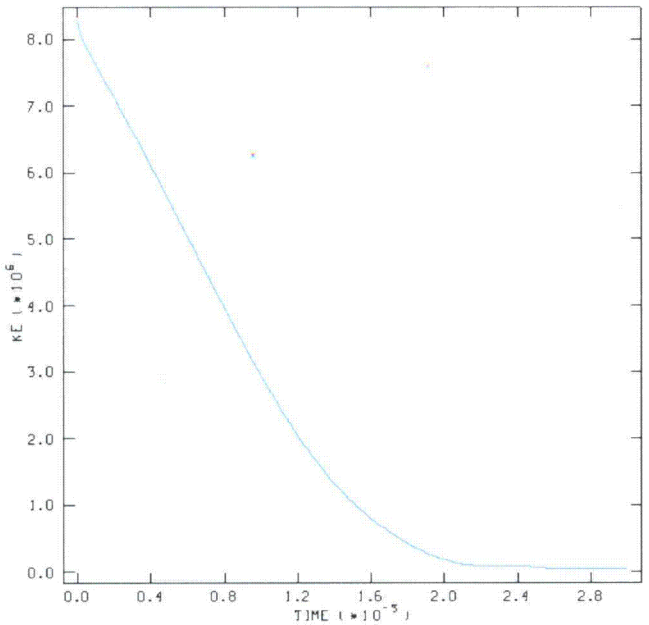


**Figure 2-111. Kinetic Energy Time History for the 831-g, ER Cylinder, Bottom Position, End Impact**

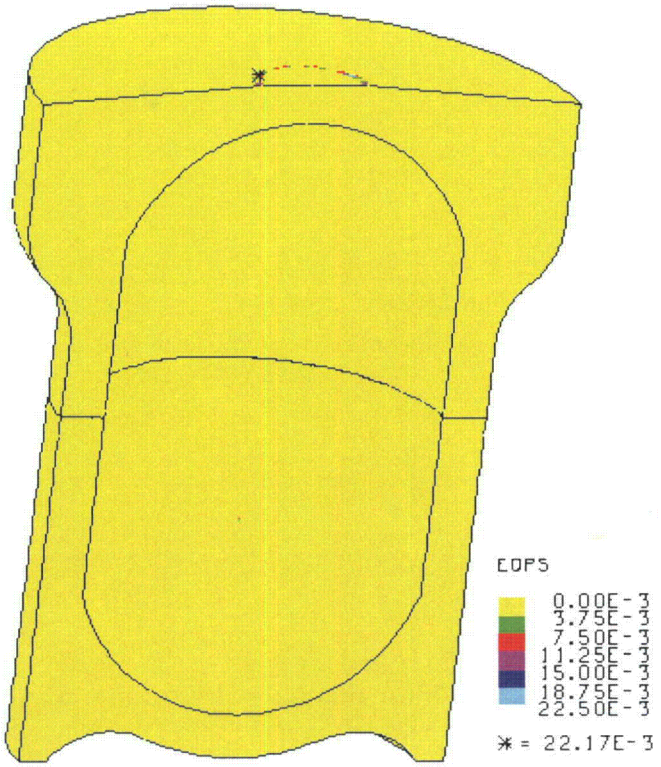


**Figure 2-112. EQPS in the TB-1 for the 831-g, ER Cylinder, Bottom Position, End Impact**

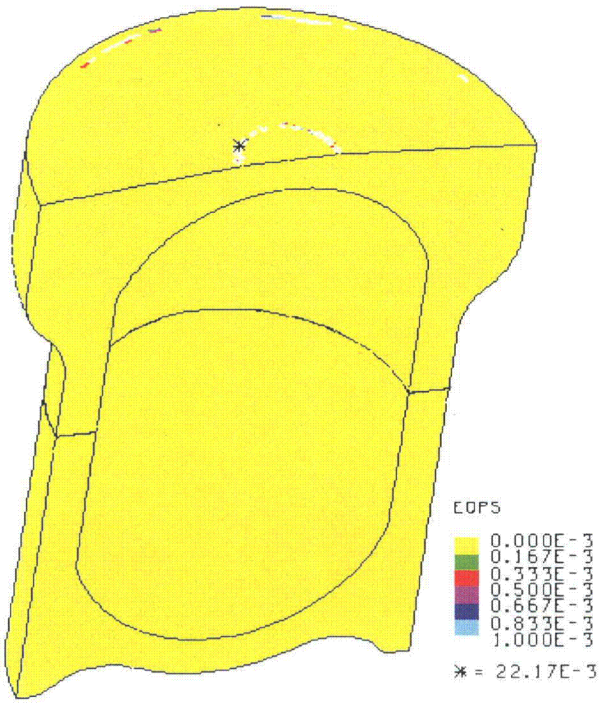


**Figure 2-113. EQPS in TB-1 (Range Zoomed in to Show All Elements with non-zero EQPS) for the 831-g, Hollow Cylinder, Bottom Position, End Impact**

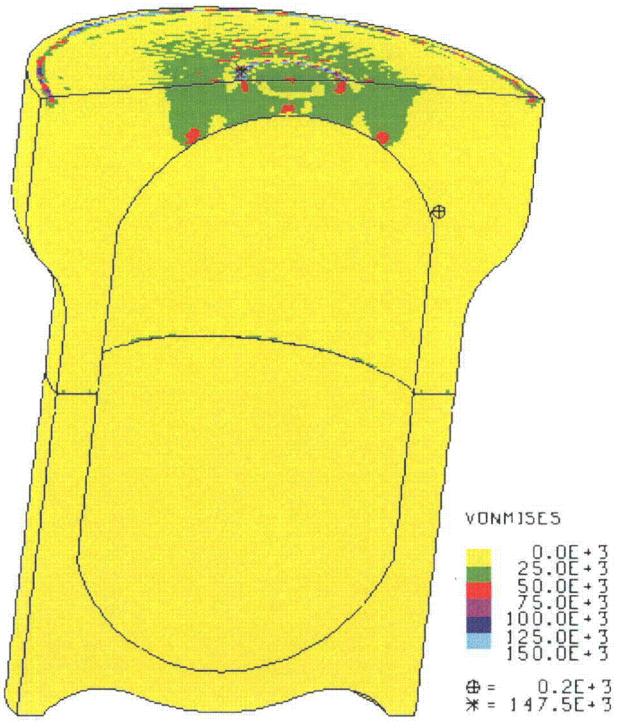


**Figure 2-114. von Mises Stress in the TB-1 for the 831-g Plutonium Metal Hollow Cylinder, Bottom Position, End Impact (Rotated Forward for Ease of Viewing)**

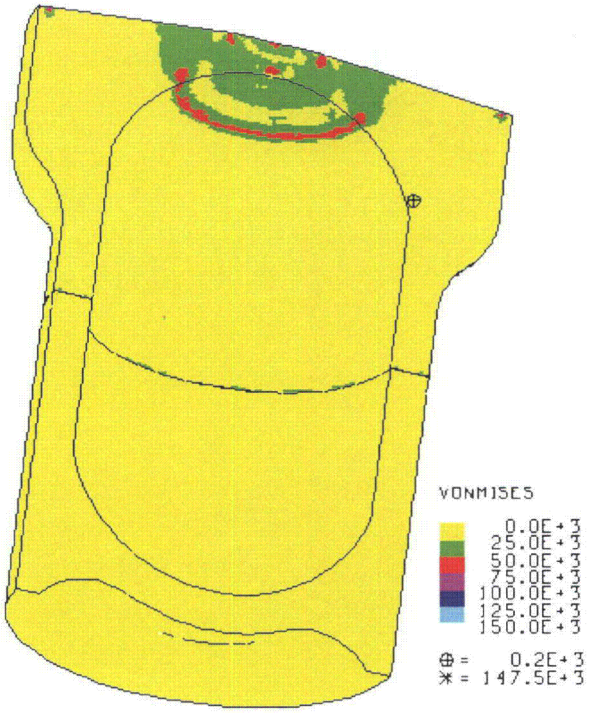


**Figure 2-115. von Mises Stress in the TB-1 for the 831-g, Plutonium Metal Hollow Cylinder, Bottom Position, End Impact (Rotated Backward for Ease of Viewing)**

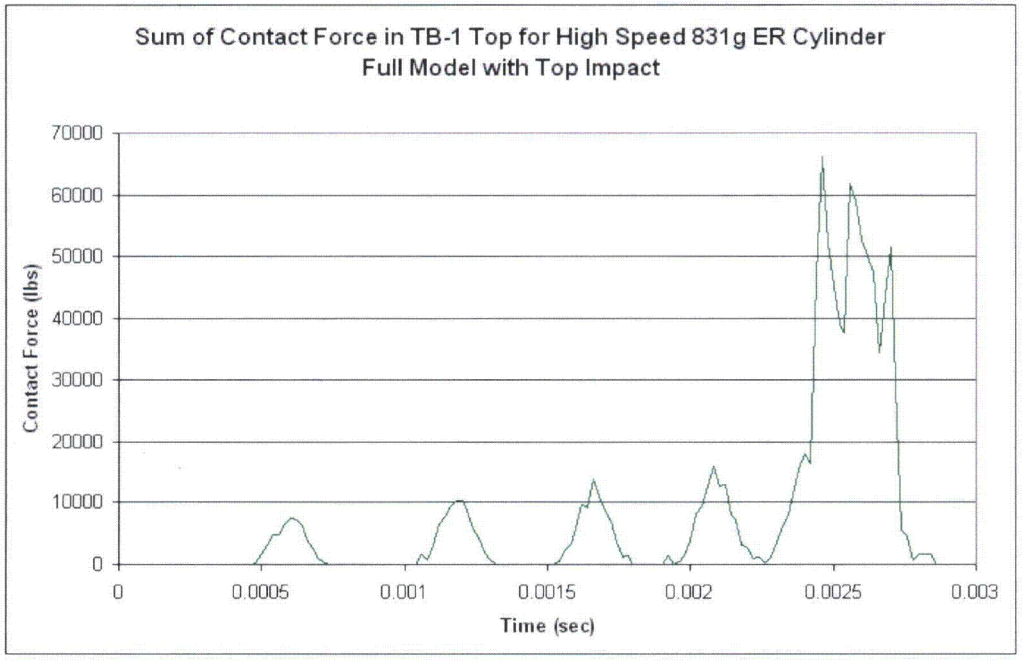


**Figure 2-116. Summed Contact Force on the TB-1 Top for a 831-g, Plutonium Metal Hollow Cylinder, Top Impact**

*2.12.5.4.3 Run 2 - 831-g Angled Cylinder with Bottom Initial Location and a Top Impact*

The top end impact model for the plutonium metal hollow cylinder with angled orientation is shown in Figure 2-117. The cylinder is located at the bottom of the T-Ampoule so that its net impact velocity with the top of the T-Ampoule is maximized. The post-impact deformation is shown in Figure 2-118 and its kinetic energy history in Figure 2-119. The plutonium metal hollow cylinder deforms but maintains much of its original shape because of its conservatively assumed "infinitely ductile," with hardening material constitutive model definition (despite its alpha Pu being a relatively brittle material in reality). If the plutonium metal hollow cylinder were modeled as a brittle material with very low ductility, it would effectively shatter and present a much less concentrated load on the T-Ampoule and TB-1.

Average stress-triaxiality versus EQPS is shown in Figures 2-120 and 2-121 for the 19 elements extending beyond the tested Bao-Wierzbicki strain locus. All of these elements are at high stress triaxiality and low EQPS. The Tearing Parameter values for these same 19 elements are shown in Figure 2-122, and all are below the critical Tearing Parameter value of 1.012 for Ti-6Al-4V. These elements are highlighted in red Figure 2-123, but note that these elements are still below even the initiation of a ductile tear.

Peak EQPS in the TB-1 vessel is shown in Figures 2-124 and 2-125 to be about 2.4%, and only in some localized outer contact regions with the redwood overpack (contact modeling artifact). The von Mises stresses (see Figures 2-126 and 2-127) peak at 148.2 ksi, just above the elevated-temperature minimum yield strength for the TB-1 of 141 ksi, but more importantly, through-thickness TB-1 stress values are less than 50 ksi, below yield. The time at which the peak value of the von Mises stress occurs coincides with the peak value of the contact force (summed over the lid area). A plot of this force as a function of time is shown in Figure 2-128. A maximum contact load of 54,509 lbs is applied to the inner surface of the TB-1 lid during the impact.

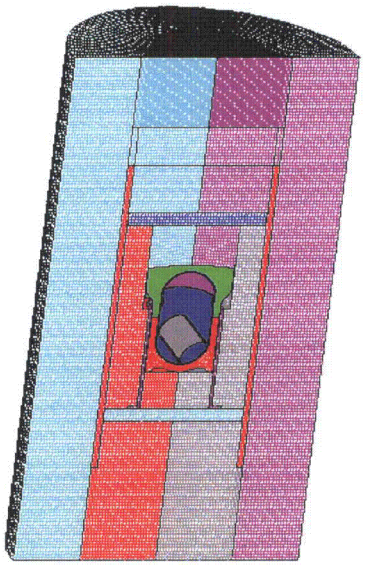

**Figure 2-117. Finite Element Mesh for the 831-g, Angled, ER Cylinder, Bottom Position, End Impact**

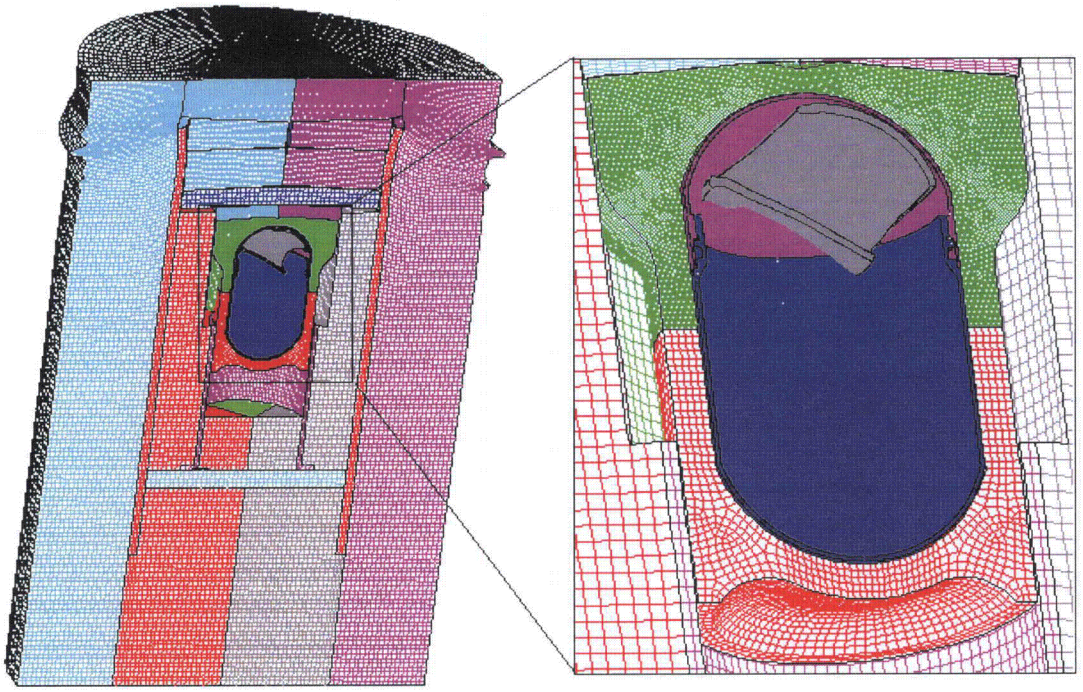

**Figure 2-118. Finite Element Mesh for the 831-g, Angled, ER, Cylinder, Bottom Position, End Impact – Final Displacement**

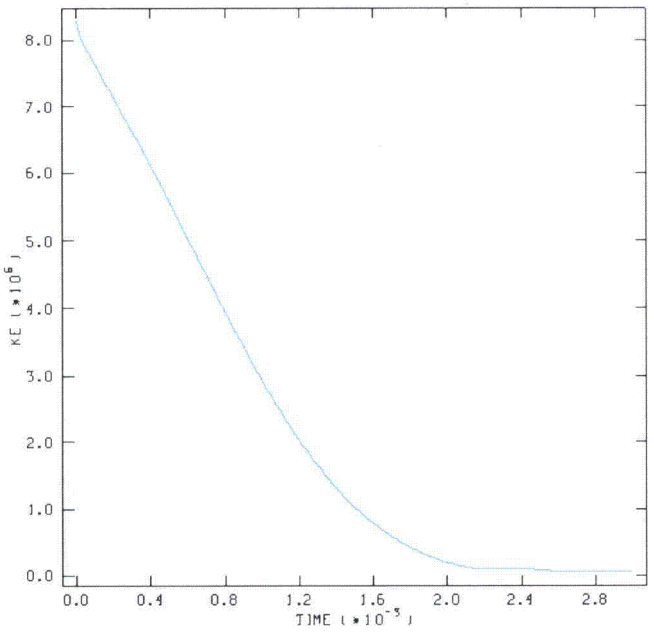


**Figure 2-119. Kinetic Energy Time History for the 831-g, Angled, Plutonium Metal Hollow Cylinder, Bottom Position, End Impact**

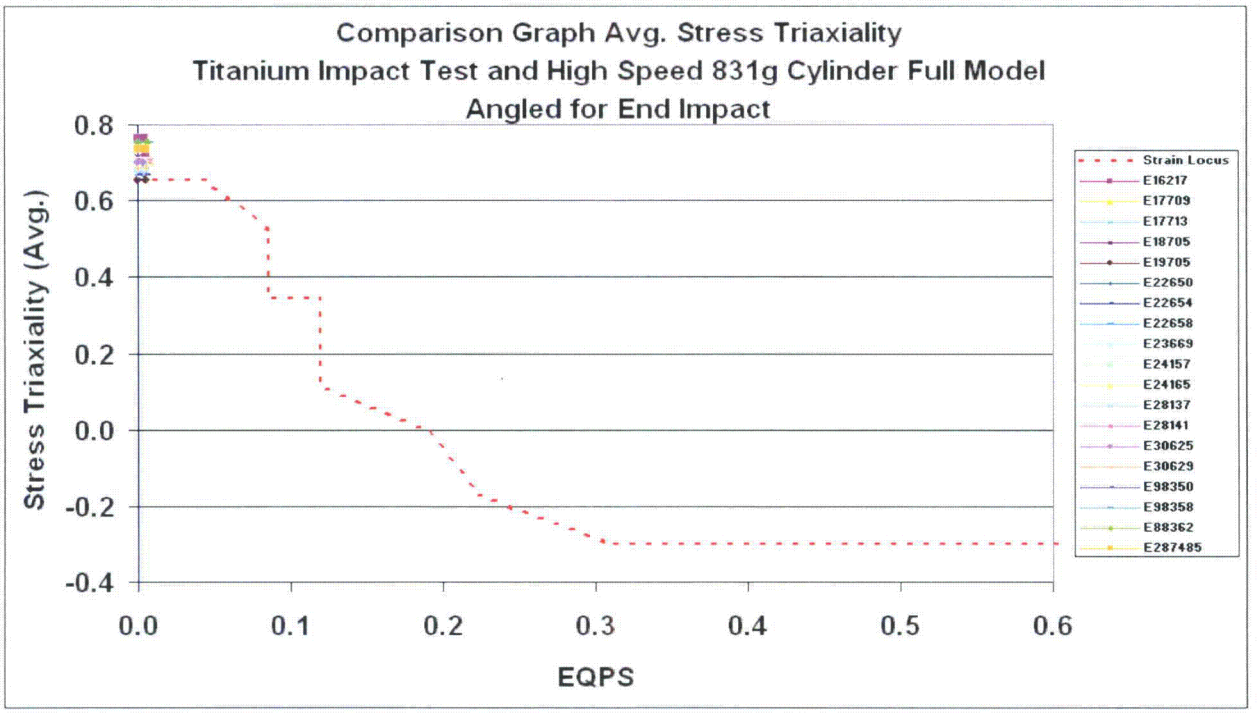


**Figure 2-120. Graph of Average Stress Triaxiality versus EQPS of Elements Exceeding the Experimental Strain Locus for the 831-g, Angled, Plutonium Metal Hollow Cylinder, Bottom Position, End Impact**

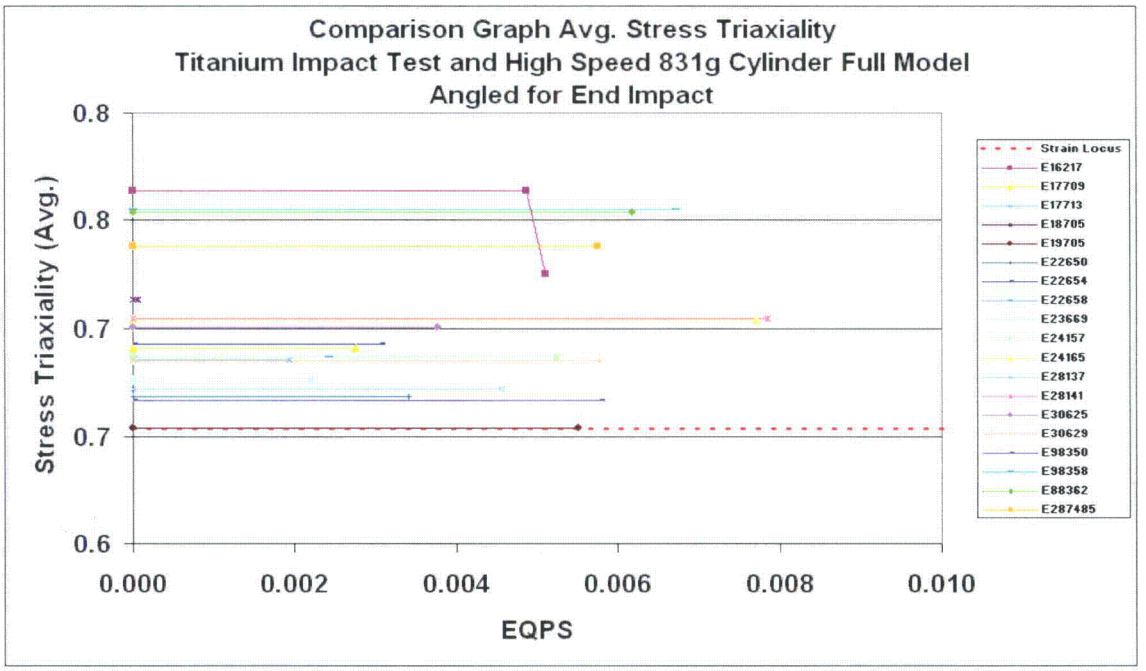


**Figure 2-121. Graph of Average Stress Triaxiality versus EQPS of Elements Exceeding the Experimental Strain Locus (Zoomed In) for the 831-g, Angled, Plutonium Metal Hollow Cylinder, Bottom Position, End Impact**

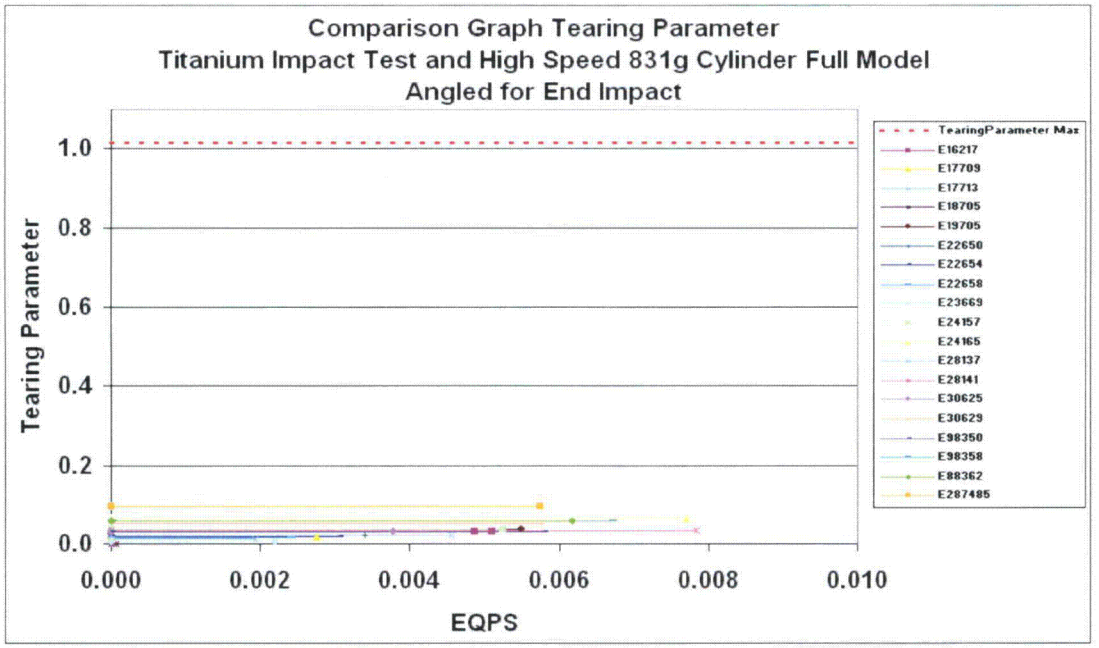


**Figure 2-122. Graph of Tearing Parameter versus EQPS for Elements Exceeding the Experimental Strain Locus for the 831-g, Angled, Plutonium Metal Hollow Cylinder, Bottom Position, End Impact**

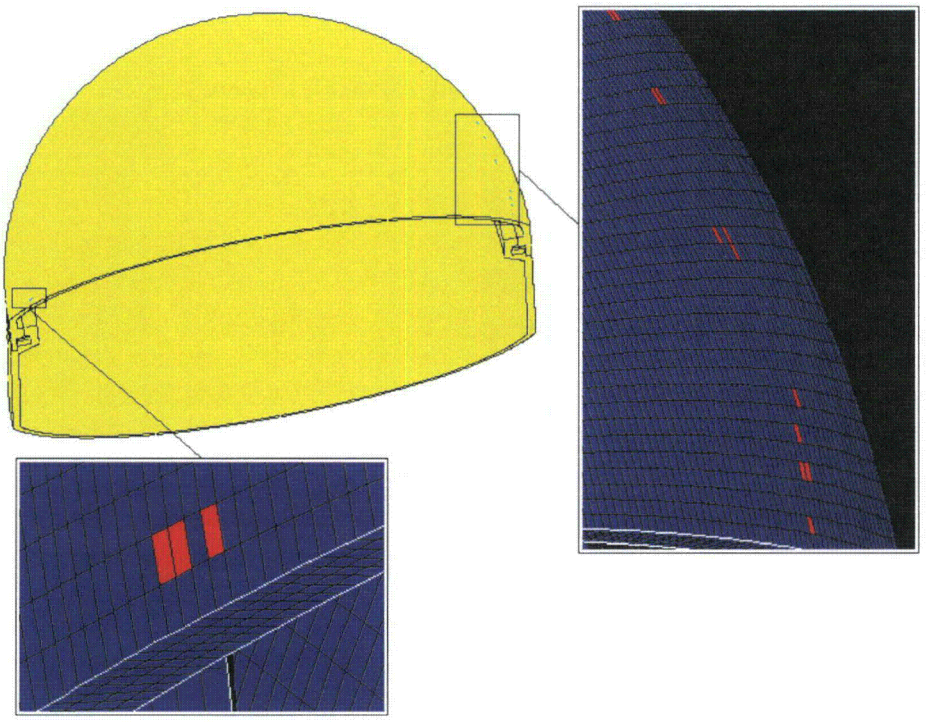

**Figure 2-123. Plot of Elements Exceeding the Experimental Strain Locus for the 831-g, Angled, Plutonium Metal Hollow Cylinder, Bottom Position, End Impact**

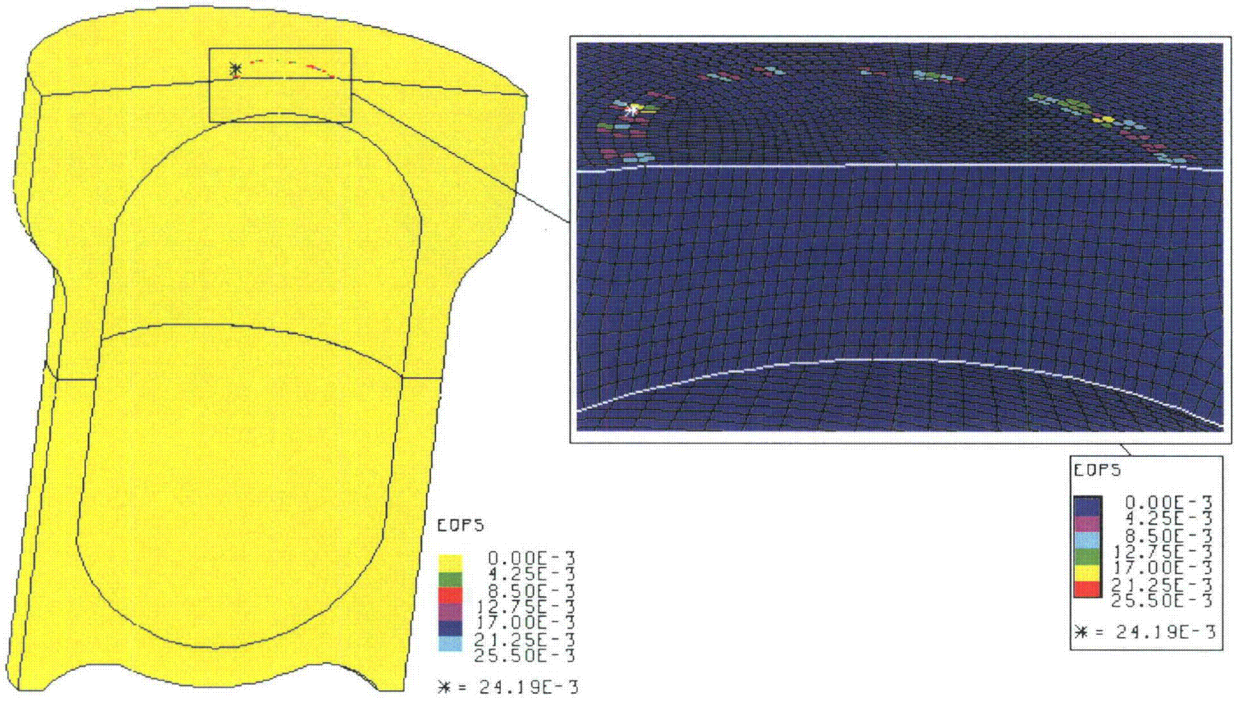


**Figure 2-124. Plot of EQPS in the TB-1 for the 831-g Angled, ER, Cylinder, Bottom Position, End Impact**

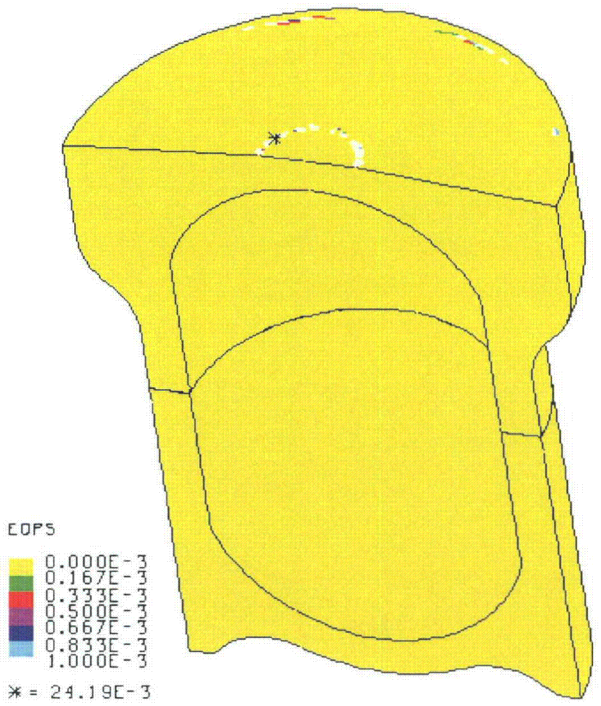


**Figure 2-125. Plot of EQPS in the TB-1 (Range Zoomed in to Show all Elements with Non-Zero EQPS) for the 831-g, Angled, Plutonium Metal Hollow Cylinder, Bottom Position, End Impact**

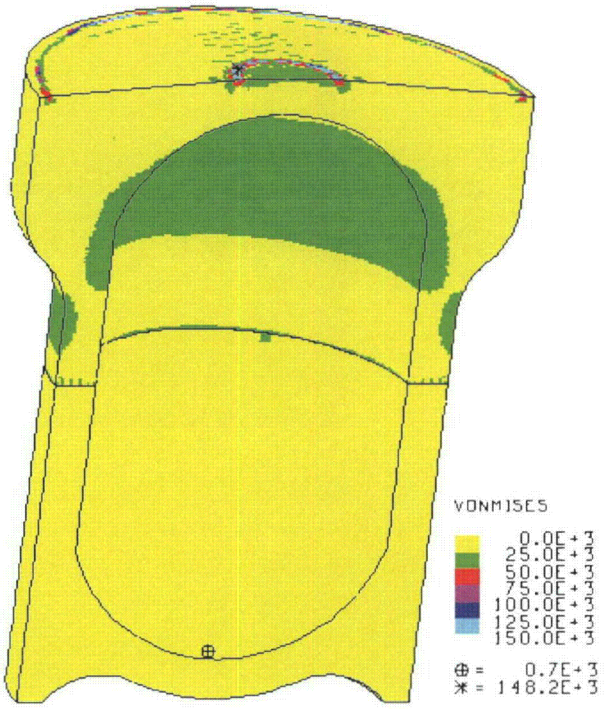


**Figure 2-126. Plot of von Mises Stress in the TB-1 for the 831-g, Angled, Plutonium Metal Hollow Cylinder, Bottom Position, End Impact**

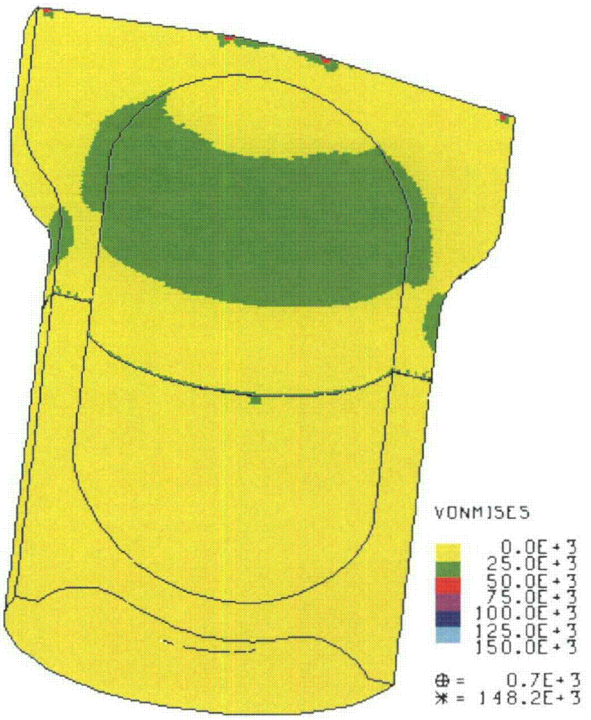


**Figure 2-127. Plot of von Mises Stress in the TB-1 for the 831-g, Angled, Plutonium Metal Hollow Cylinder, Bottom Position, End Impact**

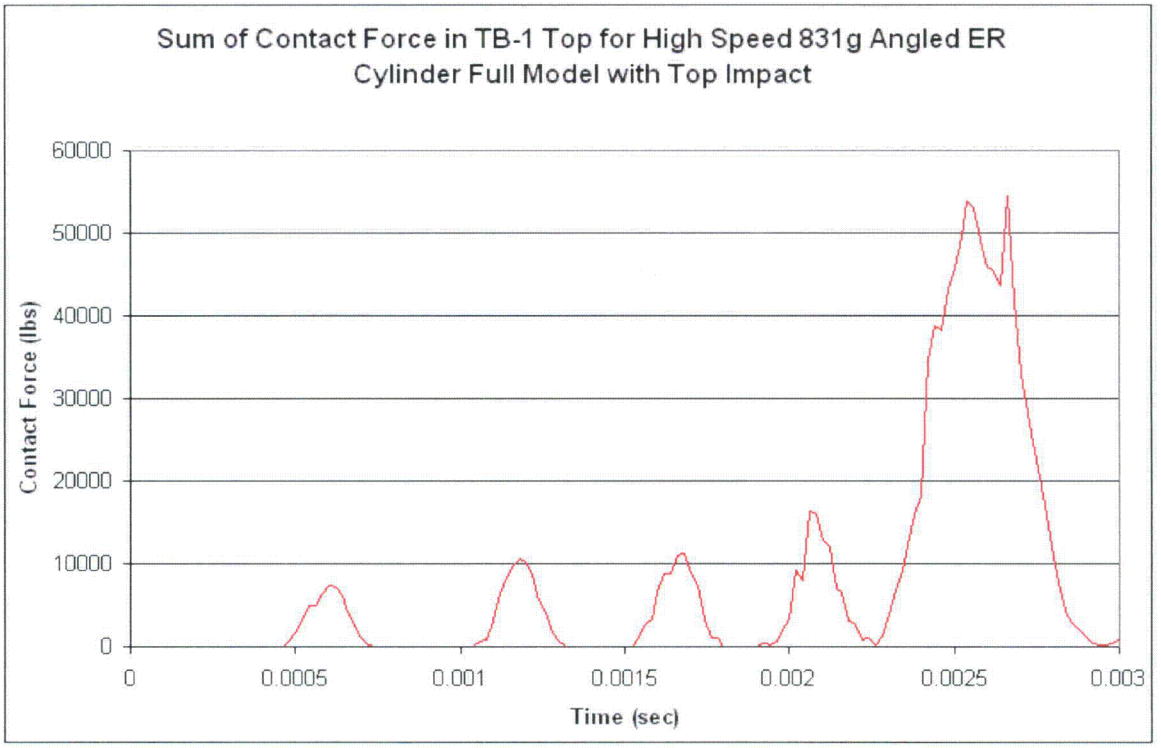


**Figure 2-128. Plot of Contact Force in the TB-1 for the 831-g, Angled Plutonium Metal Hollow Cylinder, Bottom Position, End Impact**

*2.12.5.4.4 Run 3 – 831-g Angled Plutonium Metal Hollow Cylinder with Bottom Initial Location and a CGOC Impact*

The lid end CG-over-corner impact model for the plutonium metal hollow cylinder is shown in Figure 2-129. The cylinder is located at the bottom of the T-Ampoule so that its net impact velocity with the top of the T-Ampoule is maximized. The post-impact deformation is shown in Figure 2-130 and its kinetic energy history in Figure 2-131. The plutonium metal hollow cylinder deforms slightly more than the previous case because of the slightly more side-impact-like orientation but maintains much of its original shape because of its conservatively "infinitely ductile" material constitutive model definition. If the plutonium metal hollow cylinder were modeled as a brittle material with very low ductility, it would effectively shatter and present a much less concentrated load on the T-Ampoule and TB-1.

Average stress-triaxiality versus EQPS is shown in Figures 2-132 and 2-133 for the 126 elements extending beyond the tested Bao-Wierzbicki strain locus. All of these elements are at relatively high stress triaxiality and low EQPS. The Tearing Parameter values for these same 126 elements are shown in Figure 2-134 and all are still safely below the critical Tearing Parameter value of 1.012 for Ti-6Al-4V. These elements are highlighted in red in Figures 2-135 through 2-137, but these elements are still below the critical value. Note that this impact analysis case produced the highest value of Tearing Parameter, 0.6177, which still yields a minimum factor of safety of 1.012 divided by 0.6177 equals 1.64 against even the initiation of a ductile tear. With all the analysis conservatisms in the model, the factor of safety is greater, and the T-Ampoule eutectic barrier integrity is maintained.

Peak EQPS in the TB-1 containment vessel is shown in Figures 2-138 and 2-139 to be about 18.5%, although this peak is only in a highly, localized, outer corner region where there is a slight contact over closure issue with the redwood overpack. This is a minor modeling artifact that produces localized plasticity that otherwise would not exist. It occurs when the redwood compresses well into its "lock-up" phase and becomes analytically stiffer than it would realistically be, due to limitations in the orthotropic crush constitutive model of the redwood. Nonetheless, through-thickness plasticity is non-existent and the TB-1 integrity is maintained. The von Mises stresses (see Figure 2-140) peak is 196 ksi (due to the localized redwood contact), above the elevated-temperature minimum yield strength for the TB-1 of 141 ksi, but more importantly, through-thickness TB-1 stress values are less than 35 ksi, below yield.

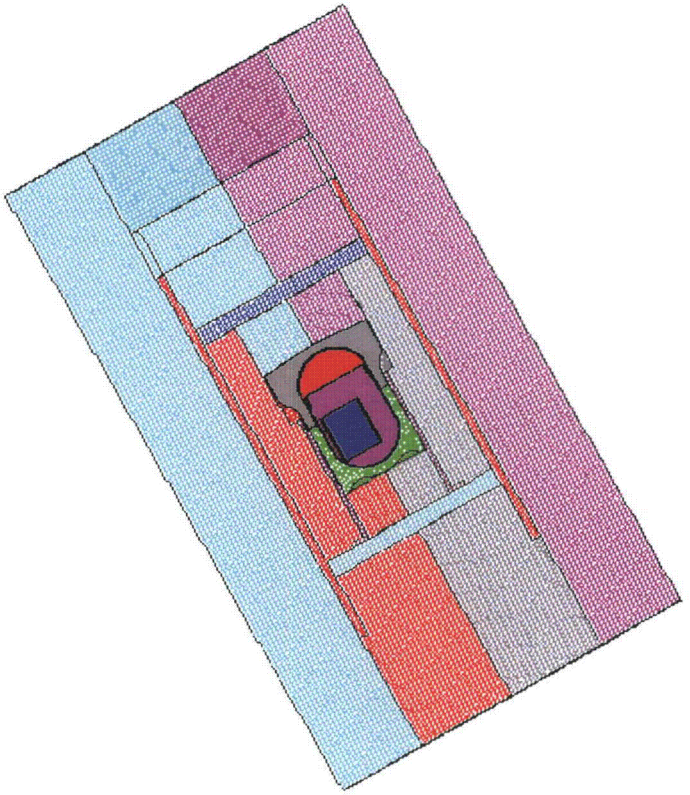

**Figure 2-129. Finite Element Mesh for the 831-g, Angled, ER Cylinder, Bottom Position, CGOC Impact**

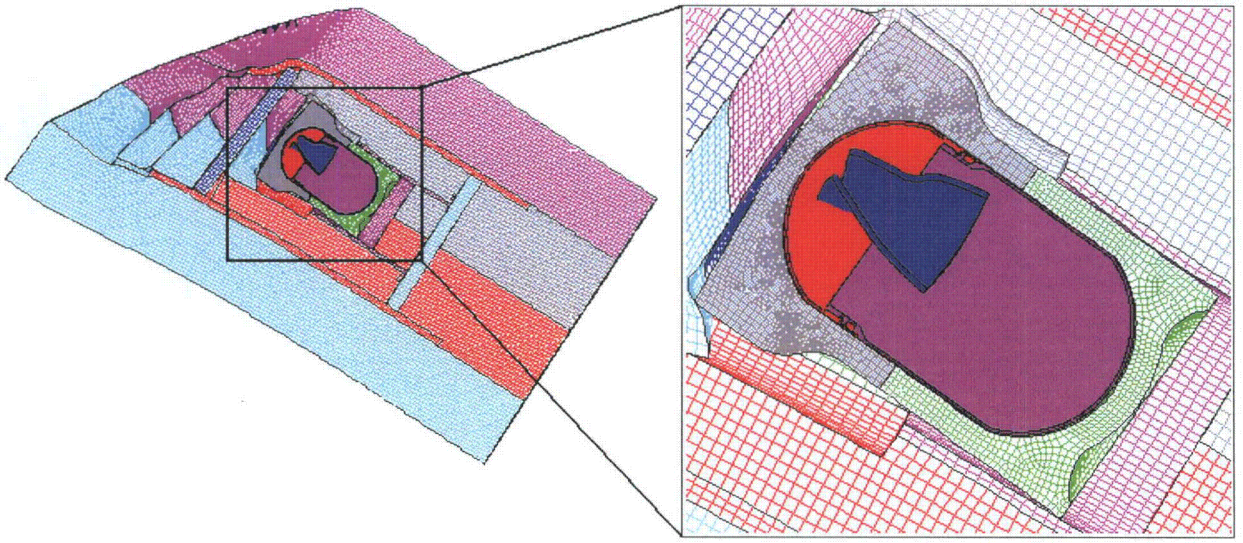

**Figure 2-130. Finite Element Mesh for the 831-g, Angled, ER Cylinder, Bottom Position, CGOC Impact – Final Displacement**

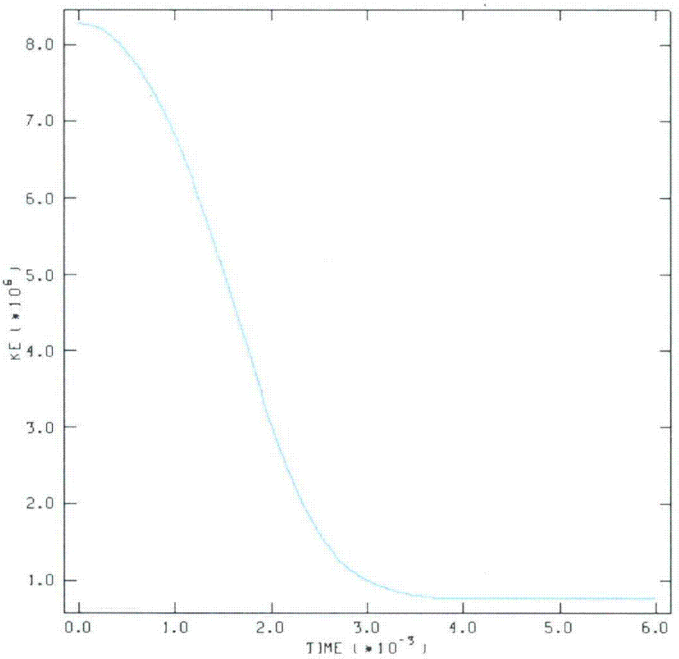


**Figure 2-131. Kinetic Energy Time History for the 831-g, Angled, Plutonium Metal Hollow Cylinder, Bottom Position, CGOC Impact**

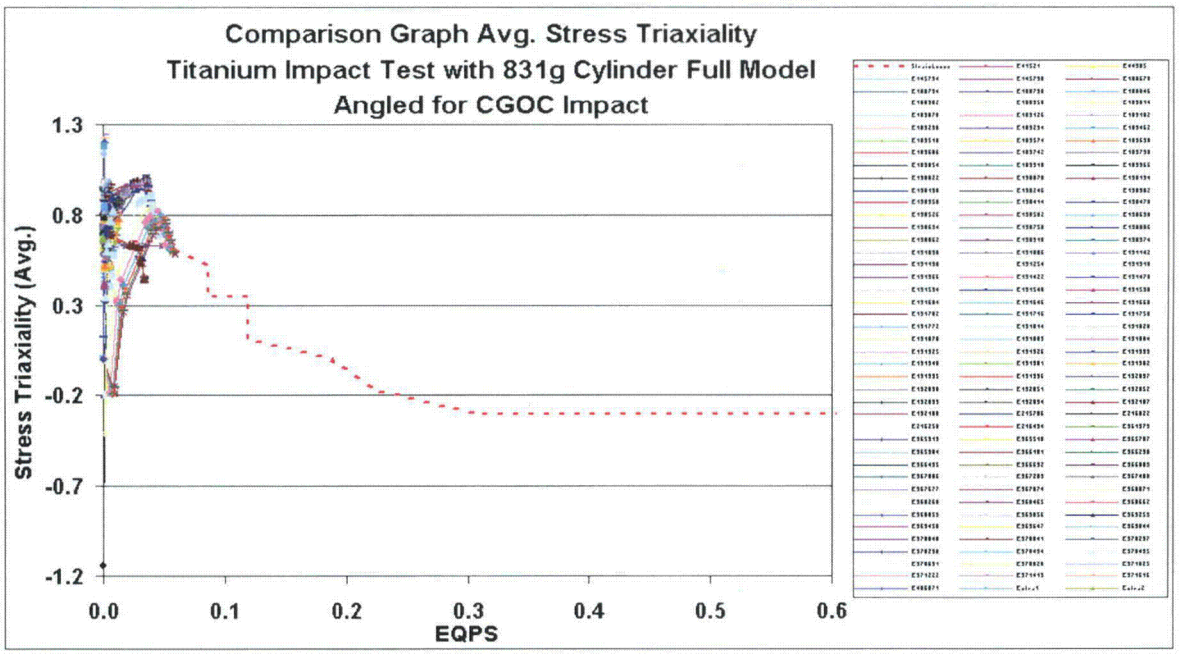


**Figure 2-132. Graph of Average Stress Triaxiality versus EQPS of Elements Exceeding the Experimental Strain Locus for the 831-g, Angled, Plutonium Metal Hollow Cylinder, Bottom Position, CGOC Impact**

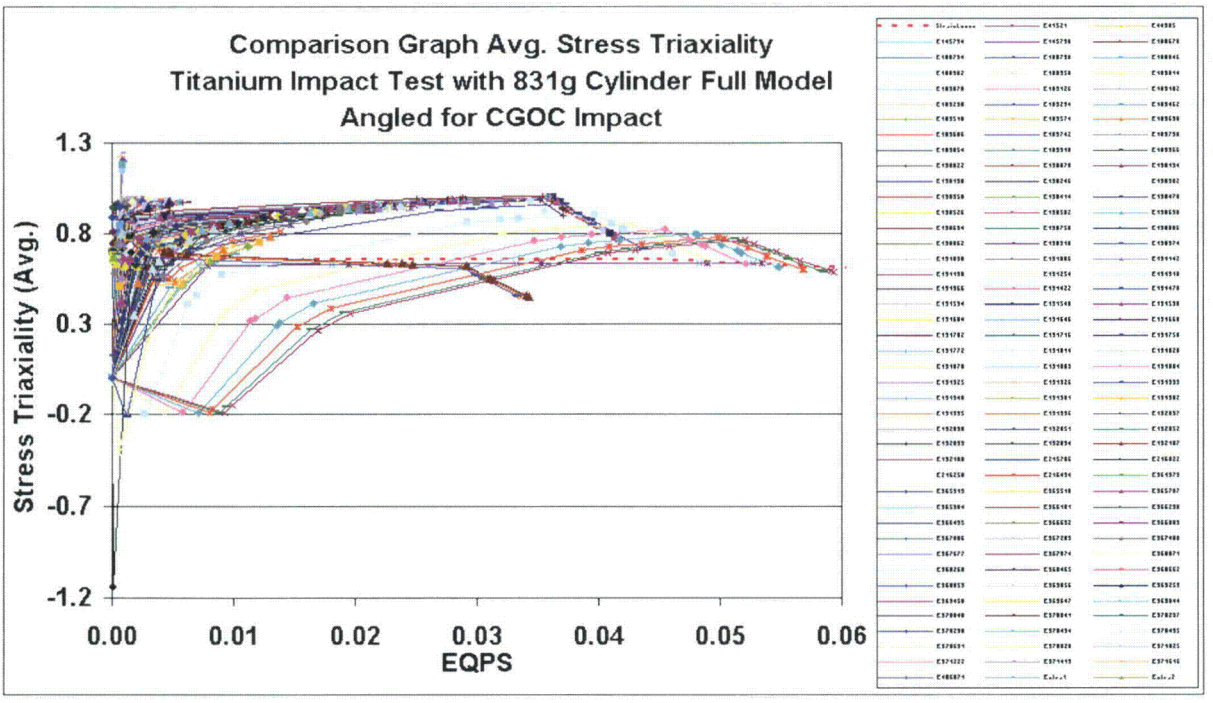


**Figure 2-133. Graph of Average Stress Triaxiality versus EQPS of Elements Exceeding the Experimental Strain Locus (Zoomed in) for the 831-g, Angled, Plutonium Metal Hollow Cylinder, Bottom Position, CGOC Impact**

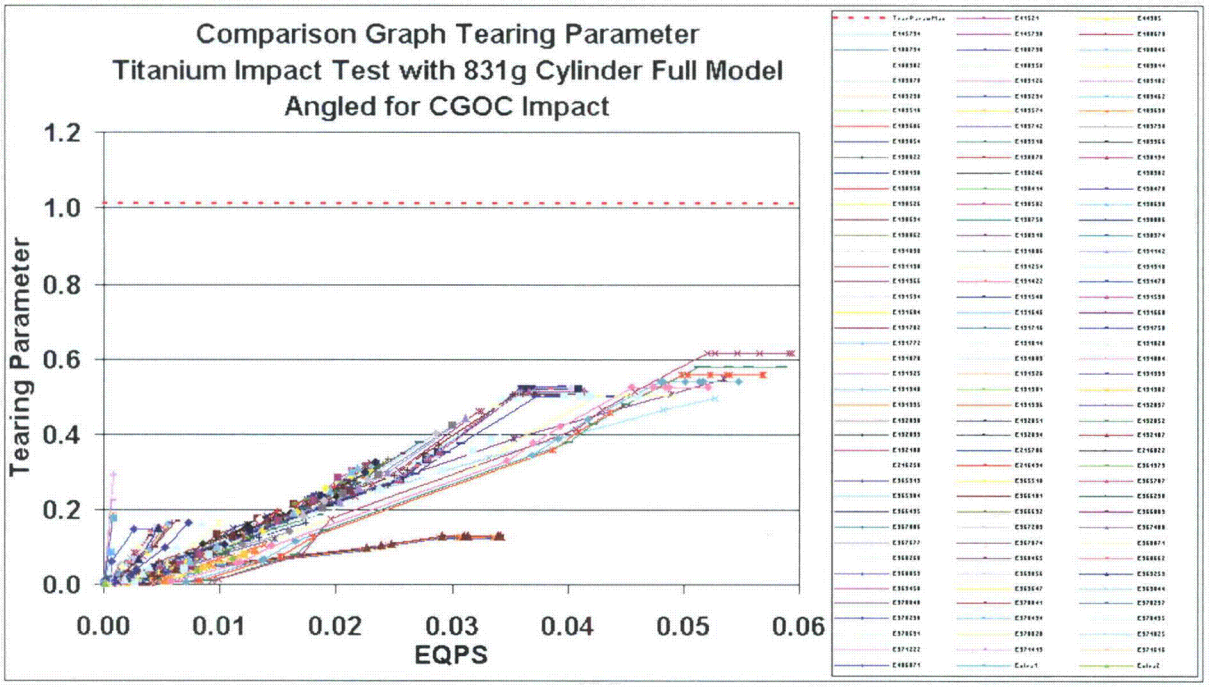


**Figure 2-134. Graph of Tearing Parameter versus EQPS of Elements Exceeding the Experimental Strain Locus for the 831-g Angled, Plutonium Metal Hollow Cylinder, Bottom Position, CGOC Impact**

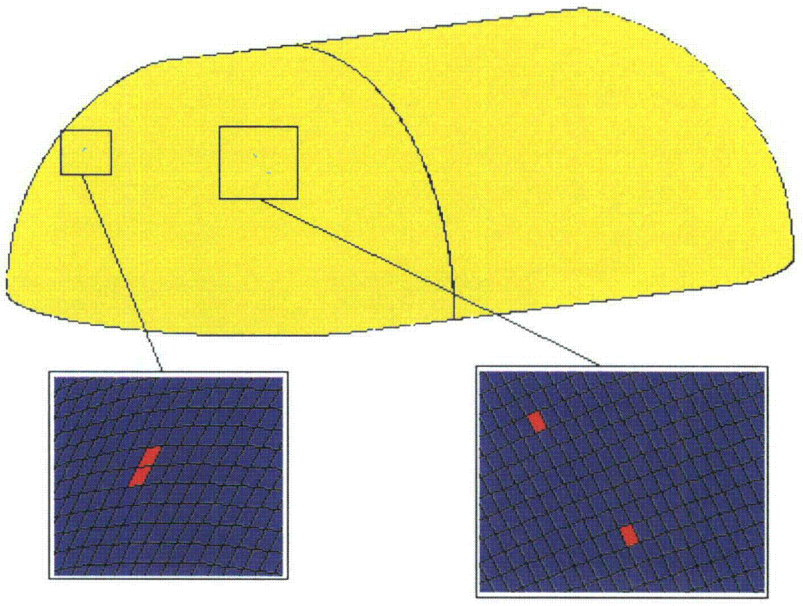

**Figure 2-135. Plot of Elements Exceeding the Experimental Strain Locus for the 831-g, Angled, Plutonium Metal Hollow Cylinder, Bottom Position, CGOC Impact**

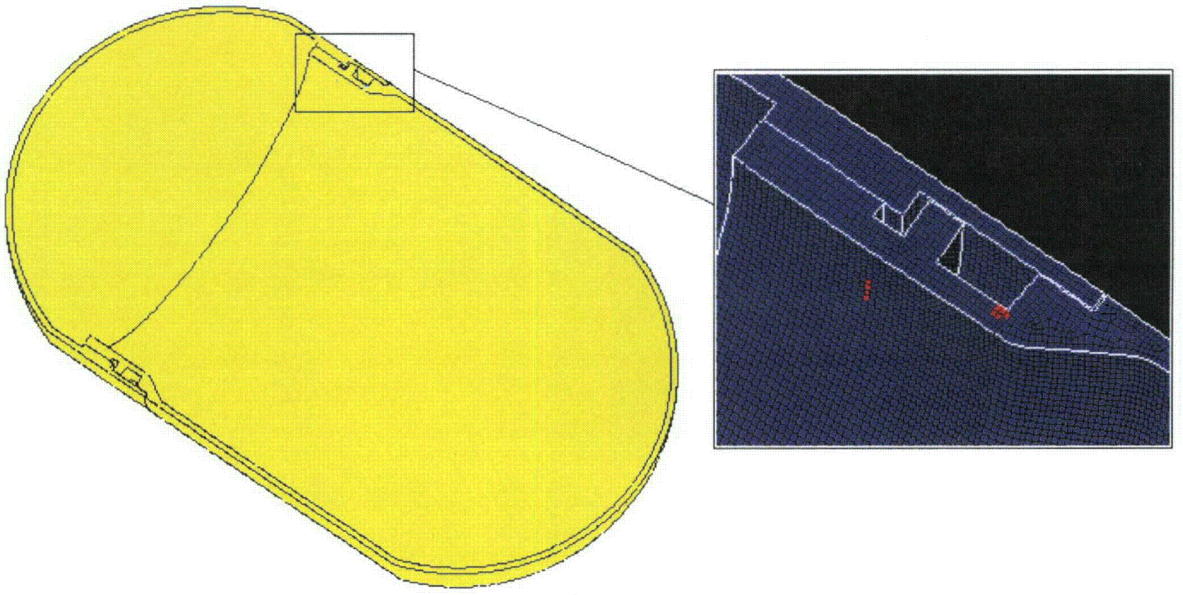

**Figure 2-136. Plot of Elements Exceeding the Experimental Strain Locus for the 831-g, Angled, Plutonium Metal Hollow Cylinder, Bottom Position, CGOC Impact**

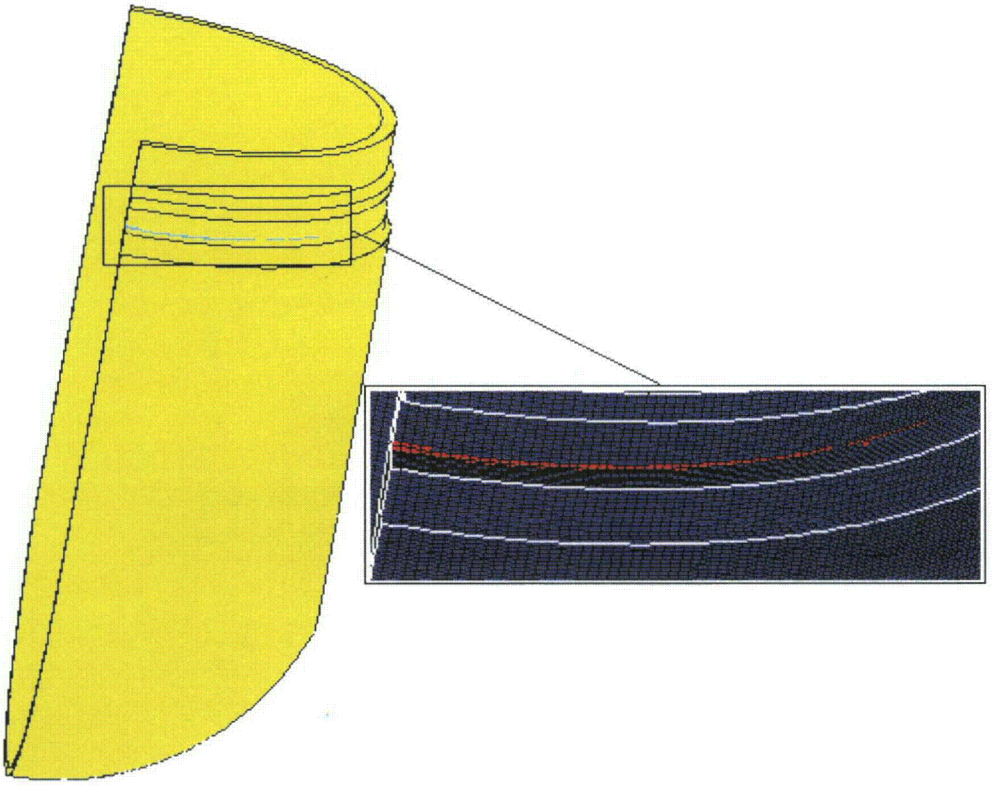

**Figure 2-137. Plot of Elements Exceeding the Experimental Strain Locus for the 831-g, Angled, Plutonium Metal Hollow Cylinder, Bottom Position, CGOC Impact**

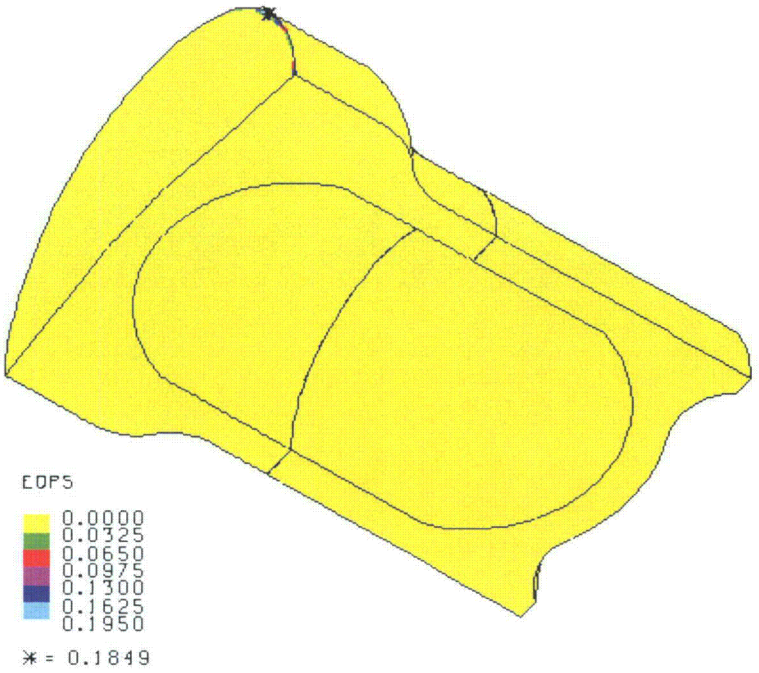


**Figure 2-138. Plot of EQPS in the TB-1 for the 831-g, Angled, Plutonium Metal Hollow Cylinder, Bottom Position, CGOC Impact**

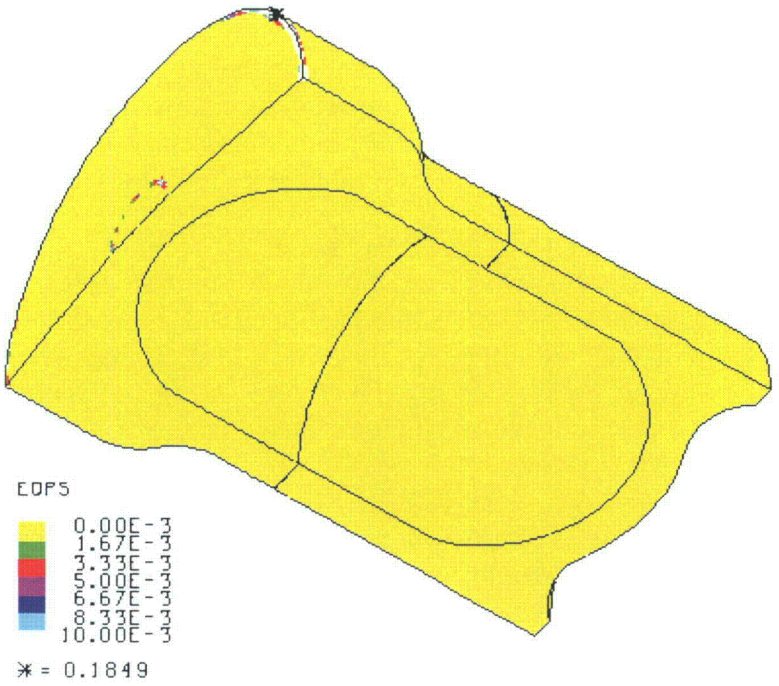


**Figure 2-139. Plot of EQPS in the TB-1 for the 831-g, Angled, Plutonium Metal Hollow Cylinder, Bottom Position, CGOC Impact**

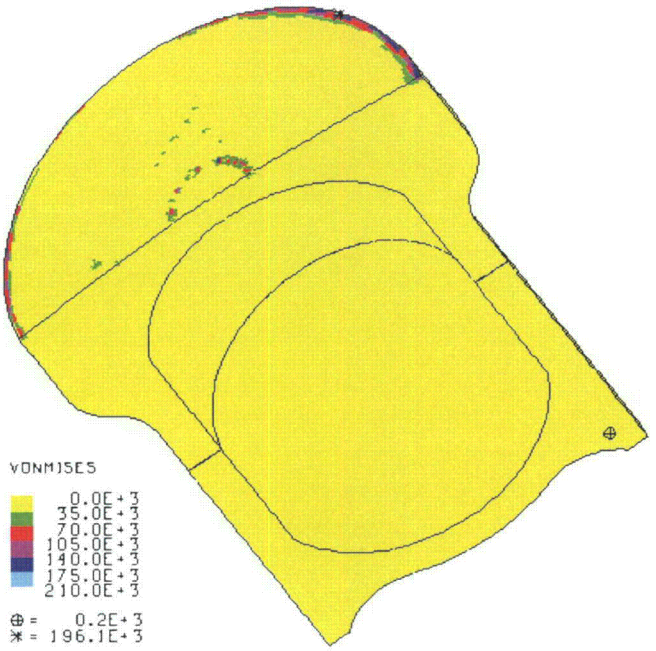


**Figure 2-140. Plot of von Mises Stress in the TB-1 for the 831-g, Angled, Plutonium Metal Hollow Cylinder, Bottom Position, CGOC Impact**

*2.12.5.4.5 Run 4 – 831-g Plutonium Metal Hollow Cylinder Side Impact*

The side impact model for the hollow plutonium metal hollow cylinder is shown in Figure 2-141. The cylinder is located at the far side of the T-Ampoule so that its net impact velocity with the side of the T-Ampoule is maximized. The post-impact deformation is shown in Figure 2-142 and its kinetic energy history in Figure 2-143. The plutonium metal hollow cylinder deforms much more than the previous case because of its weaker side-impact orientation.

Average stress-triaxiality versus EQPS is shown in Figures 2-144 and 2-145 for the 67 elements extending beyond the tested Bao-Wierzbicki strain locus. All of these elements are at relatively high stress triaxiality and low EQPS. The Tearing Parameter values for these same 67 elements are shown in Figure 2-146 and all are still below the critical Tearing Parameter value of 1.012 for Ti-6Al-4V. These elements are highlighted in red in Figures 2-147 and 2-148, but these elements are still below the critical value and do not indicate failure; T-Ampoule integrity is maintained.

Peak EQPS in the TB-1 containment vessel is shown in Figures 2-149 and 2-150 to be about 27.4%, although this peak is only in a highly localized outer corner region where there is a slight contact overclosure issue with the redwood overpack. A slight (<1% EQPS) dent is visible in Figure 2-150 from the internal impact of the plutonium metal hollow cylinder with the TB-1 wall (via the T-Ampoule). Through-thickness plasticity is non-existent and the TB-1 integrity is maintained. The von Mises stresses (see Figures 2-151 and 2-152) peak at 222 ksi (due to the localized redwood contact), which is above the elevated-temperature minimum yield strength for the TB-1 of 141 ksi, but more importantly, through-thickness TB-1 stress values are less than 37.5 ksi, below yield.

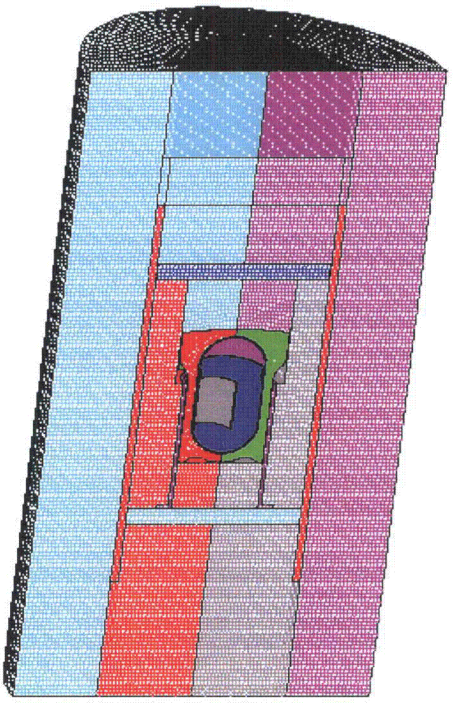

**Figure 2-141. Finite Element Mesh for the 831-g, ER, Cylinder, Far Side Position, Side Impact**

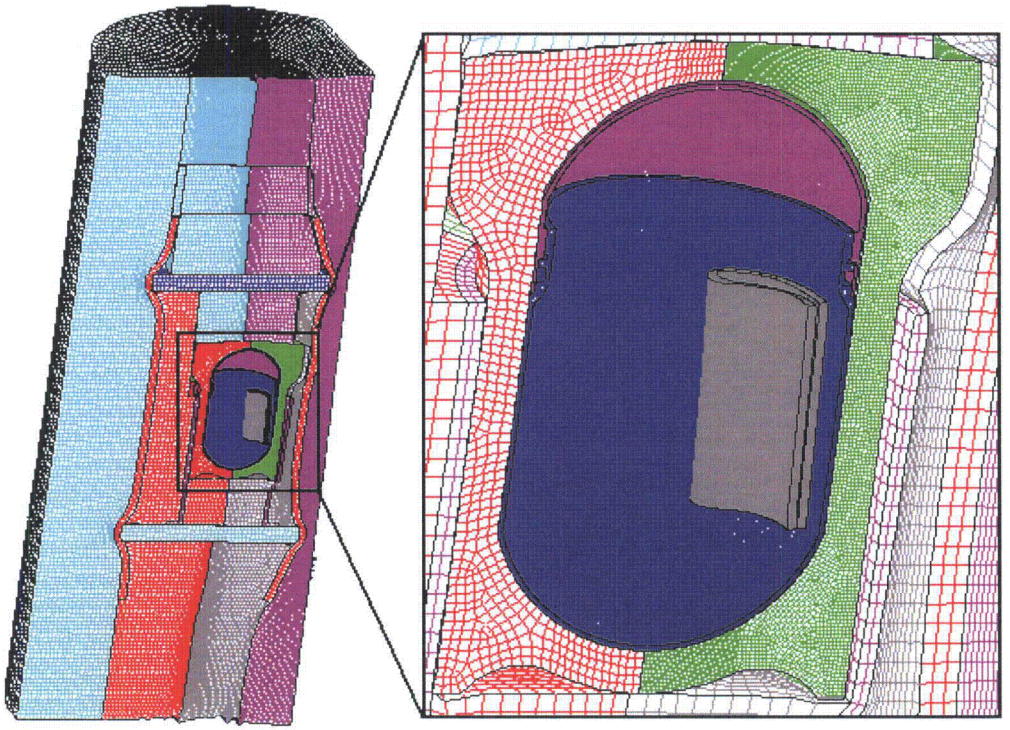

**Figure 2-142. Finite Element Mesh for the 831-g, Plutonium Metal Hollow Cylinder, Far Side Position, Side Impact – Final Displacement**

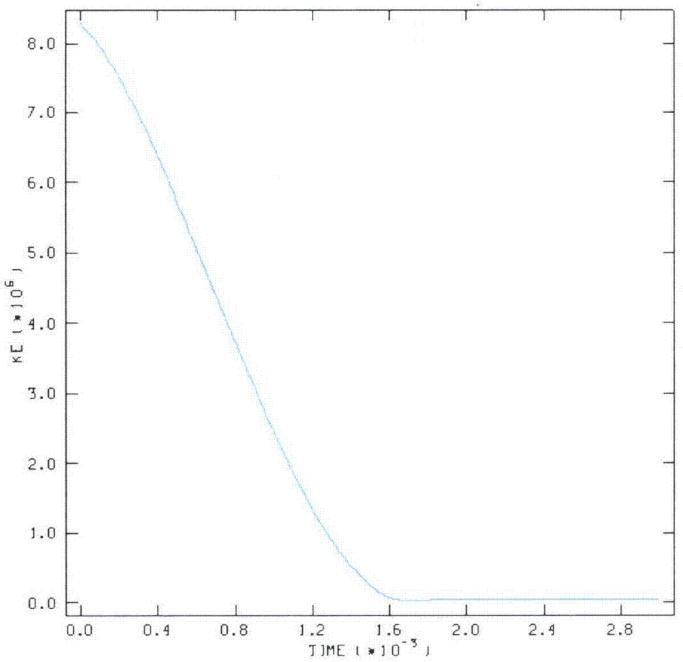


**Figure 2-143. Kinetic Energy Time History for the 831-g, ER, Cylinder, Far Side Position, Side Impact**

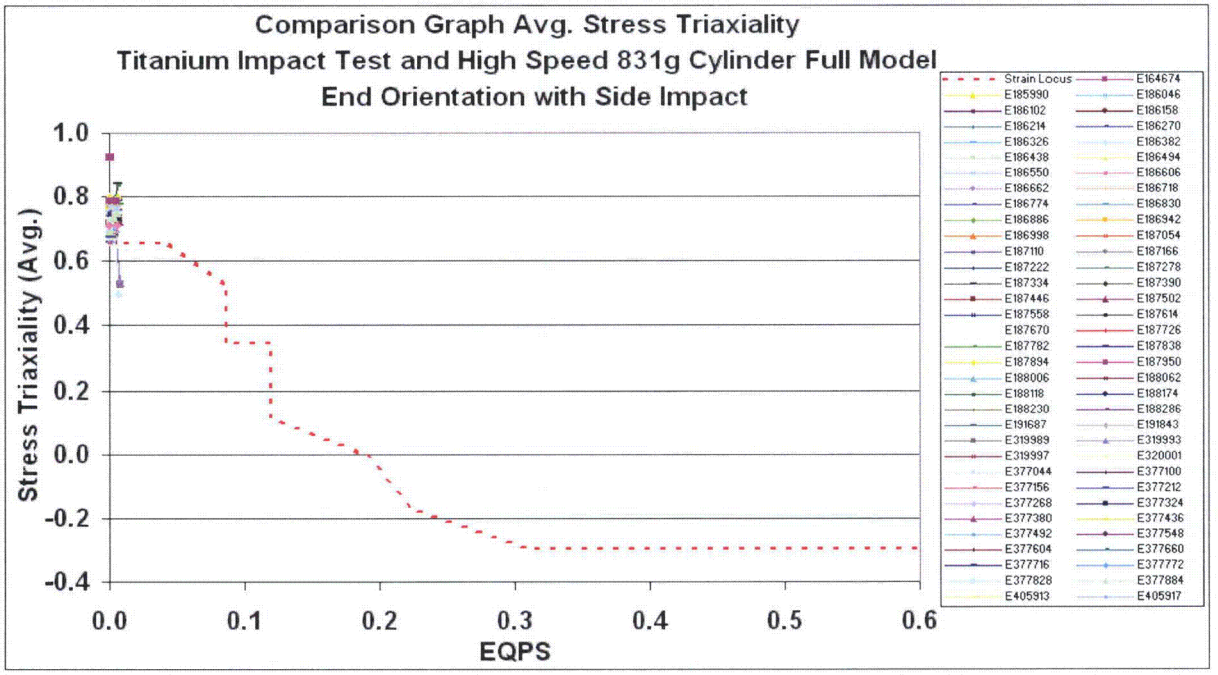


**Figure 2-144. Graph of Stress Triaxiality versus EQPS of Elements Exceeding the Experimental Strain Locus for the 831-g, Plutonium Metal Hollow Cylinder, Far Side Position, Side Impact**

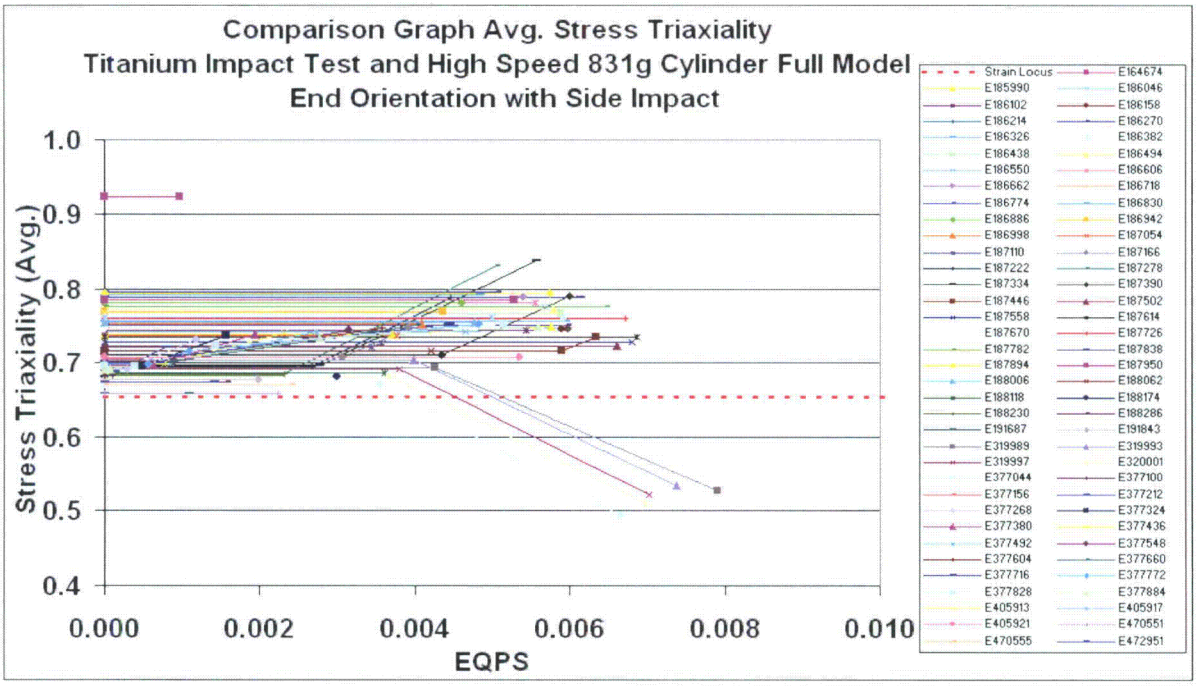


**Figure 2-145. Graph of Stress Triaxiality versus EQPS of Elements Exceeding the Experimental Strain Locus (Zoomed In) for the 831-g, Plutonium Metal Hollow Cylinder, Far Side Position, Side Impact**

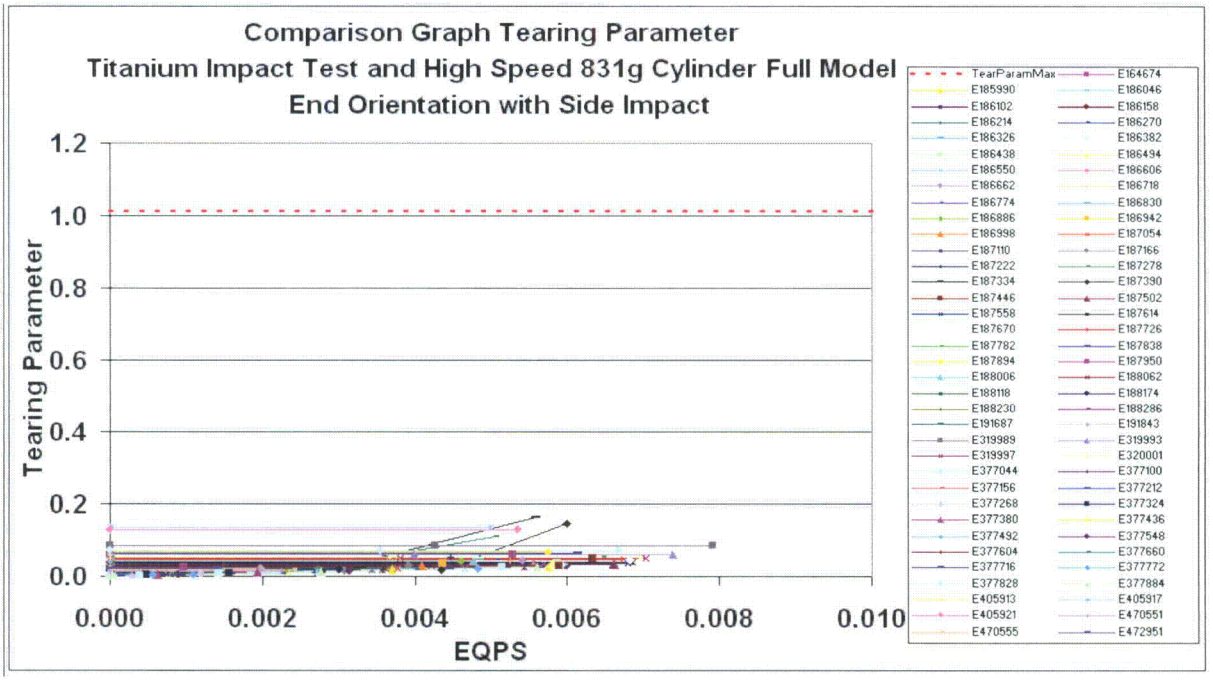


**Figure 2-146. Graph of Tearing Parameter versus EQPS of Elements Exceeding the Experimental Strain Locus for the 831-g, Plutonium Metal Hollow Cylinder, Far Side Position, Side Impact**

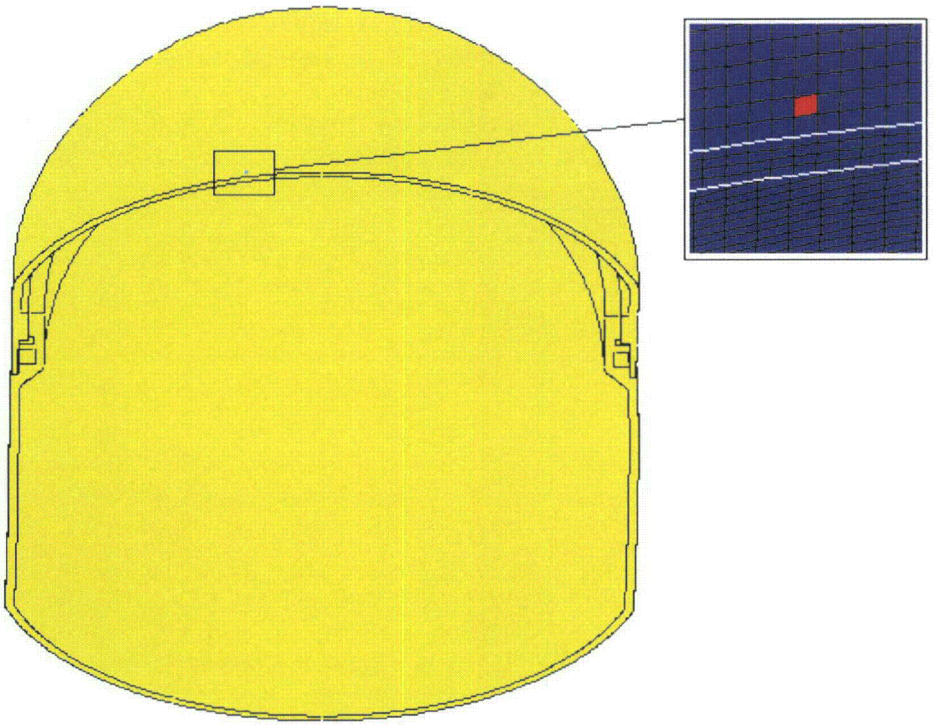

**Figure 2-147. Plot of Elements Exceeding the Experimental Strain Locus for the 831-g, Plutonium Metal Hollow Cylinder, Far Side Position, Side Impact**

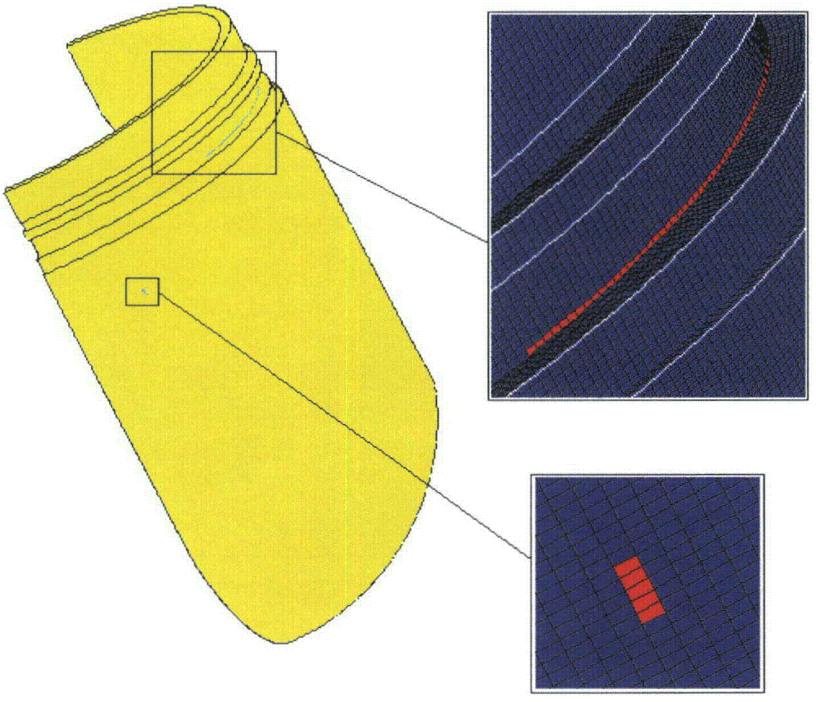

**Figure 2-148. Plot of Elements Exceeding the Experimental Strain Locus for the 831-g, Plutonium Metal Hollow Cylinder, Far Side Position, Side Impact**

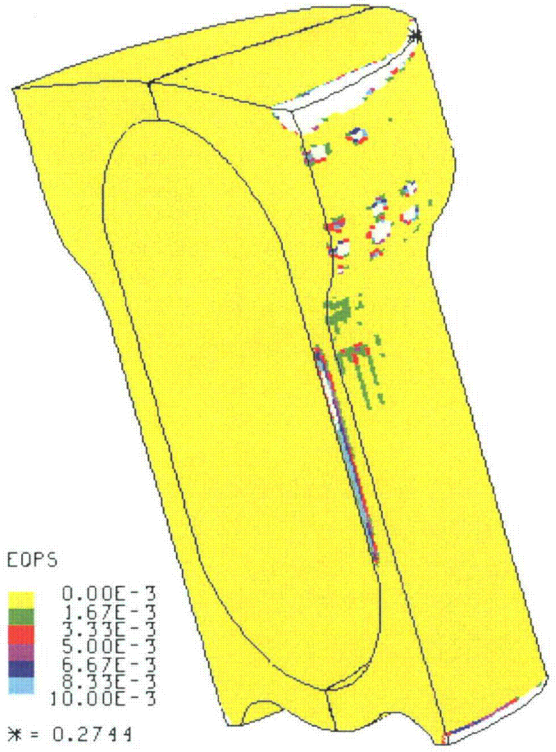


**Figure 2-149. Plot of EQPS in the TB-1 for the 831-g, ER, Cylinder, Far Side Position, Side Impact**

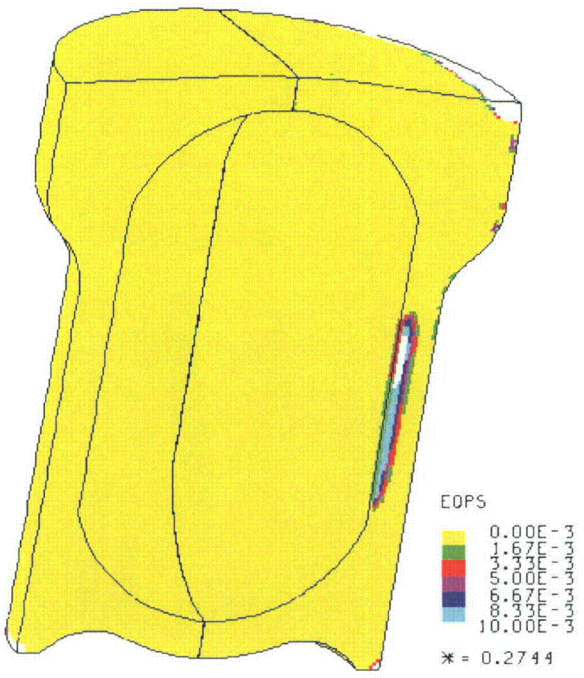


**Figure 2-150. Plot of EQPS in the TB-1 for the 831-g, ER Cylinder, Far Side Position, Side Impact**

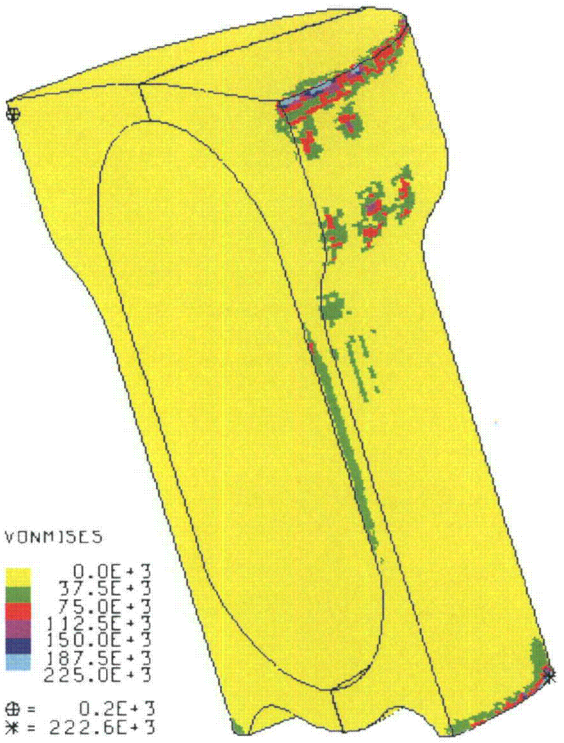


**Figure 2-151. Plot of von Mises Stress in the TB-1 for the 831-g, ER Cylinder, Far Side Position, Side Impact**

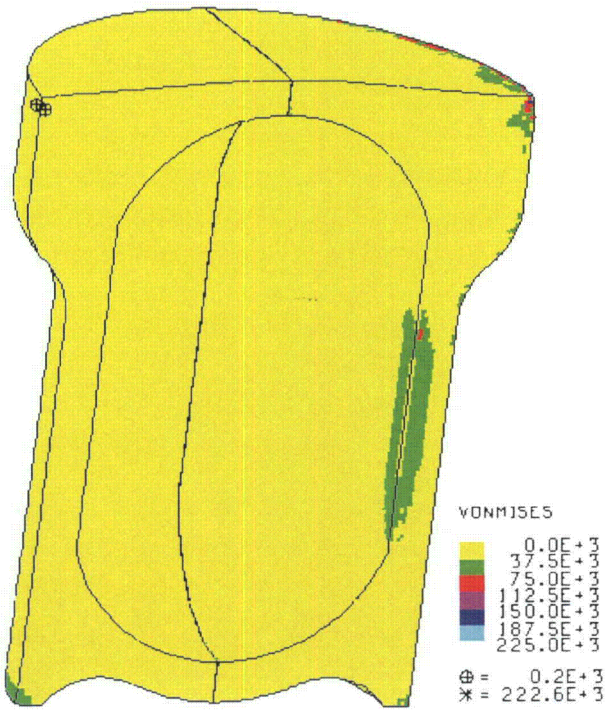


**Figure 2-152. Plot of von Mises Stress in the TB-1 for the 831-g, ER, Cylinder, Far Side Position, Side Impact**

*2.12.5.4.6 Run 5 - 831-g Angled Plutonium Metal Hollow Cylinder Side Impact*

The side impact model for the plutonium metal hollow cylinder, angled orientation, is shown in Figure 2-153. The cylinder is located at the far side of the T-Ampoule so that its net impact velocity with the side of the T-Ampoule is maximized, but also angled to present a sharp corner impact with the T-Ampoule surface. The post-impact deformation is shown in Figure 2-154 and its kinetic energy history in Figure 2-155. The plutonium metal hollow cylinder deforms moderately but maintains much of its original shape because of its conservatively "infinitely ductile" material constitutive model definition.

Average stress-triaxiality versus EQPS is shown in Figures 2-156 and 2-157 for the 91 elements extending beyond the tested Bao-Wierzbicki strain locus. All of these elements are at relatively high stress triaxiality and low EQPS. The Tearing Parameter values for these same 91 elements are shown in Figure 2-158, and all are still below the critical Tearing Parameter value of 1.012 for Ti-6Al-4V. These elements are highlighted in red Figure 2-159, but these elements are still below the critical value and do not indicate failure; T-Ampoule integrity is maintained.

Peak EQPS in the TB-1 vessel is shown in Figures 2-160 and 2-161 to be about 26.7%, although this peak is only in a highly localized outer corner region where there is a slight contact overclosure issue with the redwood overpack. Through-thickness plasticity is non-existent and the TB-1 integrity is maintained. The von Mises stresses (see Figures 2-162 and 2-163) peak at 221 ksi (due to the localized redwood contact), which is above the elevated-temperature minimum yield strength for the TB-1 of 141 ksi, but more importantly, through-thickness TB-1 stress values are less than 112.5 ksi, below yield.

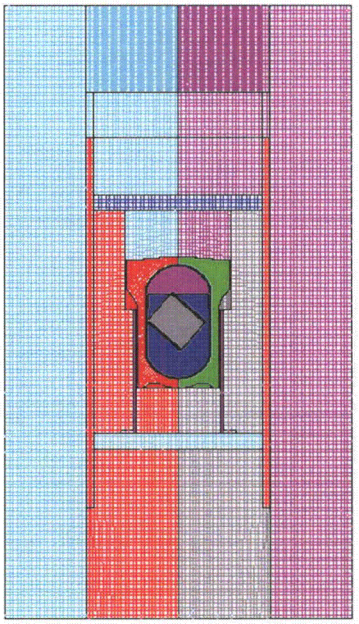

**Figure 2-153. Finite Element Mesh for the 831-g, Angled, ER Cylinder, Far Side Position, Side Impact**

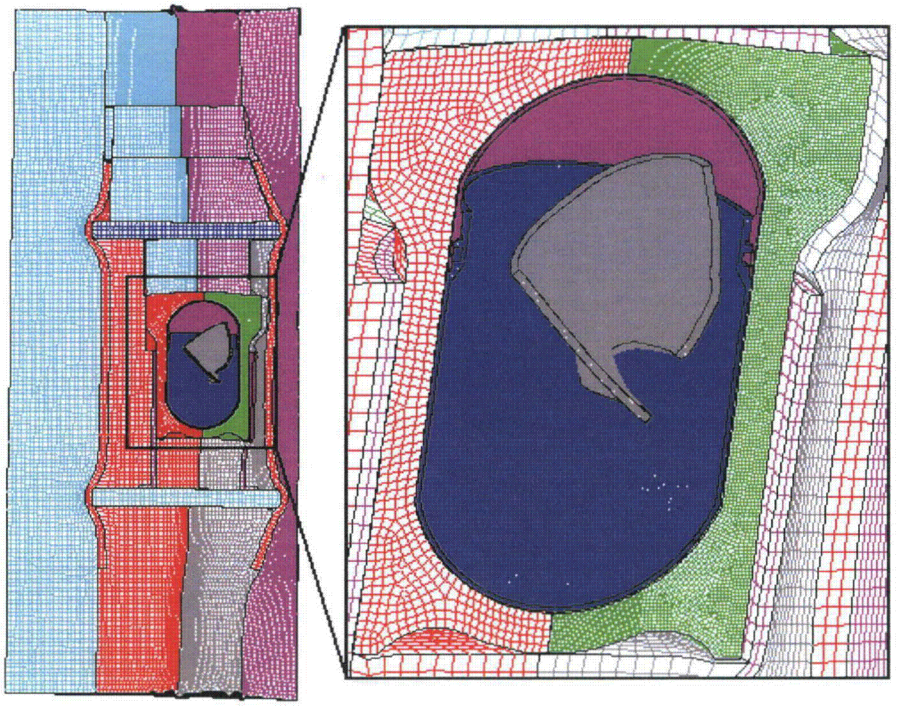

**Figure 2-154. Finite Element Mesh for the 831-g, Angled, ER Cylinder, Far Side Position, Side Impact – Final Displacement**

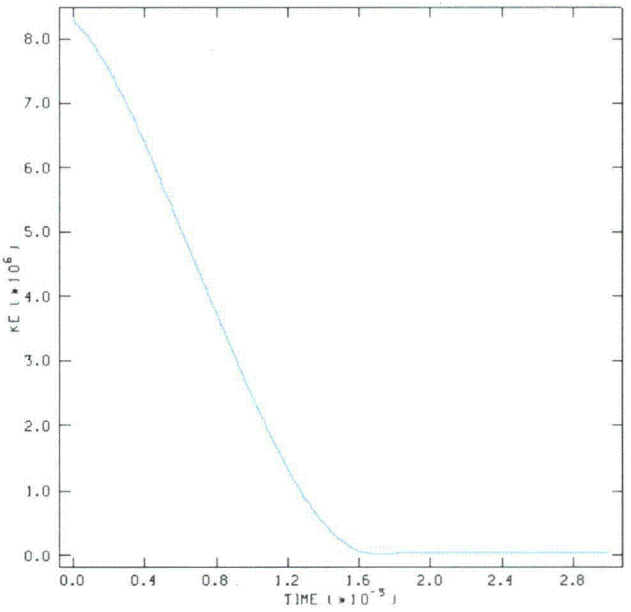


**Figure 2-155. Kinetic Energy Time History for the 831-g, Angled, Plutonium Metal Hollow Cylinder, Far Side Position, Side Impact**

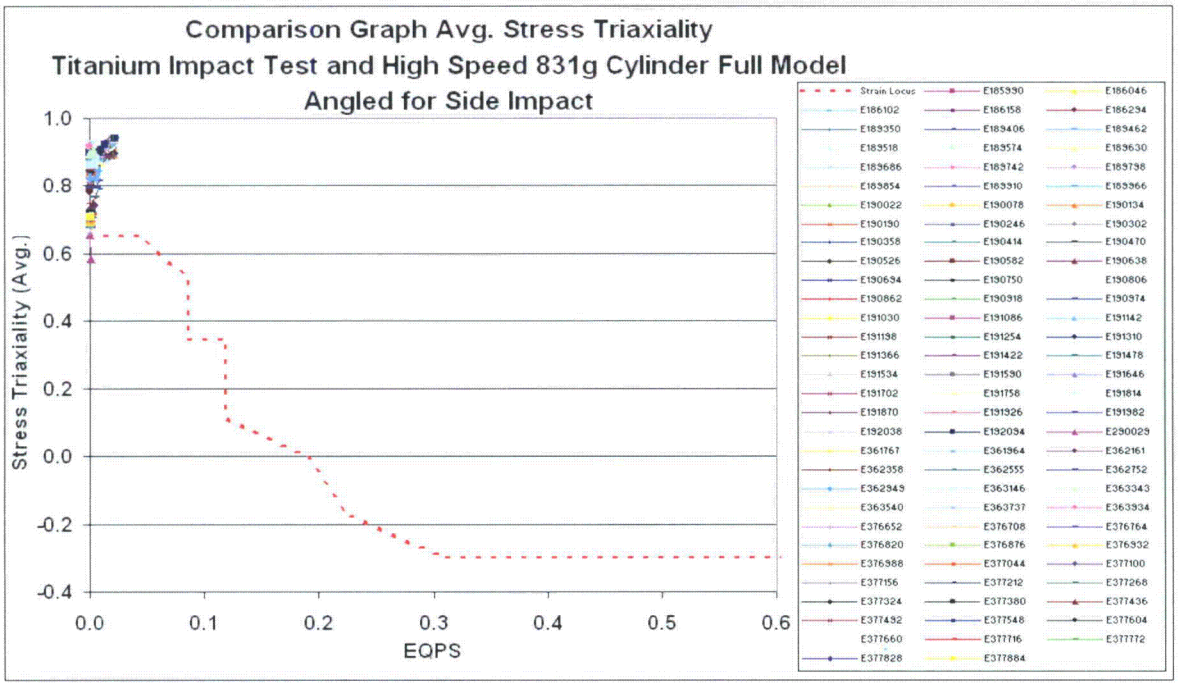


**Figure 2-156. Graph of Average Stress Triaxiality versus EQPS of Elements Exceeding the Experimental Strain Locus for the 831-g, Angled, Plutonium Metal Hollow Cylinder, Far Side Position, Side Impact**

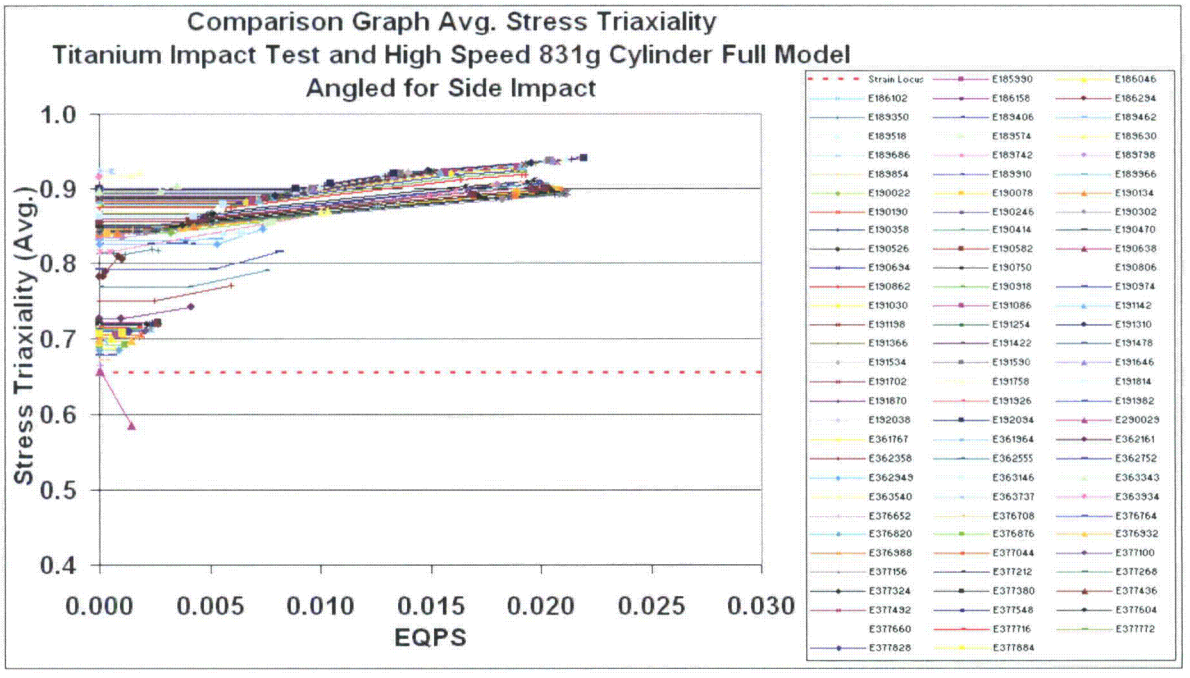


**Figure 2-157. Graph of Average Stress Triaxiality versus EQPS of Elements Exceeding the Experimental Strain Locus (Zoomed In) for the 831-g, Angled, Plutonium Metal Hollow Cylinder, Far Side Position, Side Impact**

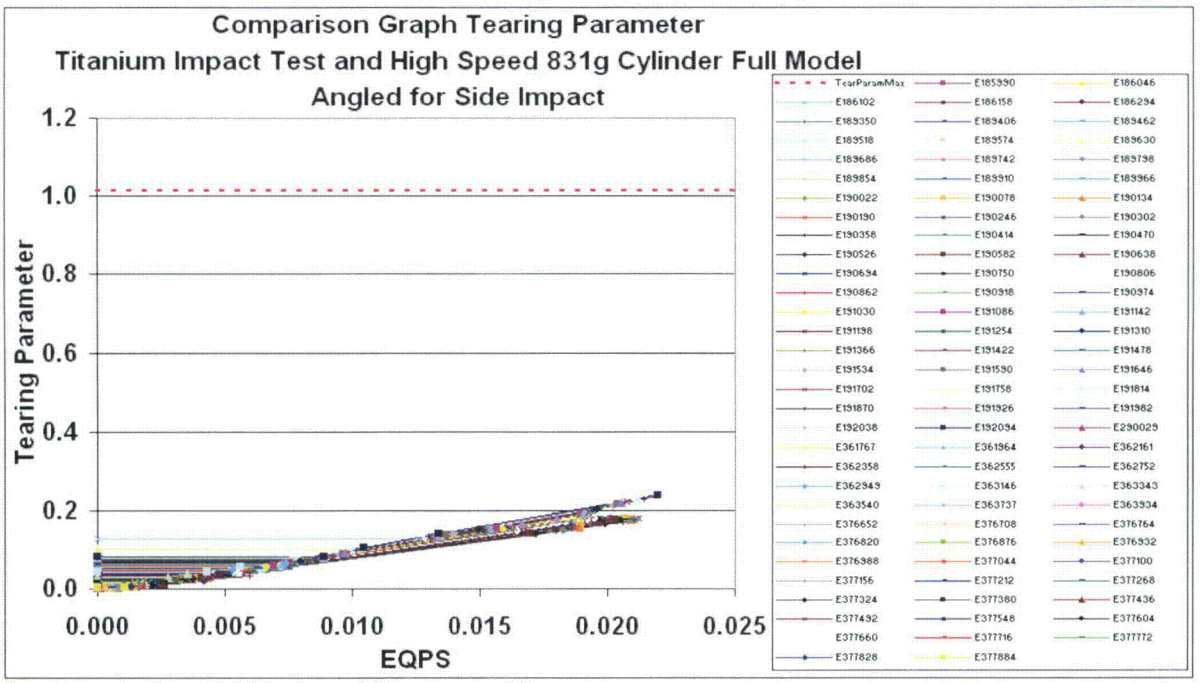


**Figure 2-158. Graph of Tearing Parameter versus EQPS of Elements Exceeding the Experimental Strain Locus for the 831-g, Angled, Plutonium Metal Hollow Cylinder, Far Side Position, Side Impact**

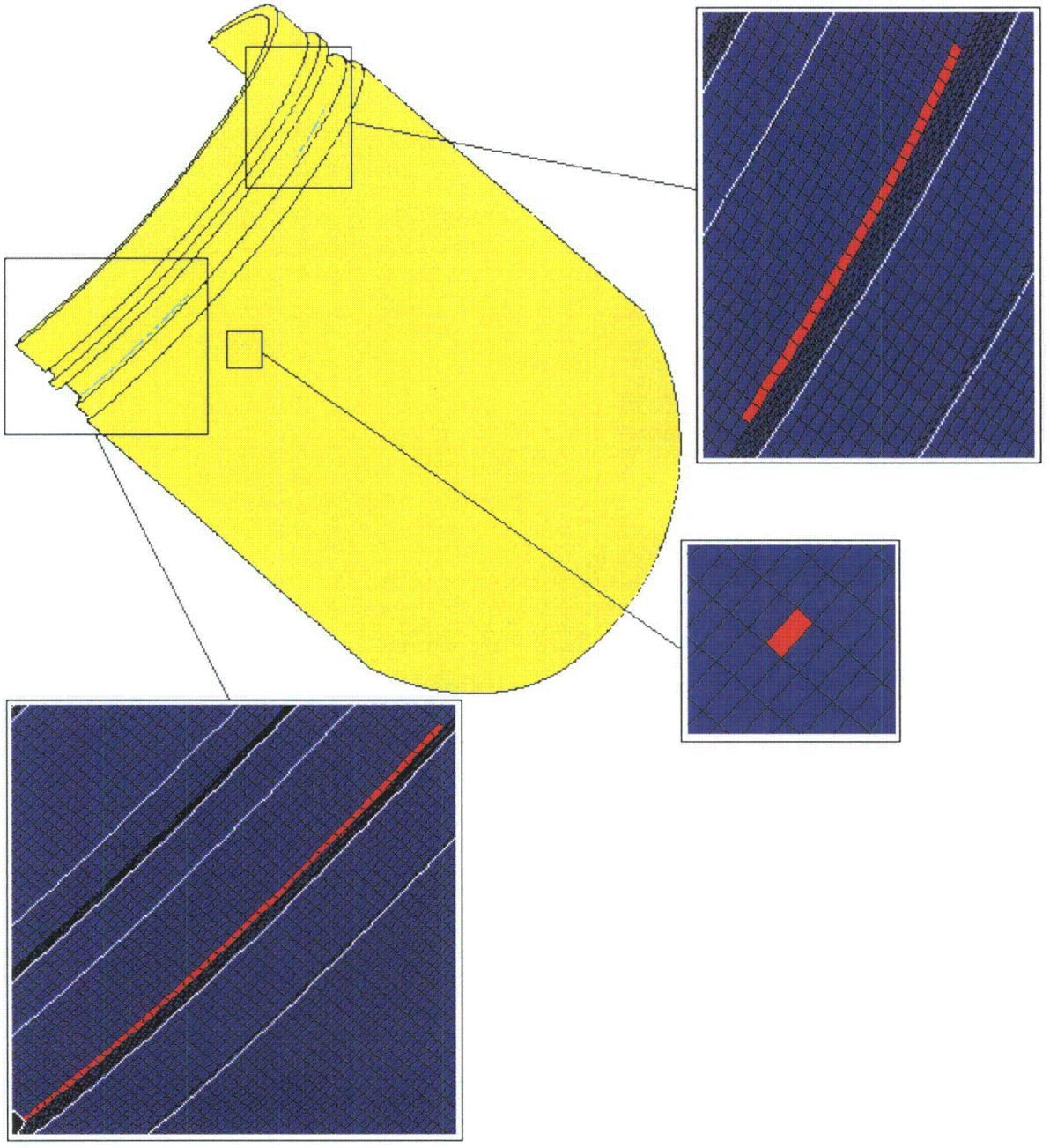

**Figure 2-159. Plot of Elements Exceeding the Experimental Strain Locus for the 831-g, Angled, Plutonium Metal Hollow Cylinder, Far Side Position, Side Impact**

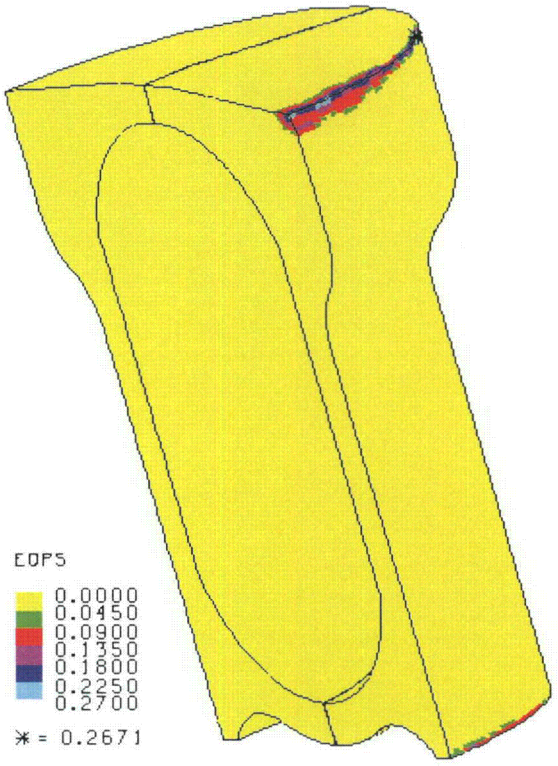


**Figure 2-160. Plot of EQPS in the TB-1 for the 831-g, Angled, ER Cylinder, Far Side Position, Side Impact**

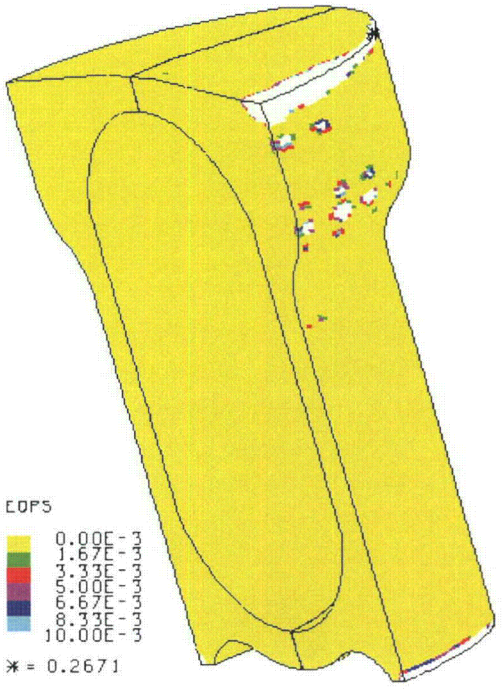


**Figure 2-161. Plot of EQPS in the TB-1 for the 831-g, Angled, ER Cylinder, Far Side Position, Side Impact**

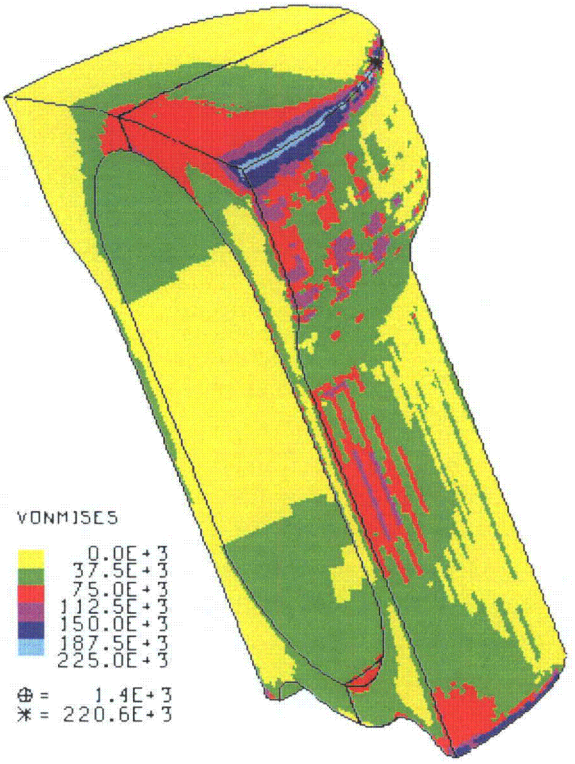


**Figure 2-162. Plot of von Mises Stress in the TB-1 for the 831-g, Angled, Plutonium Metal Hollow Cylinder, Far Side Position, Side Impact**

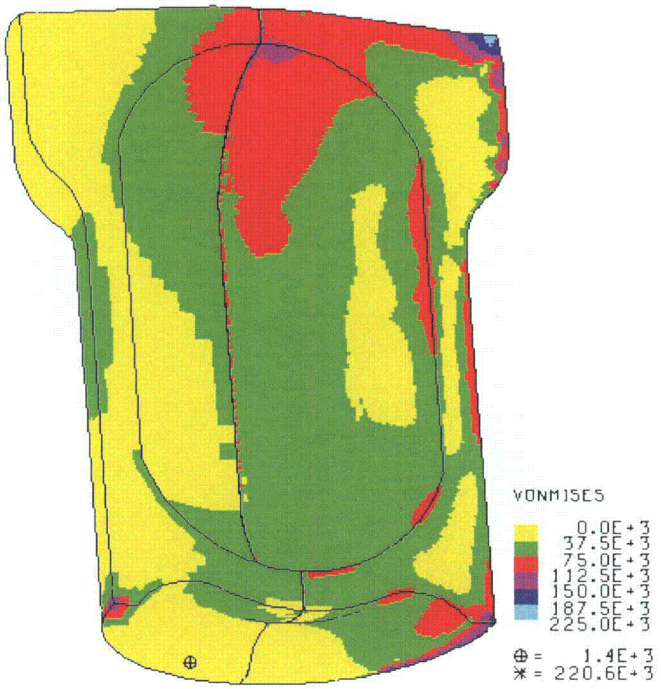


**Figure 2-163. Plot of von Mises Stress in the TB-1 for the 831-g, Angled, Plutonium Metal Hollow Cylinder, Far Side Position, Side Impact**

*2.12.5.4.7 Run 6 - 731-g Plutonium Metal Hollow Cylinder Top Impact*

The top end impact model for the slightly smaller (731 g) plutonium metal hollow cylinder, oriented axially (with the impact direction, as opposed to angled) is shown in Figure 2-164. Note that the cylinder is located at the bottom of the T-Ampoule so that its net impact velocity with the top of the T-Ampoule is maximized. The post-impact deformation is shown in Figure 2-165 and its kinetic energy history in Figure 2-166. This slightly shorter plutonium metal hollow cylinder still exhibits buckling, despite its conservatively "strongest shape" definition.

Equivalent Plastic Strain (EQPS) in the TB-1 vessel is shown in Figure 2-167 to be less than 2.7%, and only in some localized outer contact regions with the redwood overpack. The von Mises stresses (see Figures 2-168 and 2-169) peak at 148.5 ksi, is just above the elevated-temperature minimum yield strength for the TB-1 of 141 ksi, but more importantly, through-thickness TB-1 stress values are in the less-than-25 ksi range, below yield. The time at which the peak value of the von Mises stress occurs coincides with the peak value of the contact force (summed over the lid area). A plot of this force as a function of time is shown in Figure 2-170. A maximum contact load of 66,273 lbs is applied to the inner surface of the TB-1 lid during the impact. No T-Ampoule elements exceeded the tested B-W strain locus, and the peak Tearing Parameter value (see Table 2-11, run #6) of 0.1507 was below the critical Tearing Parameter value of 1.012 for Ti-6Al-4V. Note that the peak Tearing Parameter value for the T-Ampoule in this 731 g, plutonium metal hollow cylinder impact case is slightly larger than that of the 831 g cylinder impact, because the shorter plutonium metal hollow cylinder has a slightly higher net impact velocity with the T-Ampoule.

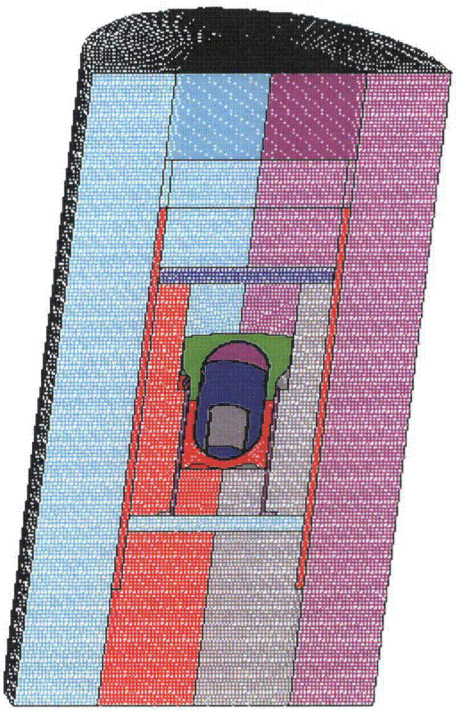

**Figure 2-164. Finite Element Mesh for the 731-g, ER, Cylinder, Bottom Position, Top Impact**

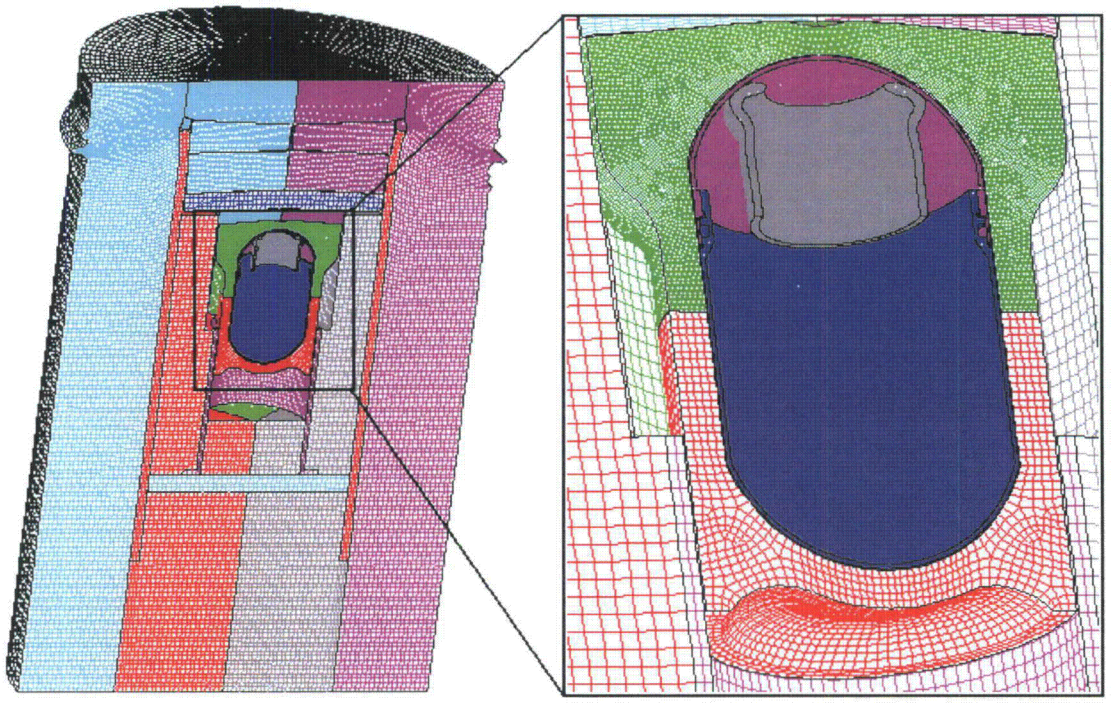

**Figure 2-165. Finite Element Mesh for the 731-g, ER, Cylinder, Bottom Position, Top Impact – Final Displacement**

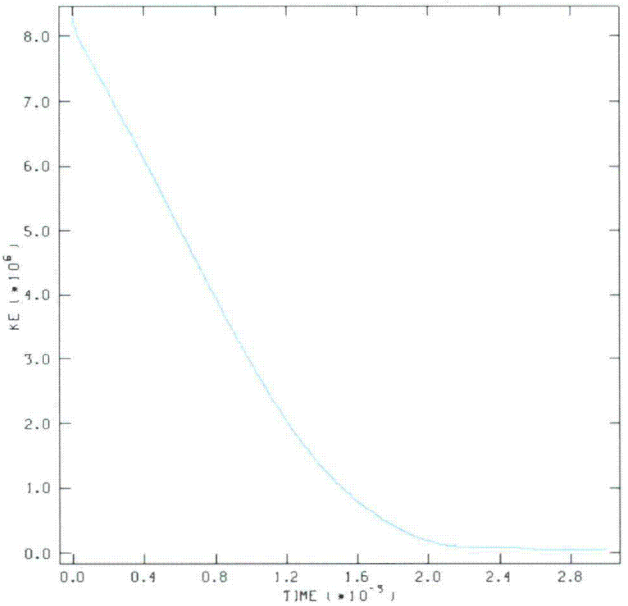


**Figure 2-166. Kinetic Energy Time History for the 731-g, ER, Cylinder, Bottom Position, Top Impact**

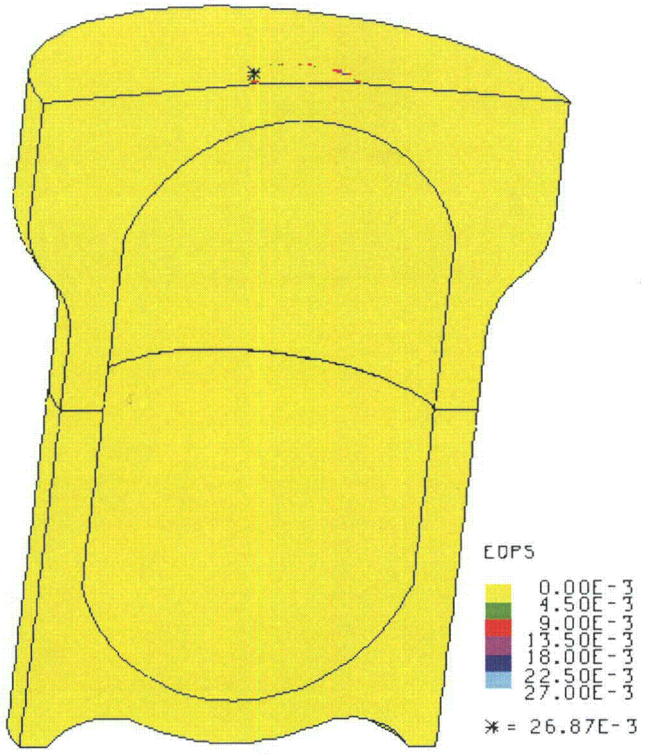


**Figure 2-167. EQPS in the TB-1 for the 731-g, Plutonium Metal Hollow Cylinder, Bottom Position, Top Impact**

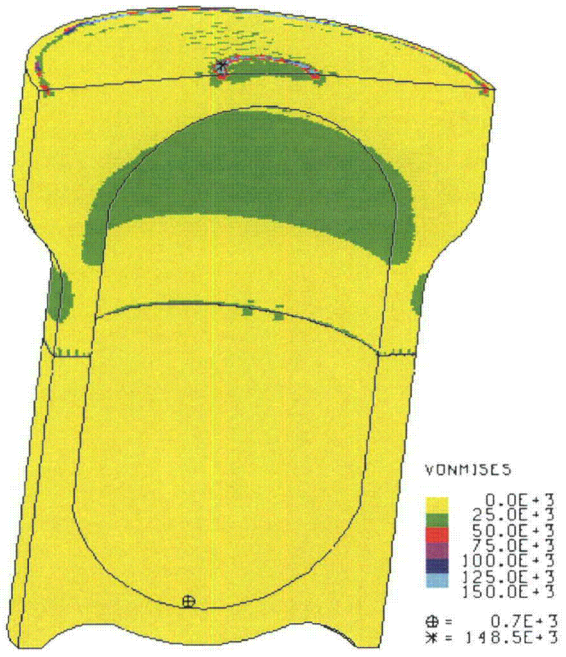


**Figure 2-168. von Mises Stress in the TB-1 for the 731-g, ER, Cylinder, Bottom Position, Top Impact**

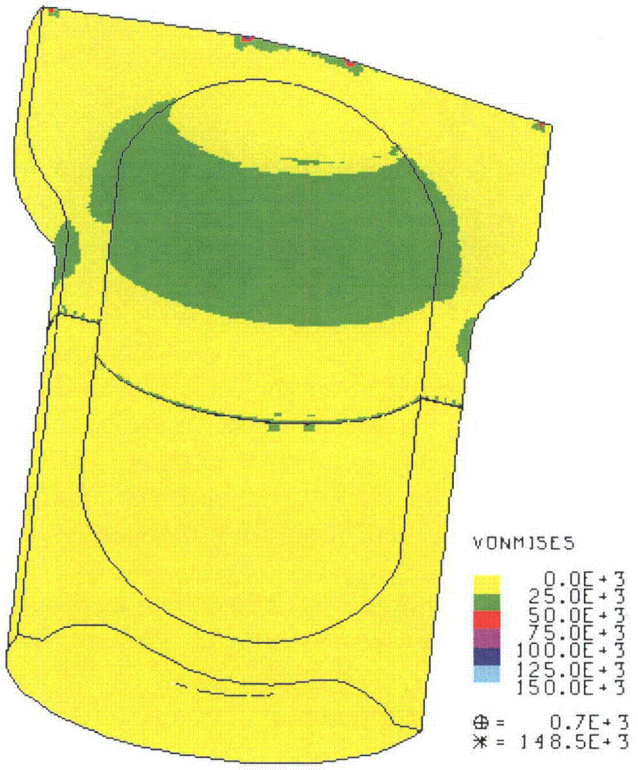


**Figure 2-169. von Mises Stress in the TB-1 for the 731-g, ER, Cylinder, Bottom Position, Top Impact**

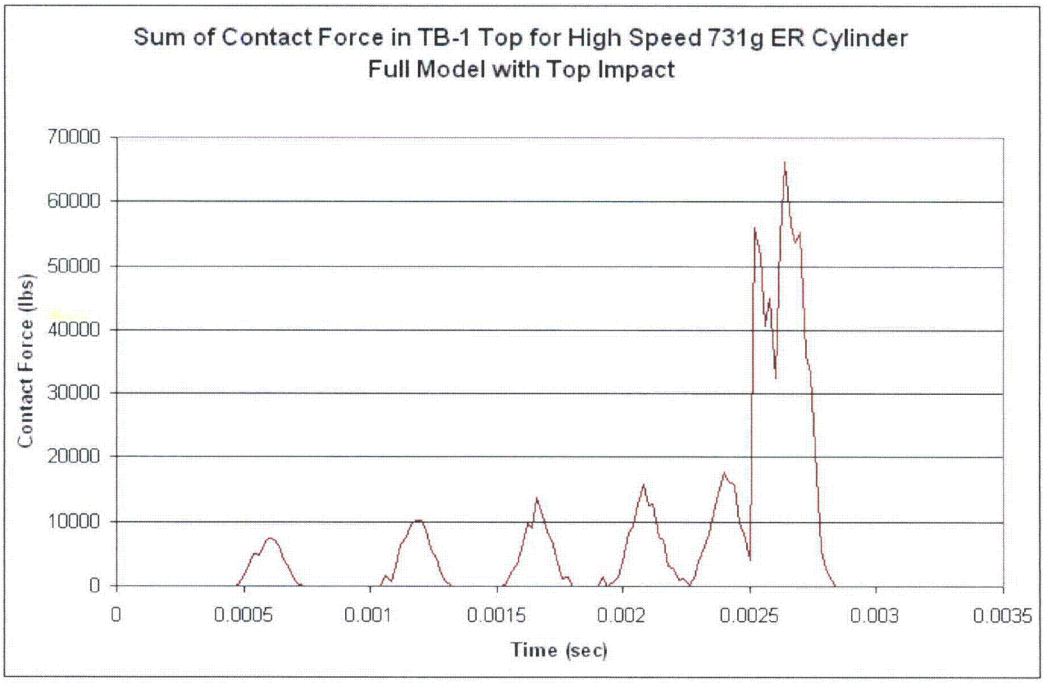


**Figure 2-170. Contact Forces in the TB-1 for the 731-g, ER, Cylinder, Bottom Position, Top Impact**

*2.12.5.4.8 Run 7 - 731-g, Angled, Plutonium Metal Hollow Cylinder Top Impact*

The top end impact model for the shorter 731 g plutonium metal hollow cylinder, oriented angled, is shown in Figure 2-171. The cylinder is located at the bottom of the T-Ampoule so that its net impact velocity with the top of the T-Ampoule is maximized. The post-impact deformation is shown in Figure 2-172 and its kinetic energy history in Figure 2-173. The plutonium metal hollow cylinder deforms but maintains much of its original shape because of its conservatively "infinitely ductile" material constitutive model definition (despite its alpha Pu being a relatively brittle material in reality).

Average stress-triaxiality versus EQPS is shown in Figures 2-174 and 2-175 for the 21 elements extending beyond the tested Bao-Wierzbicki strain locus. All of these elements are at high stress triaxiality and low EQPS. The Tearing Parameter values for these same 21 elements are shown in Figure 2-176, and all are below the critical Tearing Parameter value of 1.012 for Ti-6Al-4V. These elements are highlighted in red Figure 2-177, but note that these elements are still below the initiation of a ductile tear, thus T-Ampoule integrity is maintained.

Peak EQPS in the TB-1 vessel, shown in Figure 2-178, is about 2.4% and is only in some localized outer contact regions with the redwood overpack. The von Mises stresses (see Figures 2-179 and 2-180) peak at 148.5 ksi, is just above the elevated-temperature minimum yield strength for the TB-1 of 141 ksi, but more importantly, through-thickness TB-1 stress values are less than 25 ksi, below yield. The time at which the peak value of the von Mises stress occurs coincides with the peak value of the contact force (summed over the lid area). A plot of this force as a function of time is shown in Figure 2-181. A maximum contact load of 58,873 lbs is applied to the inner surface of the TB-1 during the impact.

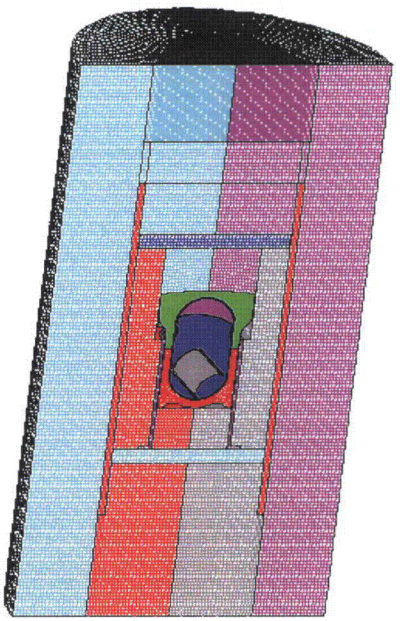

**Figure 2-171. Finite Element Mesh for the 731-g, Angled, ER Cylinder, Bottom Position, Top Impact**

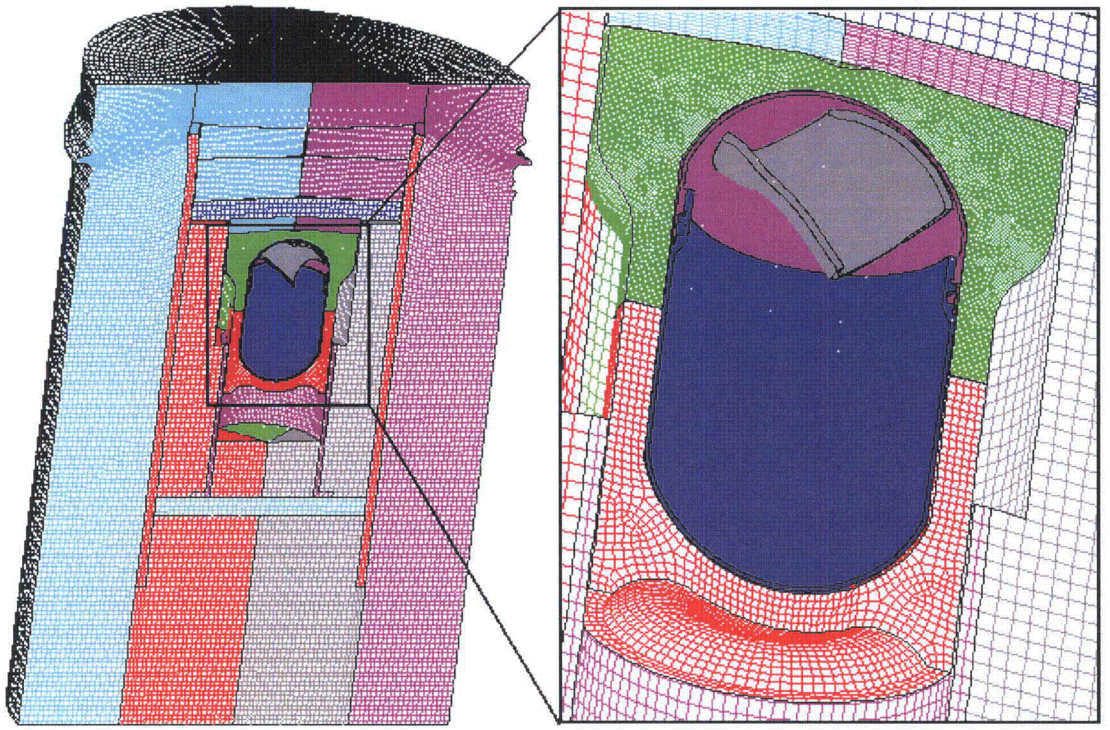

**Figure 2-172. Finite Element Mesh for the 731-g, Angled, ER Cylinder, Bottom Position, Top Impact – Final Displacement**

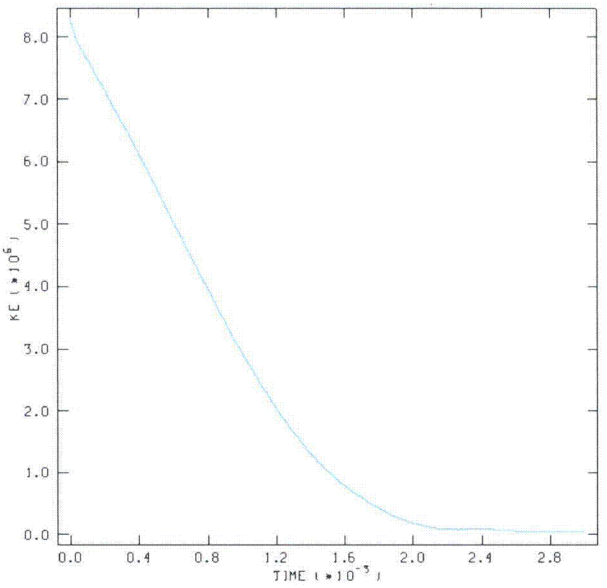


**Figure 2-173. Kinetic Energy Time History for the 731-g, Angled, Plutonium Metal Hollow Cylinder, Bottom Position, Top Impact**

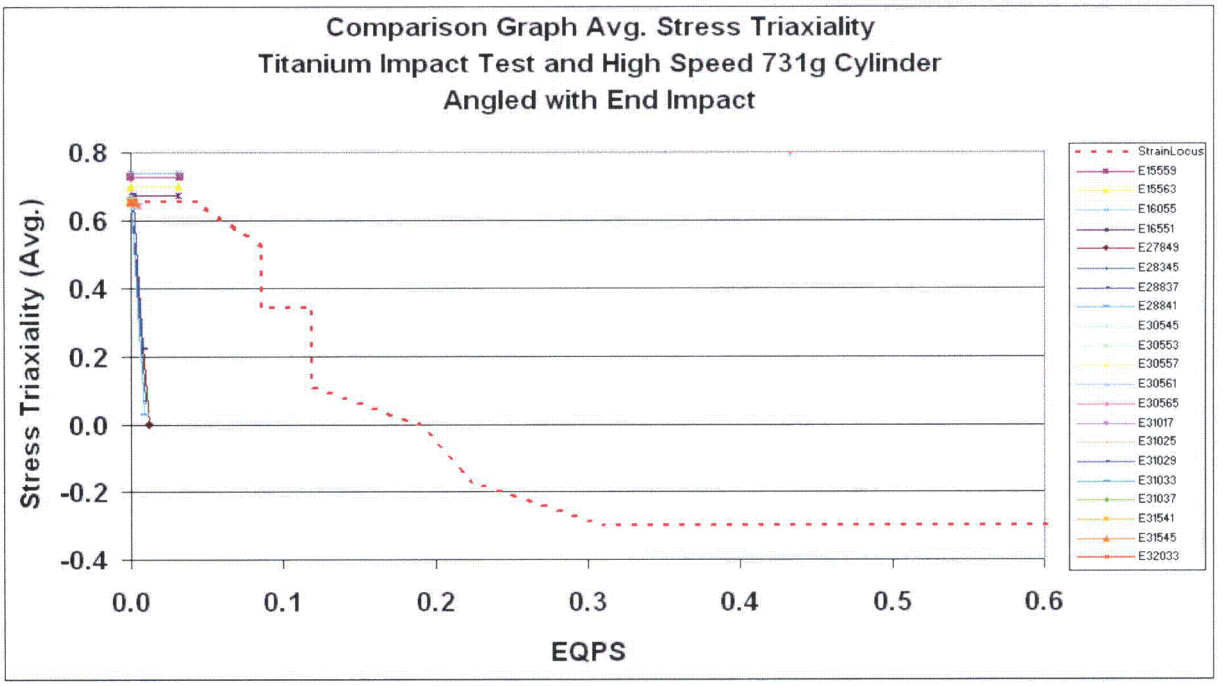


**Figure 2-174. Graph of Average Stress Triaxiality versus EQPS of Elements Exceeding the Experimental Strain Locus for the 731-g, Angled, Plutonium Metal Hollow Cylinder, Bottom Position, Top Impact**

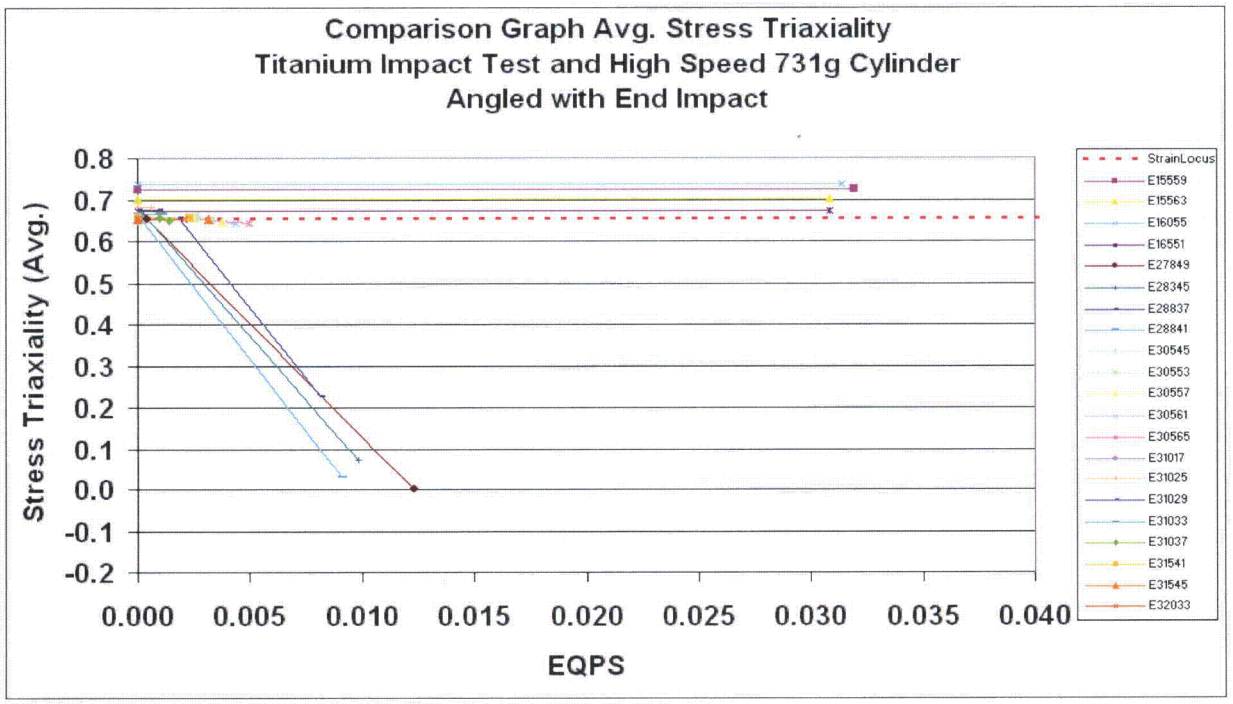


**Figure 2-175. Graph of Average Stress Triaxiality versus EQPS of Elements Exceeding the Experimental Strain Locus (Zoomed In) for the 731-g, Angled, Plutonium Metal Hollow Cylinder, Bottom Position, Top Impact**

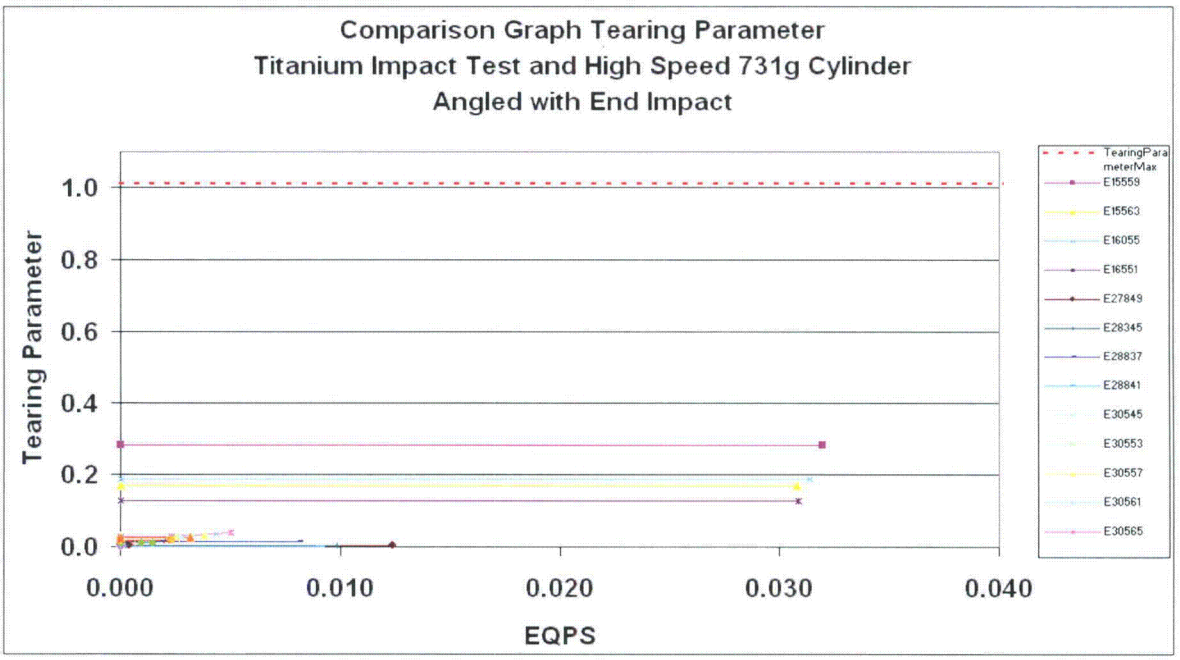


**Figure 2-176. Graph of Tearing Parameter versus EQPS of Elements Exceeding the Experimental Strain Locus for the 731-g, Angled, Plutonium Metal Hollow Cylinder, Bottom Position, Top Impact**

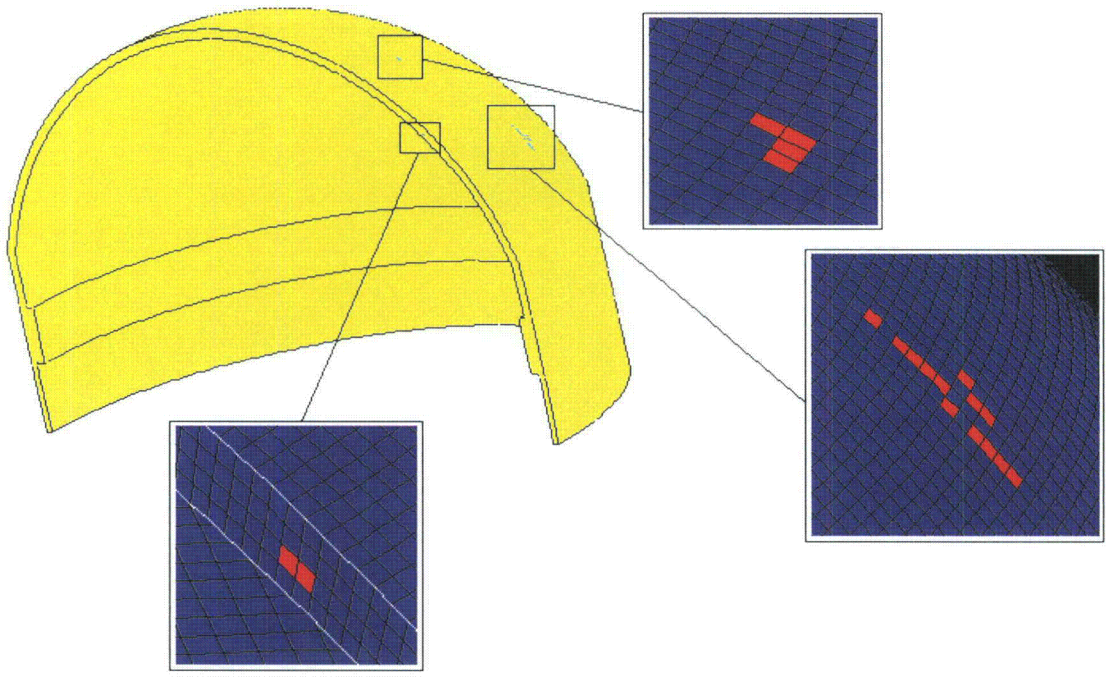

**Figure 2-177. Plot of Elements Exceeding the Experimental Strain Locus for the 731-g, Angled, Plutonium Metal Hollow Cylinder, Bottom Position, Top Impact**

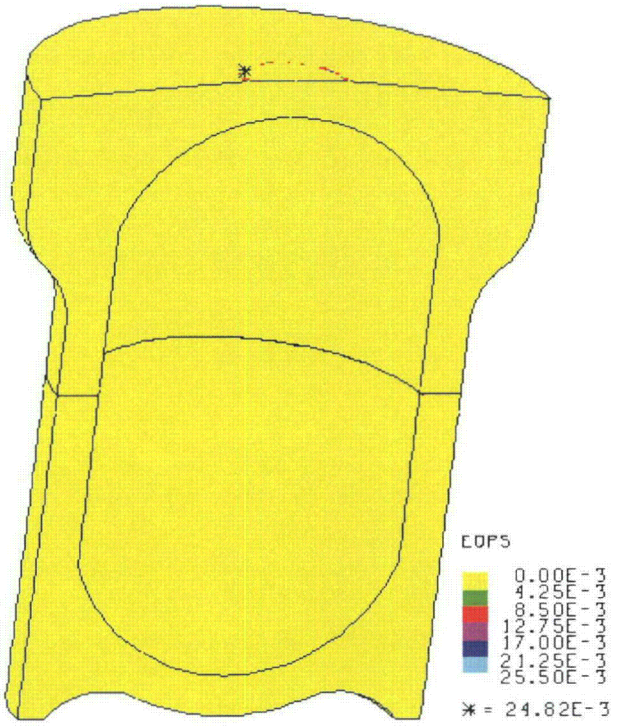


**Figure 2-178. Plot of EQPS in the TB-1 for the 731-g, Angled, Plutonium Metal Hollow Cylinder, Bottom Position, Top Impact**

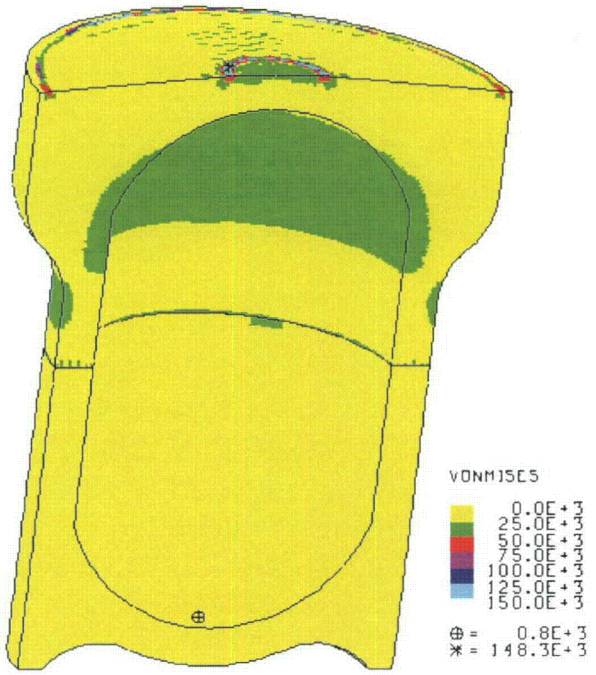


**Figure 2-179. Plot of von Mises Stress for the 731-g, Angled, Plutonium Metal Hollow Cylinder, Bottom Position, Top Impact**

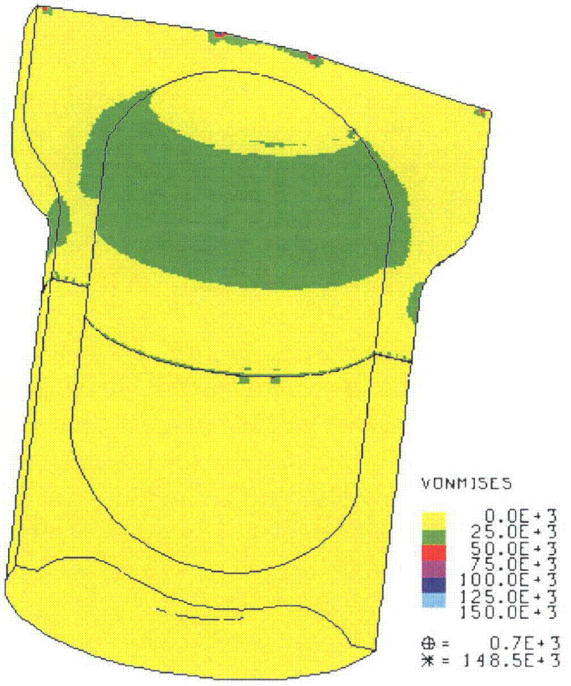


**Figure 2-180. Plot of von Mises Stress for the 731-g, Angled, Plutonium Metal Hollow Cylinder, Bottom Position, Top Impact**

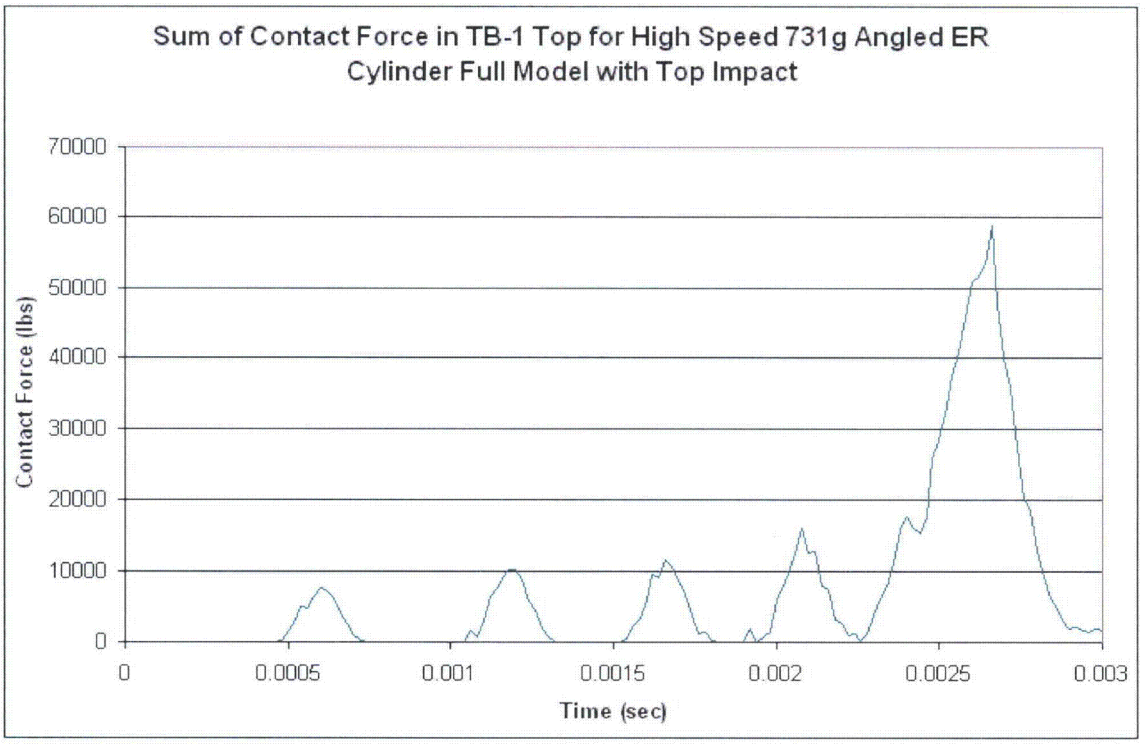


**Figure 2-181. Plot of Contact Force for the 731-g, Angled, Plutonium Metal Hollow Cylinder, Bottom Position, Top Impact**

*2.12.5.4.9 Run 8 - 731-g Angled Plutonium Metal Hollow Cylinder CGOC Impact*

The lid end CG-over-corner impact model for the shorter 731 g plutonium metal hollow cylinder is shown in Figure 2-182. The cylinder is located at the bottom of the T-Ampoule so that its net impact velocity with the top of the T-Ampoule is maximized. The post-impact deformation is shown in Figure 2-183 and its kinetic energy history in Figure 2-184. The plutonium metal hollow cylinder deforms slightly more than the previous case because of the slightly more side-impact-like orientation but maintains much of its original shape because of its conservatively "infinitely ductile" material constitutive model definition.

Average stress-triaxiality versus EQPS is shown in Figures 2-185 and 2-186 for the 84 elements extending beyond the tested Bao-Wierzbicki strain locus. All of these elements are at relatively high stress triaxiality and low EQPS. The Tearing Parameter values for these same 84 elements are shown in Figure 2-187 and all are still safely below the critical Tearing Parameter value of 1.012 for Ti-6Al-4V. These elements are highlighted in red in Figures 2-188 and 2-189 but these elements are still below the critical value, thus the T-Ampoule eutectic barrier integrity is maintained.

Peak EQPS in the TB-1 vessel is shown in Figure 2-190 to be about 28.5%, although this peak is only in a highly localized outer corner region where there is a slight contact over closure issue with the redwood overpack. Through-thickness plasticity is non-existent and the TB-1 integrity is maintained. The von Mises stress (see Figure 2-191) peak at 225 ksi (due to the localized redwood contact) is above the elevated-temperature minimum yield strength for the TB-1 of 141 ksi, but more importantly, through-thickness TB-1 stress values are less than 37.5 ksi, below yield.

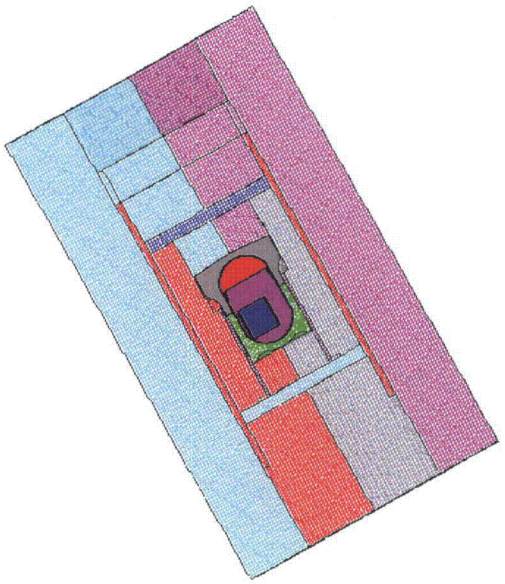

**Figure 2-182. Finite Element Mesh for the 731-g, Angled, Plutonium Metal Hollow Cylinder, Bottom Position, CGOC Impact**

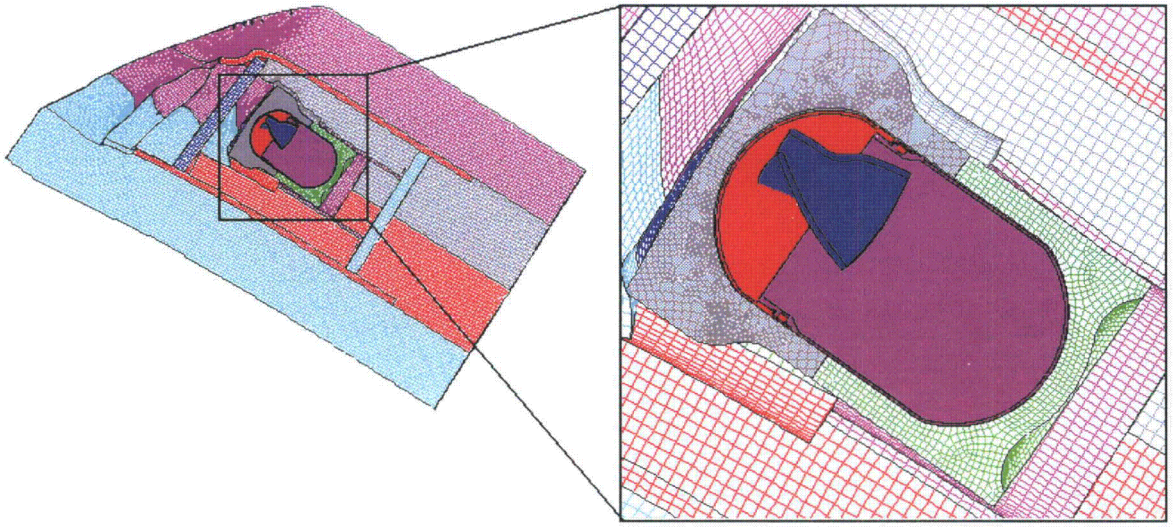

**Figure 2-183. Finite Element Mesh for the 731-g, Angled, Plutonium Metal Hollow Cylinder, Bottom Position, CGOC Impact – Final Displacement**

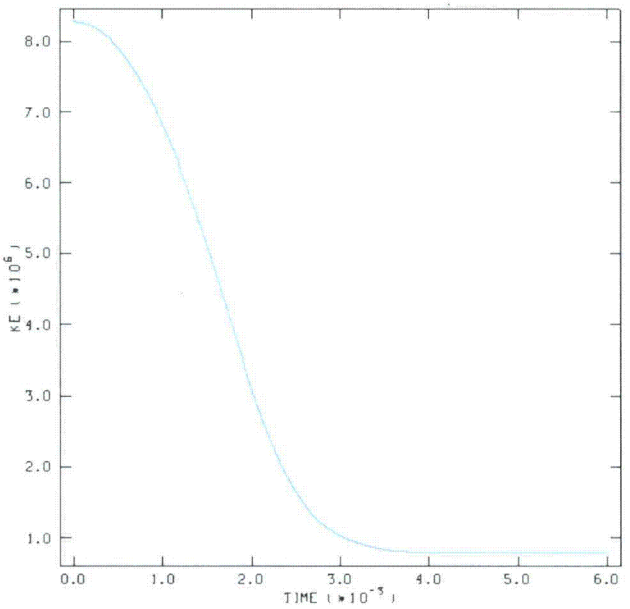


**Figure 2-184. Kinetic Energy Time History for the 731-g, Angled, Plutonium Metal Hollow Cylinder, Bottom Position, CGOC Impact**

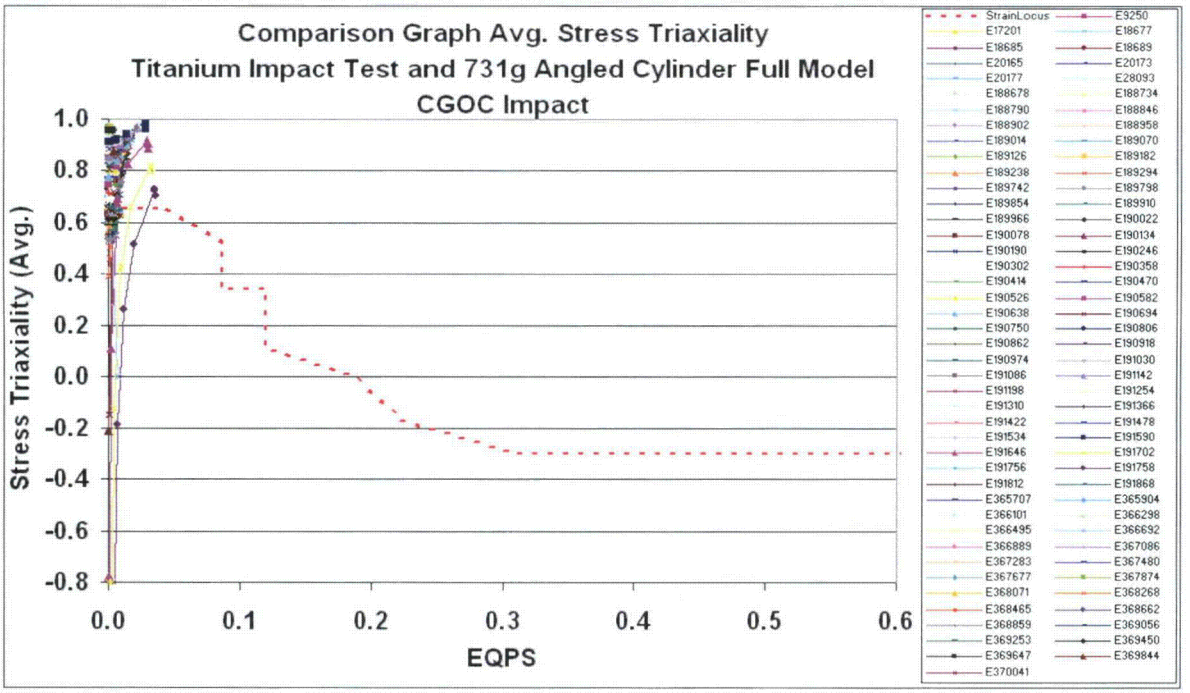


**Figure 2-185. Graph of Average Stress Triaxiality versus EQPS of Elements Exceeding the Experimental Strain Locus for the 731-g, Angled, Plutonium Metal Hollow Cylinder, Bottom Position, CGOC Impact**

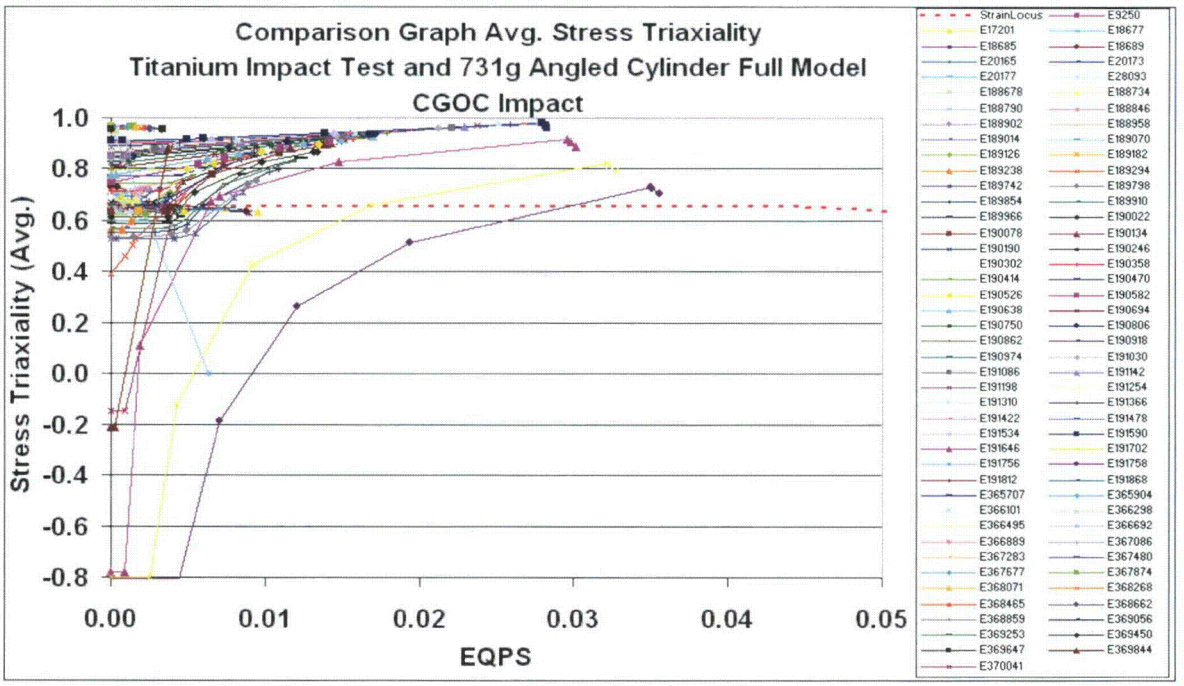


**Figure 2-186. Graph of Average Stress Triaxiality versus EQPS of Elements Exceeding the Experimental Strain Locus (Zoomed In) for the 731-g, Angled, Plutonium Metal Hollow Cylinder, Bottom Position, CGOC Impact**

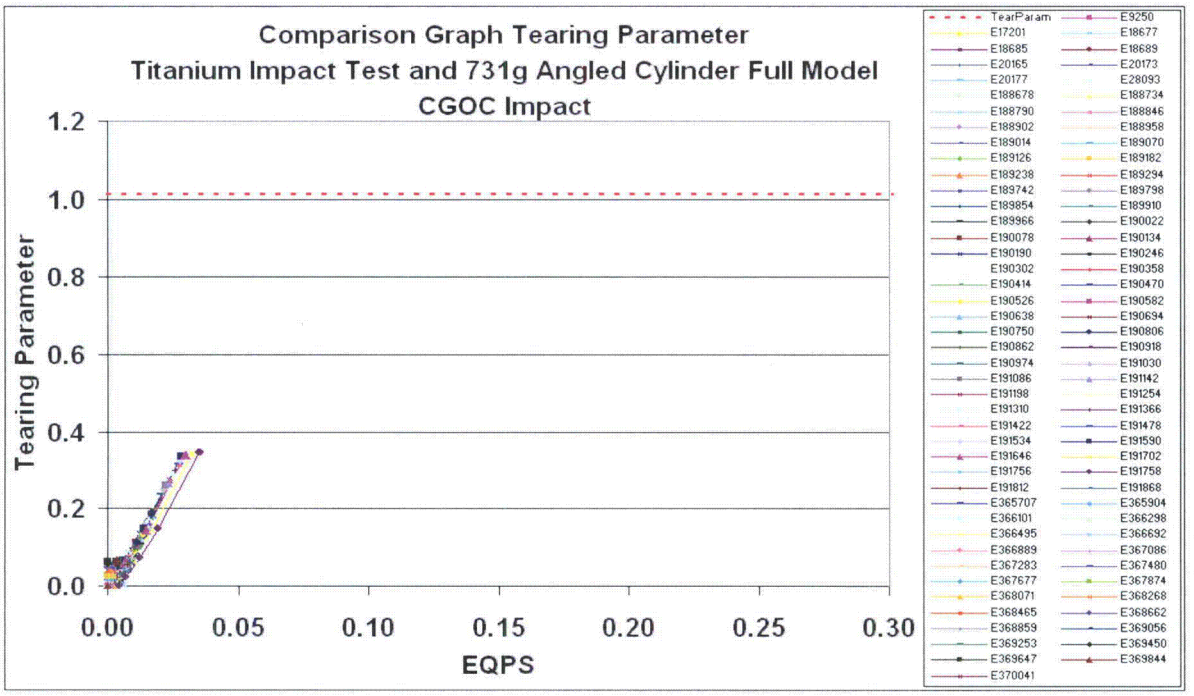


**Figure 2-187. Graph of Tearing Parameter versus EQPS of Elements Exceeding the Experimental Strain Locus for the 731-g, Angled, Plutonium Metal Hollow Cylinder, Bottom Position, CGOC Impact**

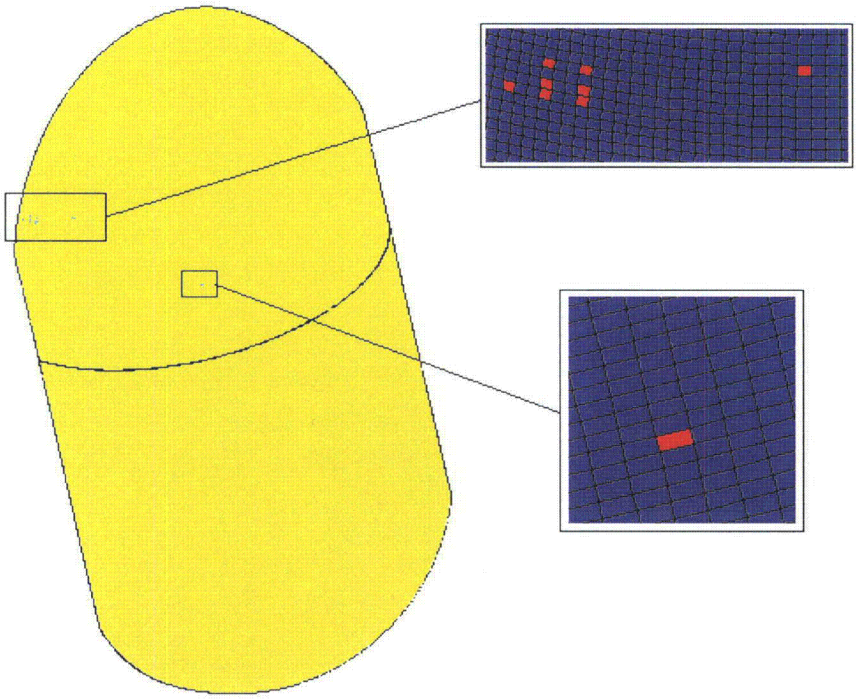

**Figure 2-188. Plot of Elements Exceeding the Experimental Strain Locus for the 731-g, Angled, Plutonium Metal Hollow Cylinder, Bottom Position, CGOC Impact**

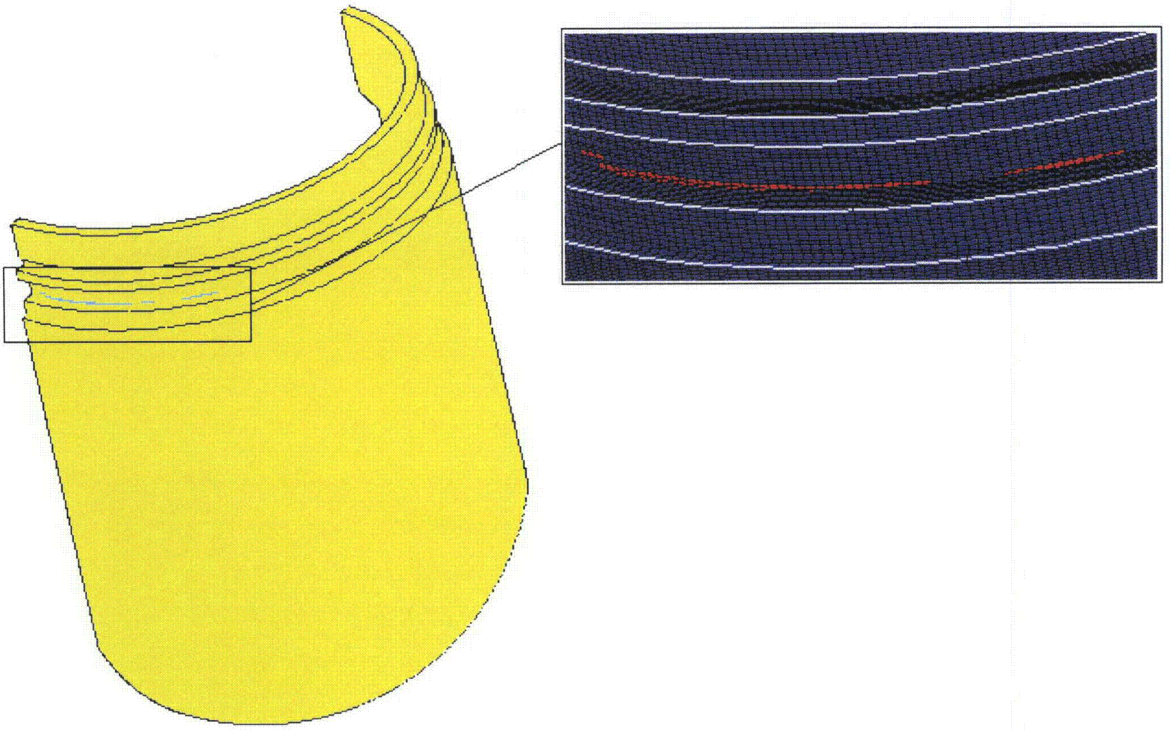

**Figure 2-189. Plot of Elements Exceeding the Experimental Strain Locus for the 731-g, Angled, Plutonium Metal Hollow Cylinder, Bottom Position, CGOC Impact**

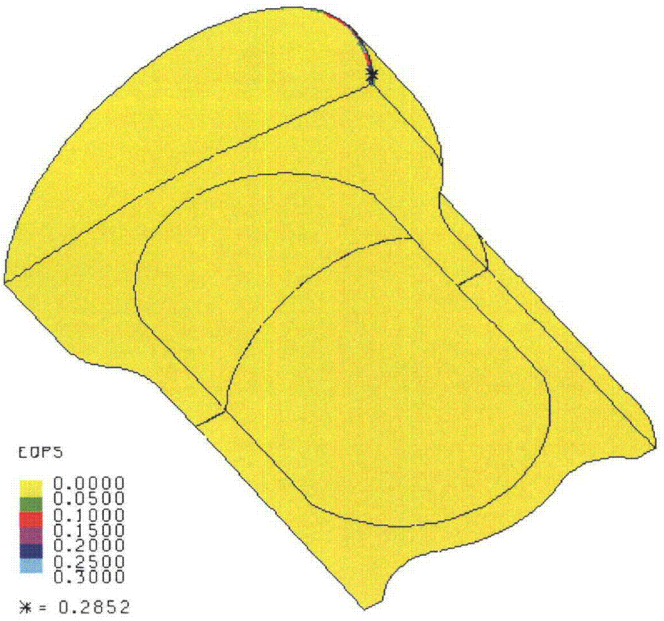


**Figure 2-190. Plot of EQPS in the TB-1 for the 731-g, Angled, Plutonium Metal Hollow Cylinder, Bottom Position, CGOC Impact**


**Figure 2-191. Plot of von Mises Stress in the TB-1 for the 731-g, Angled, Plutonium Metal Hollow Cylinder, Bottom Position, CGOC Impact**

*2.12.5.4.10 Run 9 - 731-g Plutonium Metal Hollow Cylinder Side Impact*

The side impact model for the shorter and lighter 731 g plutonium metal hollow cylinder is shown in Figure 2-192. The cylinder is located at the far side of the T-Ampoule so that its net impact velocity with the side of the T-Ampoule is maximized. The post-impact deformation is shown in Figure 2-193 and its kinetic energy history in Figure 2-194. The plutonium metal hollow cylinder deforms much more than the previous case because of its weaker side-impact-like orientation.

Average stress-triaxiality versus EQPS is shown in Figures 2-195 and 2-196 for the 63 elements extending beyond the tested Bao-Wierzbicki strain locus. All of these elements are at relatively high stress triaxiality and low EQPS. The Tearing Parameter values for these same 63 elements are shown in Figure 2-197 and all are still below the critical Tearing Parameter value of 1.012 for Ti-6Al-4V. These elements are highlighted in red Figure 2-198 but these elements are still below the critical value and do not indicate failure; T-Ampoule integrity is maintained.

Peak EQPS in the TB-1 vessel is shown in Figures 2-199 through 2-202 and is about 30%, although this peak is only in a highly localized outer corner region where there is a slight contact overclosure issue with the redwood overpack. A slight (<1% EQPS) dent is visible in Figure 2-202 from the internal impact of the plutonium metal hollow cylinder into the TB-1 wall (via the T-Ampoule). Through-thickness plasticity is non-existent and the TB-1 integrity is maintained. The von Mises stresses (see Figures 2-203 and 2-204) peak at 225 ksi (due to the localized redwood contact), above the elevated-temperature minimum yield strength for the TB-1

of 141 ksi, but more importantly, through-thickness TB-1 stress values are less than 80 ksi, below yield.

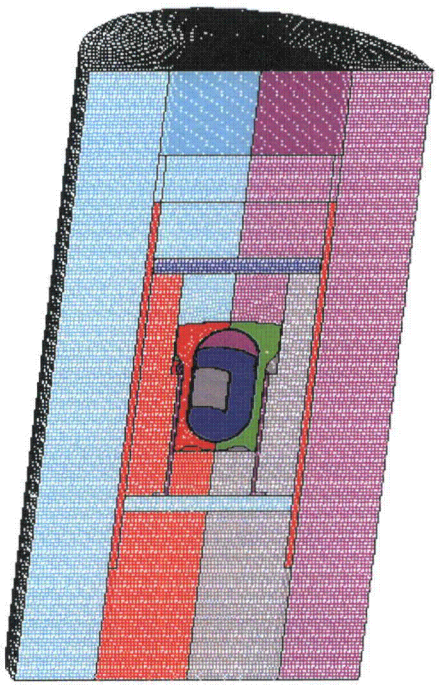

**Figure 2-192. Finite Element Mesh for the 731-g, ER, Cylinder, Far Side Position, Side Impact**

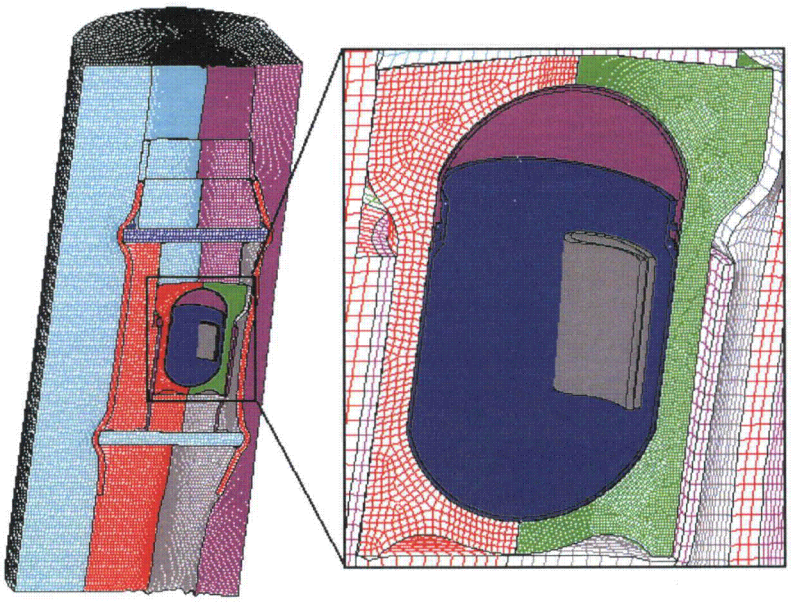

**Figure 2-193. Finite Element Mesh for the 731-g, Plutonium Metal Hollow Cylinder, Far Side Position, Side Impact – Final Displacement**

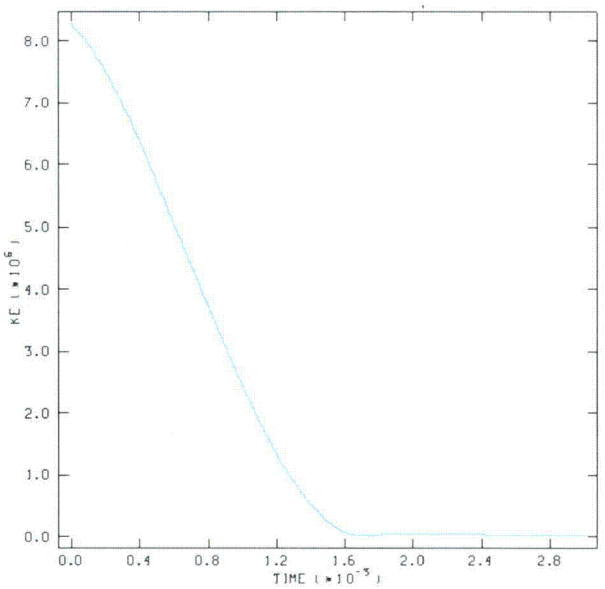


**Figure 2-194. Kinetic Energy Time History for the 731-g, ER, Cylinder, Far Side Position, Side Impact**

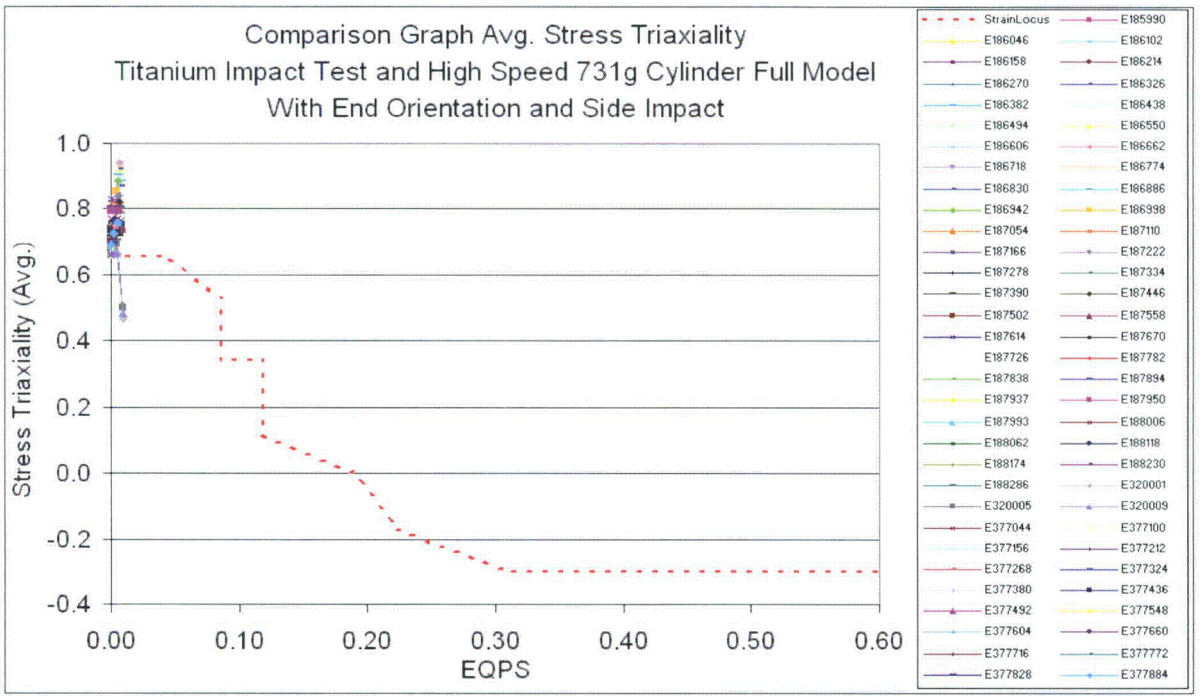


**Figure 2-195. Graph of Average Stress Triaxiality versus EQPS of Elements Exceeding the Experimental Strain Locus for the 731-g, Plutonium Metal Hollow Cylinder, Far Side Position, Side Impact**

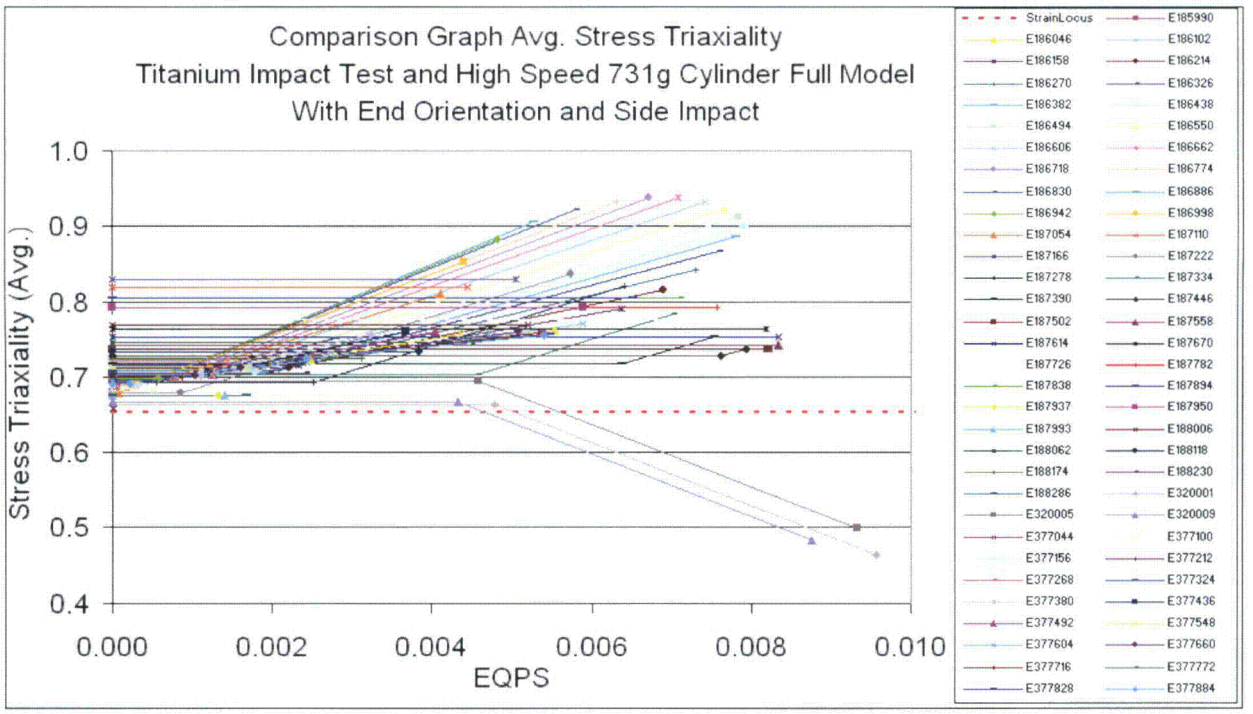


**Figure 2-196. Graph of Average Stress Triaxiality versus EQPS of Elements Exceeding the Experimental Strain Locus (Zoomed In) for the 731-g, Plutonium Metal Hollow Cylinder, Far Side Position, Side Impact**

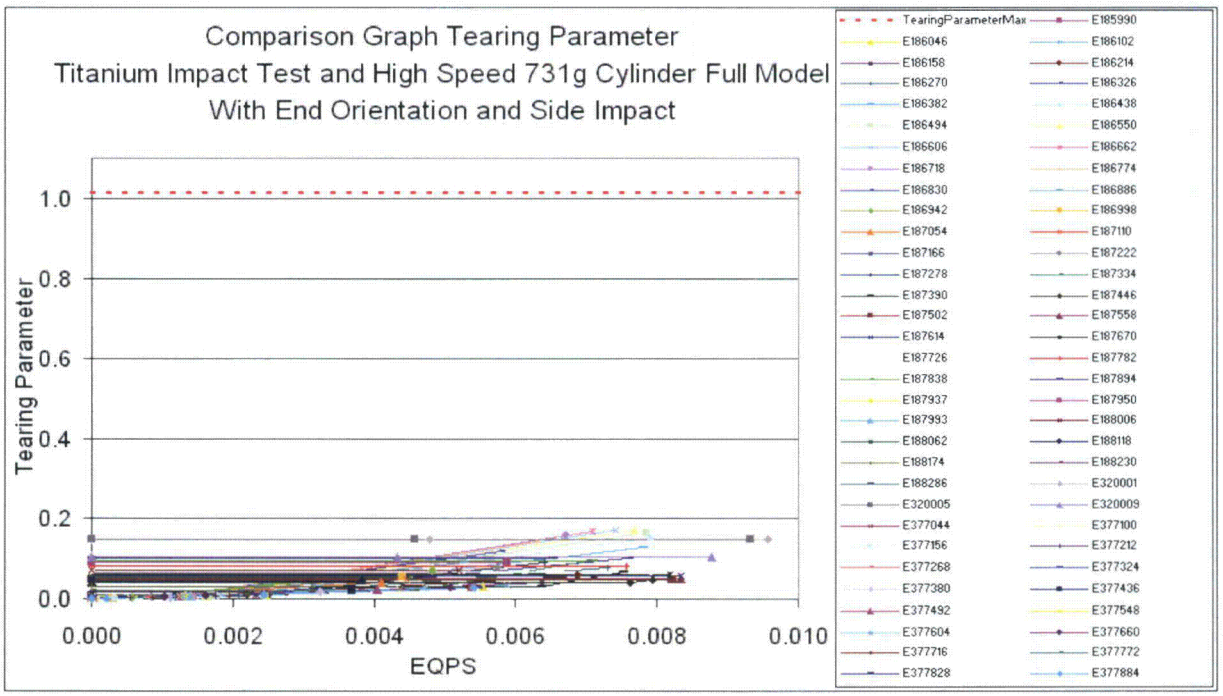


**Figure 2-197. Graph of Tearing Parameter versus EQPS of Elements Exceeding the Experimental Strain Locus for the 731-g, Plutonium Metal Hollow Cylinder, Far Side Position, Side Impact**

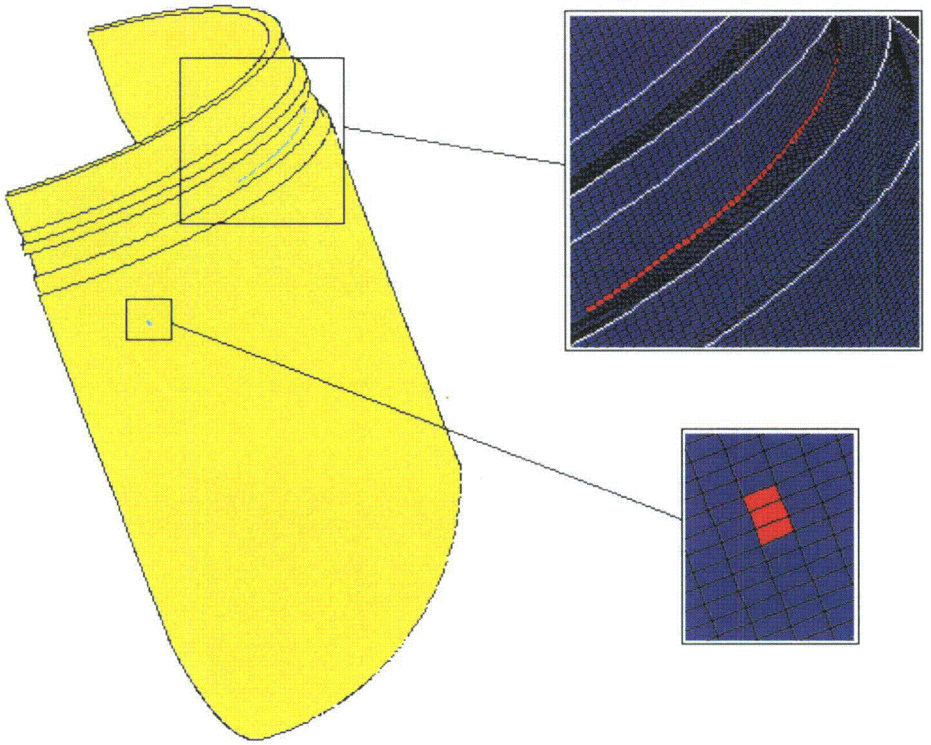

**Figure 2-198. Plot of Elements Exceeding the Experimental Strain Locus for the 731-g, Plutonium Metal Hollow Cylinder, Far Side Position, Side Impact**

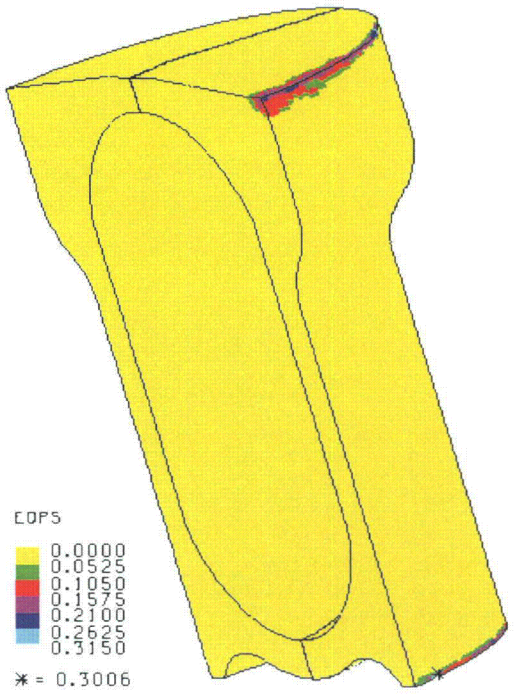


**Figure 2-199. Plot of EQPS in the TB-1 for the 731-g, ER Cylinder, Far Side Position, Side Impact**

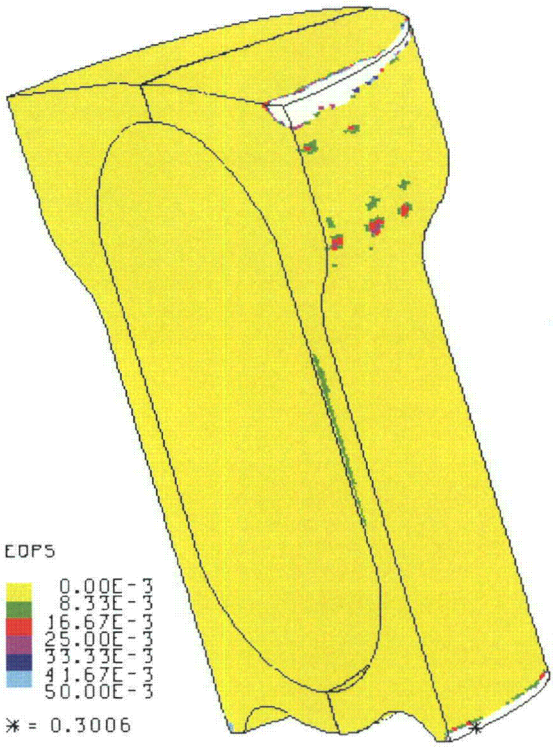


**Figure 2-200. Plot of EQPS in the TB-1 for the 731-g, ER Cylinder, Far Side Position, Side Impact**

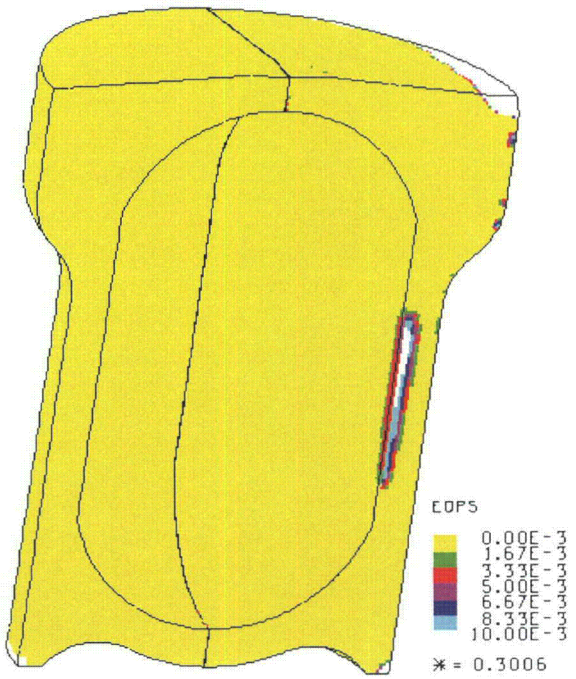


**Figure 2-201. Plot of EQPS in the TB-1 for the 731-g, ER Cylinder, Far Side Position, Side Impact**

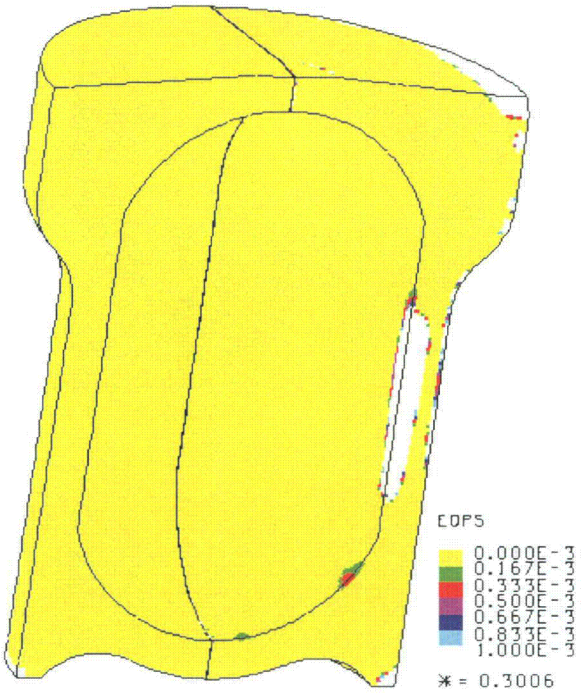


**Figure 2-202. Plot of EQPS in the TB-1 for the 731-g, Plutonium Metal Hollow Cylinder, Far Side Position, Side Impact (Range Adjusted to Highlight Small Stains in the TB-1 Not Visible in Figure 2-201)**

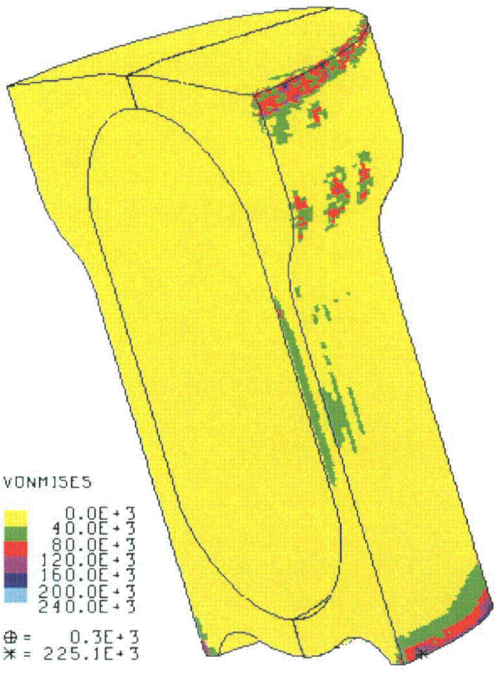


**Figure 2-203. Plot of von Mises Stress in the TB-1 for the 731-g, Plutonium Metal Hollow Cylinder, Far Side Position, Side Impact**

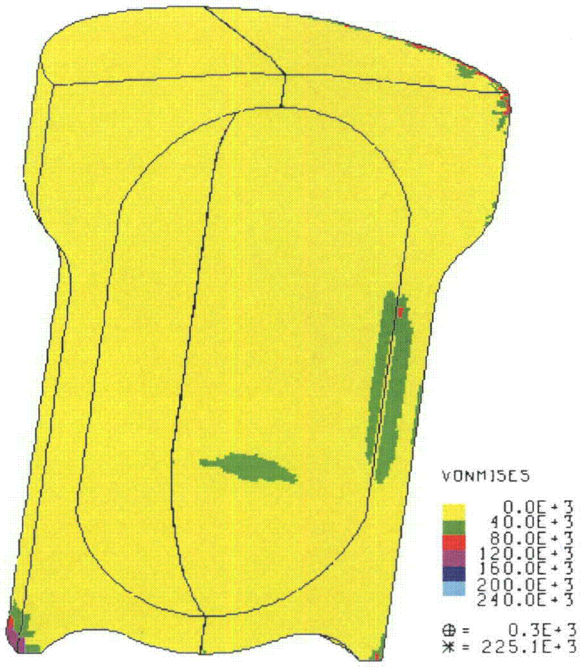


**Figure 2-204. Plot of von Mises Stress in the TB-1 for the 731-g, Plutonium Metal Hollow Cylinder, Far Side Position, Side Impact (see Figure 2-203 Rotated to Show Internal Stresses)**

*2.12.5.4.11 Run 10 - 731-g Angled Plutonium Metal Hollow Cylinder Side Impact*

The side impact model for the lighter, 731 g plutonium metal hollow cylinder, angled orientation, is shown in Figure 2-205. The cylinder is located at the far side of the T-Ampoule so that its net impact velocity with the side of the T-Ampoule is maximized, but also angled to present a sharp corner impact with the T-Ampoule surface. The post-impact deformation is shown in Figure 2-206 and its kinetic energy history in Figure 2-207. The plutonium metal hollow cylinder deforms moderately but maintains much of its original shape because of its conservatively "infinitely ductile" material constitutive model definition.

Average stress-triaxiality versus EQPS is shown in Figures 2-208 and 2-209 for the 94 elements extending beyond the tested Bao-Wierzbicki strain locus. All of these elements are at relatively high stress triaxiality and low EQPS. The Tearing Parameter values for these same 94 elements are shown in Figure 2-210 and all are still below the critical Tearing Parameter value of 1.012 for Ti-6Al-4V. These elements are highlighted in red Figure 2-211 but these elements are still below the critical value and do not indicate failure; T-Ampoule integrity is maintained.

Peak EQPS in the TB-1 vessel is shown in Figures 2-212 and 2-213 and is about 27.6%, although this peak is only in a highly localized outer corner region where there is a slight contact over closure issue with the redwood overpack. Through-thickness plasticity is non-existent and the TB-1 integrity is maintained. The von Mises stresses (see Figures 2-214 and 2-215) peak at 224 ksi (due to the localized redwood contact), above the elevated-temperature minimum yield strength for the TB-1 of 141 ksi, but more importantly, through-thickness TB-1 stress values are less than 112.5 ksi, below yield.

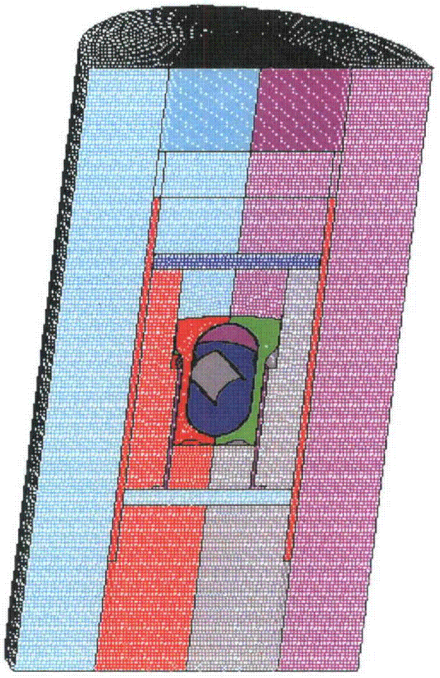

**Figure 2-205. Finite Element Mesh for the 731-g, Angled, ER Cylinder, Far Side Position, Side Impact**

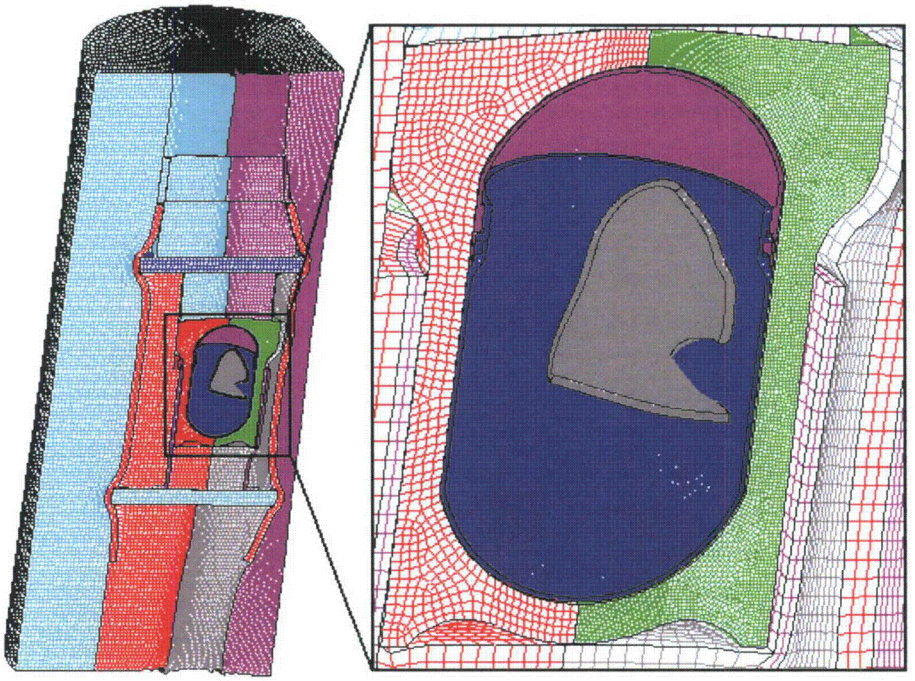

**Figure 2-206. Finite Element Mesh for the 731-g, Angled, ER Cylinder, Far Side Position, Side Impact – Final Displacement**

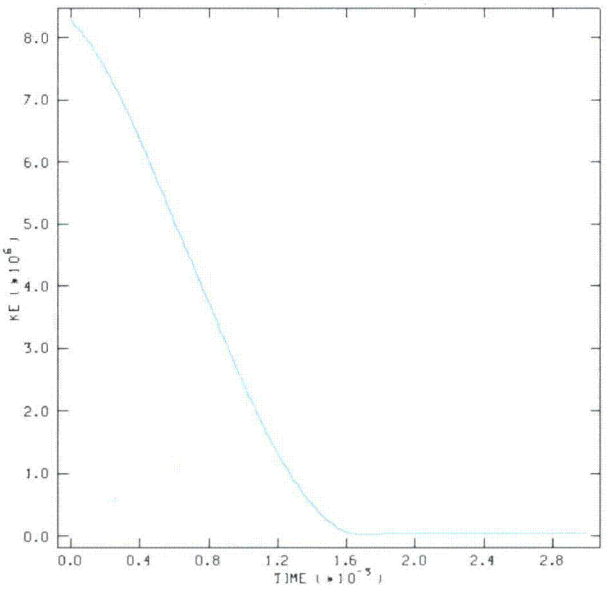


**Figure 2-207. Kinetic Energy Time History for the 731-g, Angled, Plutonium Metal Hollow Cylinder, Far Side Position, Side Impact**

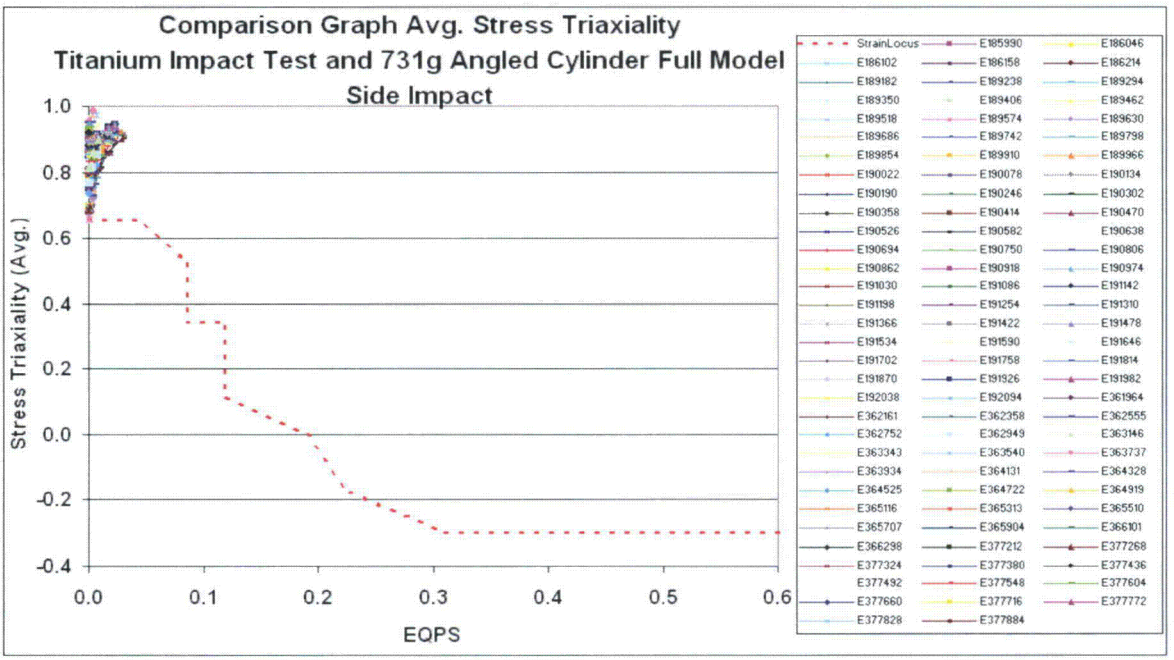


**Figure 2-208. Graph of Average Stress Triaxiality versus EQPS of Elements Exceeding the Experimental Strain Locus for the 731-g, Angled, Plutonium Metal Hollow Cylinder, Far Side Position, Side Impact**